Transport of Liquid CO_2 Derived from Steelworks Off-Gases

MSc Thesis

J.E. Krom

TU Delft and Tata Steel Netherlands

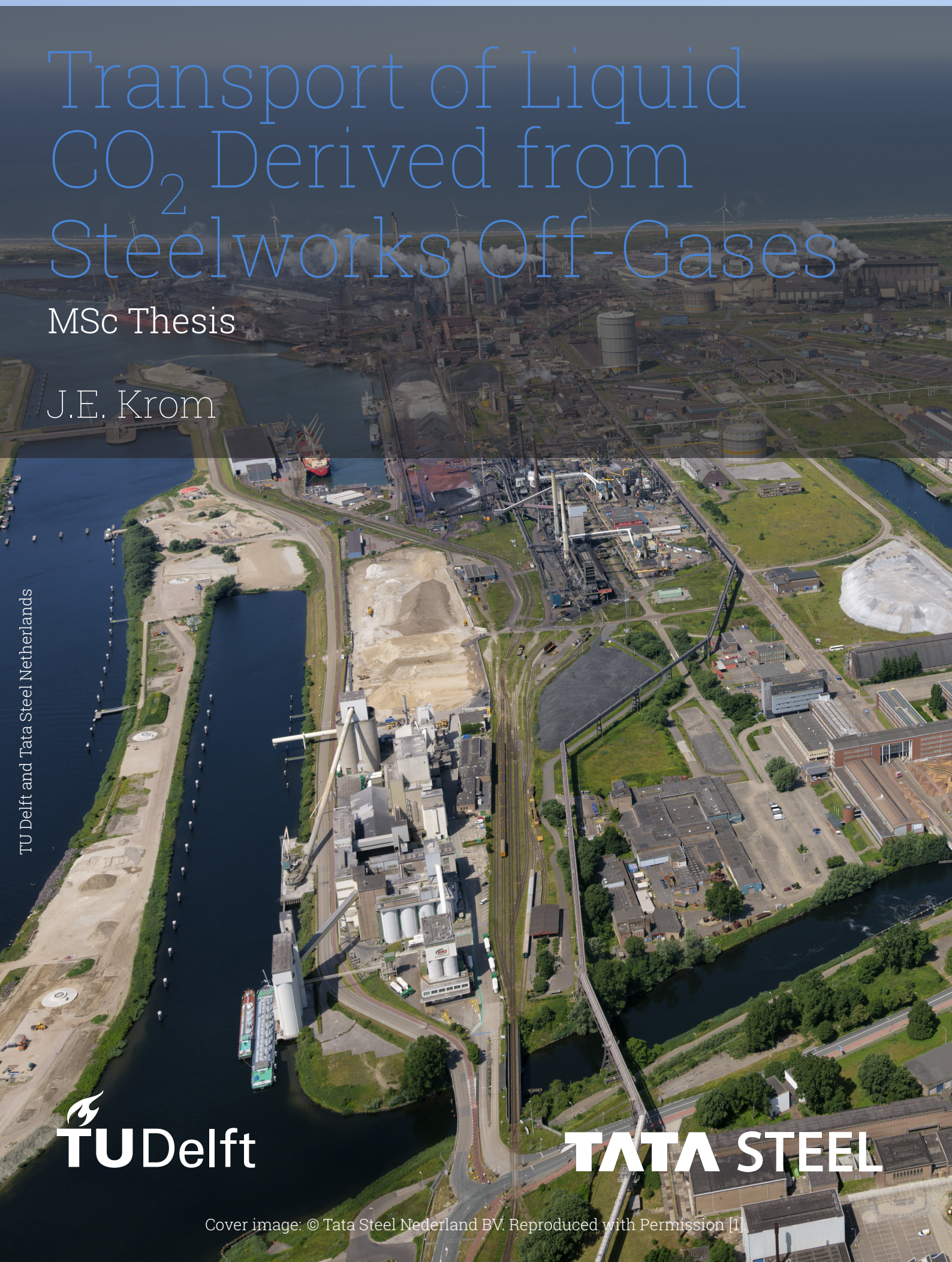

TU Delft

TATA STEEL

Transport of Liquid CO_2 Derived from Steelworks Off-Gases

MSc Thesis

by

J.E. Krom

to obtain the degree of Master of Science
at Delft University of Technology,
to be defended publicly on Tuesday, 24 February 2026 at 12:00.

Student number:	5885965	
Project duration:	May 15, 2025 – January 30, 2026	
Thesis committee:	Prof. dr. ir. T.J.H. Vlugt,	TU Delft, supervisor
	Dr. P. Van Den Broeke,	Tata Steel Netherlands, supervisor
	Dr. ir. B. Ramani,	Tata Steel Netherlands, supervisor
	Dr. ir. M. Ramdin,	TU Delft, independent member
	Dr. P. Costa,	TU Delft, independent member

Acknowledgments

First of all, I want to thank my university supervisor Thijs and company supervisors Peter and Balan for the time they have taken to support me in conducting this research. Their broad experience helped me to produce results that I hope will be useful for Tata Steel. Furthermore, their experience has also helped me produce a report I am proud of.

In addition to Peter, Balan and Thijs who personally supervised me, I also want to thank my other colleagues. Especially the other interns with whom I have shared an office space, I had plenty of insightful discussions with Tom, Cas, Lucas, Daan and Maarten. Our various interactions made this workplace very enjoyable which has greatly helped me in producing these results.

I would especially like to thank Maarten for aligning his internship objectives to my thesis, his internship project focused on modifying the pressure swing adsorption models to process HIsarna off-gas. He calculated the stream compositions based on the selected purity goals which was subsequently implemented in this work. His research results will complement my thesis and bring Tata Steel closer to realizing an operational CCS project.

My family, partner and friends have also always been a great source of motivation. I can always count on their unconditional support and encouragement which gave me a great sense of pride in my work.

J.E. Krom
IJmuiden, January 2026

Abstract

Steelworks are a hard-to-abate CO_2-producing industry but large reductions are necessary to achieve goals set by the European Union. A promising option to mitigate CO_2 emissions is to separate the CO_2 from off-gas streams and subsequently move it to permanent storage. This thesis investigates the energy requirements and costs of liquefying and transporting CO_2-rich streams to permanent storage sites.

The study focuses on ship transport of liquid CO_2 derived from HIsarna off-gas. The phase behavior of various gas streams with increasing purities of 95.5, 97.5 and 99.5 vol% CO_2 is analyzed with NIST REFPROP in the pressure and temperature range of ship transport to assess the effects of impurity content. These synthetic CO_2-rich mixtures are composed of typical impurities from the HIsarna steelmaking process with or without subsequent heat recovery from combusting CO and H_2. The impurity composition for both cases consists of N_2, CO and H_2 or N_2 and O_2 respectively.

Aspen HYSYS was utilized to configure models of open and closed liquefaction systems which were used to simulate the various synthetic mixtures to find the effects of the input streams on the energy requirements. The costs of this liquefaction equipment are analyzed by sizing it with the Aspen Process Economic Analyzer and subsequently using various cost correlations. The transportation costs were calculated for the scales of 100, 200 and 400 kt of liquefied product per year with various correlations from literature based on the selected shipping conditions.

Results show that increasing the CO_2 volume fraction will decrease energy requirements and operational costs for both open and closed liquefaction systems. The closed liquefaction system showed lower energy requirements and operational costs for all investigated mixtures compared to the open liquefaction system. Furthermore it was found that the effects of the different impurity cases, N_2, CO and H_2 or N_2 and O_2, are relatively small. The capital costs of liquefaction equipment are found to be higher for the closed liquefaction system and slightly decrease with CO_2 purity. An increase of CO_2 purity also creates a reduction in operational and capital costs for transport infrastructure. Total operational costs are found to scale linearly with yearly capacity while capital costs increase strongly sublinearly.

The findings provide insight into the effects of CO_2 purity, impurity components, liquefaction systems and process scale on the operational and capital costs of liquefaction and transport. These results can be combined with research on CO_2 separation costs to find a preferred CO_2 storage route and support CO_2 abatement in the steel industry.

List of Figures

List of Tables

Nomenclature

Abbreviations

Abbreviation	Definition
FAR	First Assessment Report
UNFCCC	United Nations Framework Convention on Climate Change
EU	European Union
RIVM	National Institute for Public Health and the Environment
PBL	Netherlands Environmental Assessment Agency
SMR	Steam Methane Reforming
DR	Direct Reduction
DRI	Direct Reduced Iron
CCS	Carbon Capture and Storage
COG	Coke Oven Gas
BF	Blast Furnace
BFG	Blast Furnace Gas
ULCOS	Ultra Low CO2 Steelmaking
ZR	Zero Reformer
BOF	Basic Oxygen Furnace
EAF	Electric Arc Furnace
IOGP	International Organization of Oil and Gas Producers
CCUS	Carbon Capture Utilization and Storage
VOC	Volatile Organic Compound
BTEX	Benzene, Toluene, Ethylbenzene, and Xylenes
GERG	Groupe Européen de Recherches Gazières
PC-SAFT	Perturbed-Chain Statistical Associating Fluid Theory
EoS	Equation of State
SRK	Soave-Redlich-Kwong
PR	Peng-Robinson
CPA	Cubic Plus Association
BIPs	Binary Interaction Parameters
MD	Molecular Dynamics
MC	Monte Carlo
COP	Coefficient of Performance
CAPEX	Capital Expenditures
PSA	Pressure Swing Adsorption
MAE	Mean Absolute Error
CEPCI	Chemical Engineering Plant Cost Index
APEA	Aspen Process Economic Analyzer
MAPE	Mean Absolute Percentage Error
VLE	Vapor Liquid Equilibrium

Symbols

Symbol	Definition	Unit
p	pressure	[kPa]
R	Gas constant	$[J \cdot mol^{-1} \cdot K^{-1}]$

Symbol	Definition	Unit
V_m	Molar volume	[$m^3 \cdot mol^{-1}$]
a	Constant	[-]
b	Constant	[-]
I	Ice	[-]
L_{CO_2}	Liquid CO_2	[-]
L_w	Liquid water	[-]
x_i	Predicted value i	[-]
y_i	Reference value i	[-]
n_{tot}	Total amount of values	[-]
V	CO_2 vapor	[-]
H	Hydrate	[-]
h	Enthalpy	[J]
μ_{JT}	Joule-Thomson Coefficient	[-]
$C_{2024,NL}$	Capital cost in the Netherlands for 2024	[€]
$C_{2010,USGC}$	Capital cost on the United States Gulf Coast for 2010	[€]
LF_{NL}	Location factor for the Netherlands	[-]
$C_{equipment}$	Capital cost of liquefaction equipment	[€]
S	Unit for size	[-]
n	Exponent for unit of size	[-]
$m_{pressure\ vessel}$	Weight of pressure vessel	[kg]
d	Diameter of pressure vessel	[m]
h	Height of pressure vessel	[m]
t_{wall}	Wall thickness of pressure vessel	[m]
ρ_{cs}	Volumetric density of carbon steel	[$kg \cdot m^{-3}$]
$p_{separator}$	internal pressure of separator	[Pa]
S_{cs}	Maximum allowable stress for carbon steel	[Pa]
$O_{equipment}$	Operational cost of liquefaction equipment	[€]
P_{total}	Total compressor work	[kW]
c_{el}	Electricity cost per kWh	[€ $\cdot$ kWh^{-1}]
C_{buffer}	Capital cost of buffer storage	[€]
$p_{shipping}$	Absolute shipping pressure	[kPa]
V_{buffer}	Volume capacity of buffer storage	[m^3]
O_{buffer}	Operational cost of buffer storage	[€]
$C_{loading\ facilities}$	Capital cost of loading facilities	[€]
M_{annual}	Annual shipping mass capacity	[kt $\cdot$ y^{-1}]
$O_{loading\ facilities}$	Operational cost of loading facilities	[€]
O_{fuel}	Operational cost for shipping fuel	[€]
s	Distance	[km]
M_{ship}	Ship mass capacity	[kt]
f	Fuel usage	[g $\cdot$ km^{-1} $\cdot$ t^{-1}]
c_{fuel}	Shipping fuel cost	[€ $\cdot$ t^{-1}]
C_{ship}	Capital cost of transport ship	[€]
O_{ship}	Operational cost of transport ship	[€]
D_{annual}	Annual days of ship usage	[d]
v	Ship speed	[km $\cdot$ h^{-1}]
$D_{loading}$	Days to load and offload the transport ship	[d]

Contents

1 Introduction

1.1. Background

The Intergovernmental Panel on Climate Change completed its First Assessment Report (FAR) in 1990, underlining the importance of climate change. The report was the most comprehensive scientific article produced to date and acted as a foundation to establish the United Nations Framework Convention on Climate Change (UNFCCC) [2]. This influential treaty is backed today by 198 parties, showing the realization of the dangers that come from human interference with the climate system and commitment to limiting the increase of greenhouse gases in the atmosphere [3]. From this treaty the Kyoto Protocol and later the Paris Agreement followed, the latter being the agreement which sets goals for the coming years. Based on this agreement, all European Union member states aim to have decreased their greenhouse gas emissions with 55 % by 2030, compared to the emissions in the year 1990, and become completely carbon neutral by 2050 [4]. These agreements show the necessity of greatly decreasing anthropogenic greenhouse gas emissions. The National Institute for Public Health and the Environment (RIVM) reported the Netherlands had decreased emissions by 35.6 % in 2023, this is a significant improvement but it is not enough yet [5]. According to the Netherlands Environmental Assessment Agency (PBL) the Netherlands is on track for a reduction in greenhouse gases between 44 and 52 % in 2030, based on the current planned projects [6]. Furthermore, the report states that the probability of achieving the 55 % reduction goal is less than 5 %. This means that the efforts to minimize the greenhouse gas emissions will have to be intensified. Tata Steel Netherlands follows these climate goals, and has set a goal of an emission reduction of 40 % by 2030 in its recent Environmental Effect Report [7]. This is not an easy achievement, steelmaking without carbon dioxide production is not possible using the current Blast Furnace plants. Since this technology has been almost perfected, with a reduction of 30 % in carbon dioxide production compared to 1990 [8], additional significant reduction of carbon dioxide production is not possible in these plants. As a result, Tata Steel Netherlands will move to a Direct Reduction plant [7]. This kind of plant is able to directly reduce iron ore using natural gas or additional hydrogen as input instead of coke, a coal product. Most direct reduction plants use natural gas as an input to produce syngas, a mix of CO and H_2, through a reformer [9]. This syngas is then fed into the reactor to reduce the iron ore. An alternative are zero reformer plants which directly inject the natural gas into the reactor where it will subsequently react into CO and H_2. These zero reformer plants could also be directly fed with H_2 to reduce its environmental impact. A direct reduction reactor is a closed-loop system in which the majority of the reactor top-gas is recycled back into the reactor. The CO_2 in this recycle stream is separated through an amine based absorption unit which produces relatively high purity CO_2. Therefore, the Direct Reduction plants are the way to a carbon neutral future [10]. Additionally, Tata Steel Netherlands has also invested significantly in the HIsarna ironmaking technology [8]. This technology can use biomass-derived carbon sources like biochar to reduce the iron ore and the process produces at least 20 % less carbon dioxide than a conventional blast furnace [11]. By combining this technology with Carbon Capture and Storage technologies, an emission reduction of 80 % is reported. Therefore, it is also a viable option for future steelmaking which should be further explored.

1.2. Objectives

As explained in the background section, Tata Steel Netherlands has serious ambitions to implement Carbon Capture and Storage in its steelmaking process. This thesis will explore the possibilities to implement this technology within the ironmaking processes of Tata Steel. Earlier research has explored the possibilities of CO_2 separation from blast furnace off-gases [12]. The main interest of this research lays in finding an efficient trade off between the level the carbon dioxide stream is purified to and subsequent transport conditions and routes. The main research question can be formulated as follows.

> What are the energy requirements and costs of transporting CO_2-rich mixtures derived from steelworks off-gases?

A literature review will first be conducted to find information about different aspects which need to be explored to answer the main research question. The following aspects will be explored in the literature study.

- What are the off-gas compositions of various steelmaking processes?
- Which requirements are set on CO_2 stream purity and composition by comparable initiatives?
- Which transportation and storage methods are employed in CCS projects?
- How can the thermodynamic properties of CO_2-rich mixtures be determined?
- How are the thermodynamic properties of CO_2-rich streams affected by impurities introduced by capture from steelmaking processes?

1.3. Search Plan

The literature review is mainly conducted with the Scopus database to have a broad coverage of scientific publications. Various keywords were used to find useful articles, examples of these keywords are CCS, pipeline, liquefaction, CCS mixtures, impurities, steelmaking, thermodynamic models and experimental. Based on the objective, the results were sorted by most citations to find fundamental research or sorted by newest to find state-of-the-art developments. Articles found through this were used as a basis to find other related research in their bibliographies that was not found using the Scopus database. Additionally, a conventional search engine was used to identify public information about CCS projects that are currently in development.

2

Literature Review

2.1. Off-gases from Steelmaking

This section reviews the different process options and the off-gases that are produced by the different steelmaking routes shown in Figure 2.1 [13]. Iron ore can be reduced in and smelted in a blast furnace or HIsarna reactor to produce pig iron, this pig iron is high in carbon content and cannot be classified as steel yet. An alternative is producing Direct Reduced Iron (DRI) through a direct reduction process, this also reduces the iron ore but does not smelt it. The pig iron or DRI is subsequently transformed to liquid steel in a Basic Oxygen Furnace (BOF) or Electric Arc Furnace (EAF). These furnaces smelt the pig iron or DRI and subsequently remove impurities and carbon through injecting pure oxygen which will bind with these components and remove them in gaseous form. The last steps in steel production can be casting, rolling and finishing to produce varying steel products.

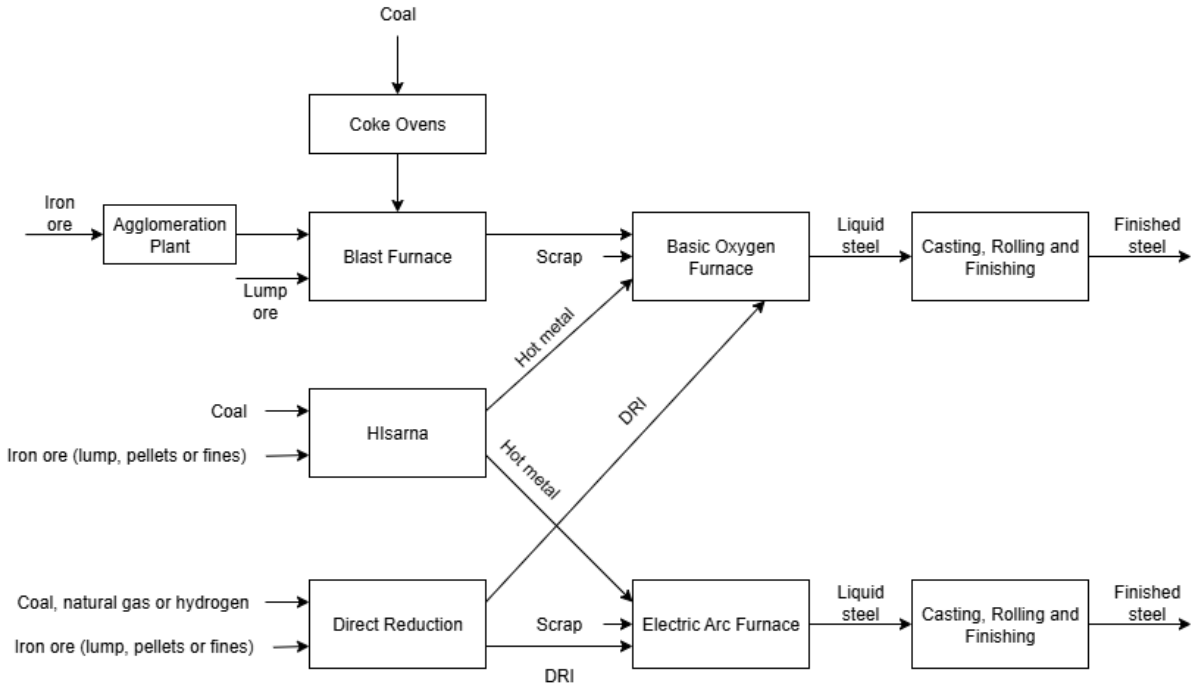

Figure 2.1: Diagram illustrating possible steel making routes based on blast furnace, HIsarna or direct reduction ironmaking and subsequent steelmaking with an Basic Oxygen Furnace or Electric Arc Furnace. Created from Carpenter [13].

2.1.1. Agglomeration Plant

A blast furnace needs a ferrous burden of a certain minimum size to allow for favorable burden permeability [14]. Lump ores, pieces of 6 to 25 mm, fit this criterion but are getting increasingly scarce and generally have poorer properties as a blast furnace burden. The smaller pieces of ore are called fines. These fines can be sintered into larger lumps, or processed into pellets through an agglomeration plant. These larger pieces can be used in the furnace without creating gas flow problems but do create an extra process step and CO_2 production. The largest share of CO_2 production in these plants come from the heating that is needed in these processes [13]. A gas powered sintering plant emits 272 kg CO_2 per ton hot metal and a gas powered pellet plant emits 43 kg CO_2 per ton hot metal [15].

2.1.2. Coke Oven Plant

A blast furnace also needs coke in addition to iron ore. The coke has a few important functions like providing structure to the burden, generate heat, generate reducing gases, provide carbon for carburization of the hot metal and act as a filter for soot and dust [14]. Coke is a coal product that is obtained by heating it in absence of air to drive off the water vapor and volatile components. This leaves a hard structure that only consists of carbon and minerals. The hardened product can fulfill the requirements for a stable blast furnace reaction. The gas that is produced in this oven is called coke oven gas and its composition is highly dependent on the origin of the utilized coal. Table 2.1 shows the composition ranges [13].

Table 2.1: COG main components volume fraction, excluding 4-12 g/m^3 H_2S, 20-30 g/m^3 benzene, toluene, and xylene, 6-8 g/m^3 ammonia, polycyclic aromatic hydrocarbons, other hydrocarbons, oxygen, nitrogen, nitrogen compounds, other sulfur compounds and water vapor [13]

Component	**Volume** $\%$
H_2	39-65
CH_4	20-42
C_xH_y	2-8.5
CO	4-7
CO_2	1-3

2.1.3. Blast Furnace Ironmaking

Blast furnaces ironmaking is the most common production method of pig iron [14]. The blast furnace is a tall furnace that is a type of counter-current reactor. It is filled with alternating layers of iron ore and coke, called the burden, from the top while at the bottom hot gas is injected that moves up in the reactor. This hot blast gasifies the coke or other injected fuel creating CO and melts the iron ore creating pig iron. The counter-current flow allows the burden to dry and slowly heat up while the ferrous burden is reduced to iron. This reduction process is possible due to the CO that is produced by gasifying the coke, it removes the oxygen from the iron ore and produces CO_2 in the reaction. Table 2.2 shows the typical composition of the gas that leaves the reactor at the top, called top gas. The N_2 comes from the air that is injected and not all the CO reacts so it is also still present next to CO_2. Lastly, there is also H_2 present that forms in the blast furnace from hydrocarbons and moisture.

Table 2.2: BFG main components volume fraction, excluding sulfur and cyanide compounds [13]

Component	**Volume** $\%$
N_2	50-55
CO	20-28
CO_2	17-25
H_2	1-5

2.1.4. Smelting Reduction Ironmaking

HIsarna is a type of smelting reduction process developed by Tata Steel in the ULCOS (Ultra Low CO_2 Steelmaking) project [16]. The reactor has a cyclone at the top where iron ore and oxygen are injected, here the iron ore is prereduced and liquefied. The liquid iron droplets are transported by gravity into a smelter that is placed directly under the cyclone, this removes the need for intermediate handling or transport. Coal is injected and subsequently gasified in this smelter to fully reduce the iron before it is tapped. While the blast furnace process is a highly mature technology, the HIsarna process provides an alternative because of the wider accepted raw material quality range and the ability of directly using coal instead of needing a coke production plant. Furthermore, the cyclone fully combusts the smelter off-gas. This means that the fuel is used more efficiently and therefore the carbon emissions are lower compared to the blast furnace route. Table 2.3 shows the predicted off-gas composition of a industrial-scale HIsarna plant[17].

Table 2.3: Predicted gas composition of an industrial-scale HIsarna plant with H_2O and normalized without H_2O [17]

Component	Volume fraction	Dry volume fraction
CO_2	50.3 %	64.5 %
H_2O	22.0 %	0.0 %
N_2	10.3 %	13.2 %
CO	15.7 %	20.1 %
H_2	1.7 %	2.2 %

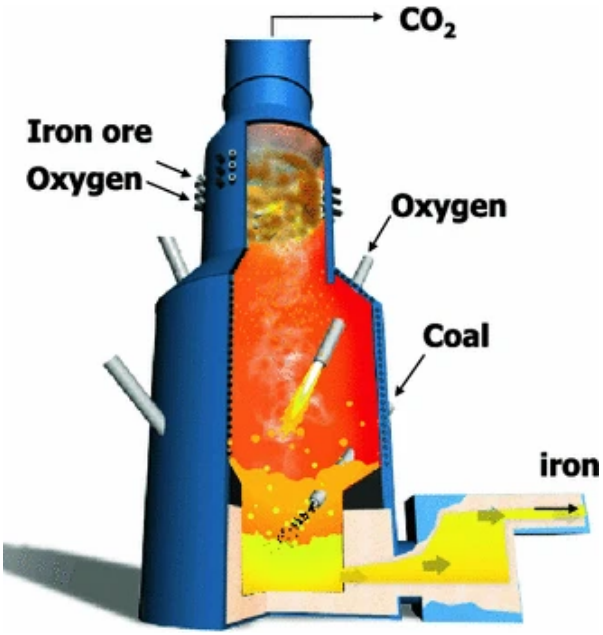

Figure 2.2: HIsarna reactor displaying the cyclone at the top where the iron ore is injected with oxygen to reduce the iron ore and where the CO_2-rich top gas leaves the reactor. Furthermore it shows the smelt bath at the bottom where coal or biochar is injected and the molten iron exits the reactor. Reproduced with permission from Springer Nature, from [16].

2.1.5. Direct Reduction Ironmaking

Direct Reduction (DR) is another type of iron production. The iron ore is not smelted in a DR process, instead the reduction of iron oxides to pure iron takes place while the ore remains in the solid phase. There are a number of different direct reduction processes possible, these processes can be classified based on the type of reactor utilized [13]. A possible option is a shaft furnace direct reduction plant. Specifically the HyL Zero Reformer (ZR) process from ENERGIRON. This process distinguishes itself with the fact that it uses natural gas as a reducing gas instead of syngas. This syngas is produced using an external reformer in other processes but the ZR technology removes this step. This simplifies the process but, more importantly, the carbon content in the direct reduced iron will increase due to using

methane as a reducing gas. This higher carbon content steel can be preferred to aid further processing. Figure 2.3 showcases the process flow diagram of the ENERGIRON ZR process. There are two product off-gas streams, numbers 30 and 31 representing the flue gas of the reducing gas heater and the almost pure CO_2 stream coming from the separation unit [10]. Table 2.4 gives the composition of the separated CO_2 stream coming from the integrated amine absorber in a ENERGIRON III reactor [9]. This kind of separator is highly selective and therefore produces a high CO_2 purity.

Table 2.4: ENERGIRON III direct reduction reactor off-gas composition with H_2O and normalized without H_2O, as reported in [9]

Component	Volume fraction	Dry volume fraction
CO_2	94.33 %	99.7 %
H_2O	5.4 %	0.0 %
H_2	1600 ppm	1690 ppm
CO	400 ppm	425 ppm

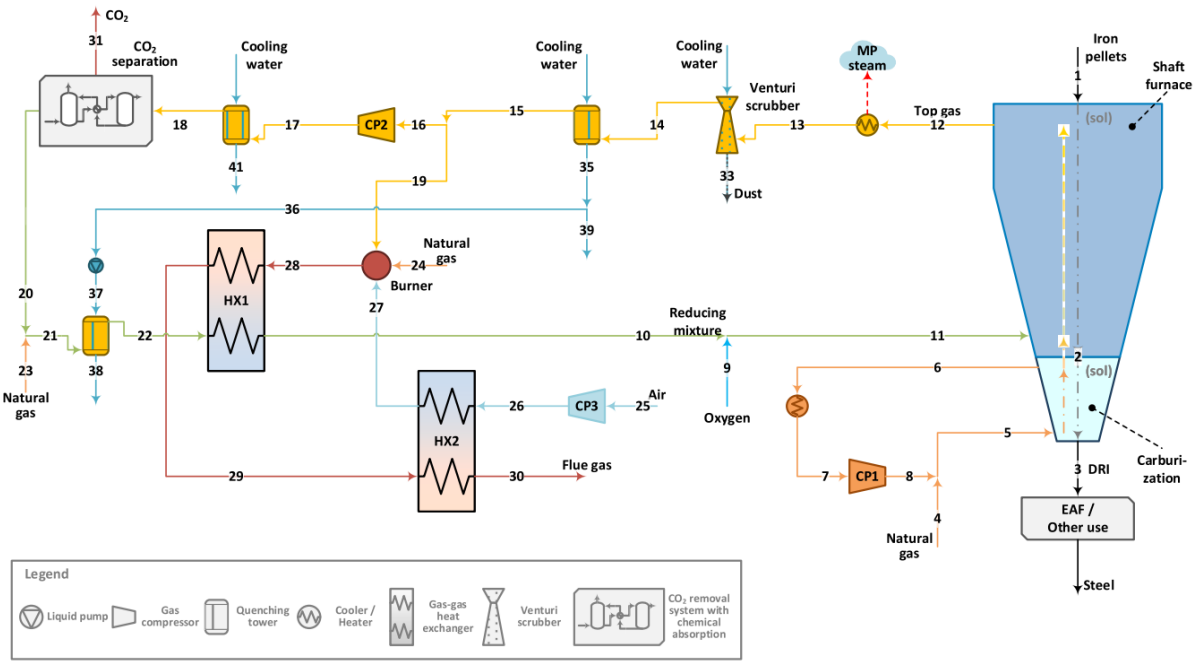

Figure 2.3: Simplified process flow diagram of ENERGIRON ZR Direct Reduction process. Reprinted from Applied Energy, Vol 376, Roberto Scaccabarozzi; Chiara Artini; Stefano Campanari; Maurizio Spinelli, Techno-Economic and CO2 Emissions Analysis of the Molten Carbonate Fuel Cell Integration in a DRI Production Plant for the Decarbonization of the Steel Industry, 124264, Copyright 2024, with permission from Elsevier [10].

2.1.6. Basic Oxygen Furnace

The Basic Oxygen Furnace (BOF) is used to produce steel from the hot metal coming from a blast furnace, direct reduction plant or smelting reduction plant and additional scrap metal can be added [13]. Steel is produced by injecting oxygen into the molten metal, oxidizing with the carbon, silicon and other elements. This process lowers the carbon content until it can be called steel. Additionally, various impurities will be removed from the hot metal and form a slag by adding fluxes like limestone and dolomite. The oxidizing of carbon will form CO and CO_2 and will form the main components of the off-gas, as shown in Table 2.5.

Table 2.5: Basic Oxygen Furnace off-gas composition, as reported in [13]

Component	Volume %
CO	55-80
CO_2	10-18
H_2	2-10
N_2	8-26

2.1.7. Electric Arc Furnace

Electric Arc Furnaces (EAF) are used to remove carbon, silicon and other impurities from iron sources, comparable to a BOF [13]. EAFs are optimized for solid charge materials and are traditionally used to process scrap metal but can also be used to process DRI and hot metal. The feed is melted through the use of carbon electrodes that can create arcs of electricity, additionally oxyfuel burners and O_2 lances may be used. Table 2.6 shows the ranges of EAF off-gas composition as reported in [18]. The ranges are relatively large because of the different iron sources that can be used in EAFs.

Table 2.6: Electric Arc Furnace off-gas composition, as reported in [18]

Component	Volume %
CO	20-50
CO_2	10-30
H_2	0-40
H_2O	10-20
N_2	20-50

2.2. Main European Carbon Storage Projects

Using the interactive map created by the International Organization of Oil and Gas Producers (IOGP) all Carbon Capture, Utilization and Storage (CCUS) projects in Europe could be identified [19]. This section covers the details of three carbon storage projects, the projects are selected based on their operational or advanced development status and yearly capacity bigger than 1 Mt CO_2. The Sleipner project meets these criteria but was excluded from this review because of the in-situ CO_2 storage and therefore lack of transportation logistics which are of interest for this project [20].

2.2.1. Porthos

Porthos is a carbon storage project located in the port of Rotterdam [21]. The CO_2 sources are four Steam Methane Reforming (SMR) hydrogen production plants located in the port [22]. The Porthos system consists of an onshore pipeline that connects several CO_2 plants in the port of Rotterdam with a compressor station located near the coast. This compressor station is connected to an offshore platform at the reservoir location through an offshore pipeline. The CO_2 rich stream is then injected from the platform into a depleted gas field with a total capacity of 37.6 Mt CO_2. The CO_2 producing plants are required to deliver the CO_2 stream at an pressure between 24 and 35 bar (g) [23]. Because this pressure is higher than the initial reservoir pressure, the compressor station is first in a bypass mode. This means that the CO_2 transport will initially take place in the gas phase. The compressor station is started at a maximum of 30 bar (g) and the CO_2 stream will be delivered in the gas phase while building up the pressure in the injection well and pipeline over time. From 75 bar (g), the transport will be in the dense phase and the injection pressure is further increased over time until a maximum of 135 bar (g). The maximum annual pump capacity is set at 9.3 Mt CO_2, the pipeline is also designed for this annual capacity.

2.2.2. Northern Endurance

The Northern Endurance project can be compared to the Porthos project, the main difference is that the CO_2 will be stored in a saline aquifer instead of a depleted gas field [24]. A saline aquifer is an underground rock formation that contains brine, in which the CO_2 can be injected. The other aspects of the system are the same as Porthos, an onshore pipeline will connect multiple CO_2 sources to

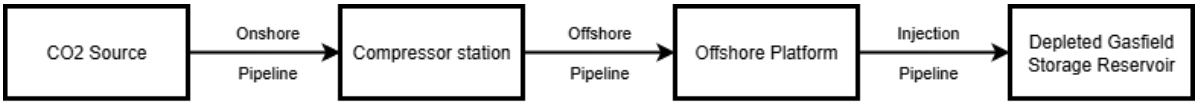

Figure 2.4: Block diagram of Porthos project logistics which consists of transporting CO_2 through an onshore pipeline to a compressor station and subsequent transportation through an offshore pipeline to an offshore platform which injects the CO_2 into a depleted gasfield storage reservoir.

a compressor station from which the CO_2 is transported through an offshore pipeline to an offshore platform which injects the CO_2 in the reservoir. The advantage of the Endurance reservoir, as shown in Table 2.7, is its much larger capacity of 450 Mt CO_2 compared to the 37.6 Mt CO_2 that can be stored in the depleted gas field used in the Porthos project. The initial three CO_2 sources will be an gas-fired power plant and two SMR hydrogen production plants [25]. The initial pipeline will be constructed from the Teesside area, an additional pipeline is also proposed to connect the Humber area with the offshore injection platform but this expansion is not included in the capacities shown in Table 2.7. The compressor station will support a maximum annual capacity of 4 Mt CO_2 in the initial stages but the pipeline will be designed and built for a maximum annual capacity of 10 Mt to allow for further scale increases. The offshore pipeline operating pressure will always be higher than 110 bar (g) to facilitate dense phase transport and will increase up to 195 bar (g) when the reservoir nears its full capacity. The operating temperature will range from 40 °C near the compressor station to the ambient seawater temperature of 10 to 16 °C [24].

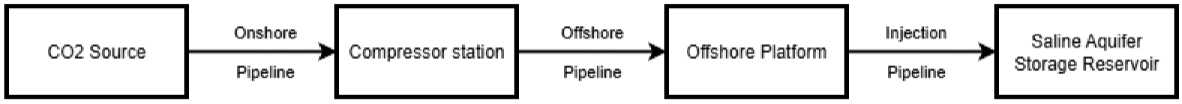

Figure 2.5: Block diagram of Northern Endurance project logistics which consists of transporting CO_2 through an onshore pipeline to a compressor station and subsequent transportation through an offshore pipeline to an offshore platform which injects the CO_2 into a saline aquifer storage reservoir.

2.2.3. Northern Lights

The Northern Lights project differentiates itself because it accepts CO_2 streams transported by ship to the injection site. CO_2 streams can be accepted from a wide range of third parties this way [26]. The injection site in Øygarden consists of a jetty where specially made CO_2 transport ships can dock and unload the CO_2 into onshore storage tanks. These storage tanks act as a buffer from which the CO_2 is subsequently injected into an offshore saline aquifer. The CO_2 is transported in the liquid phase at a pressure of 15 bar (g) and temperature of -26 °C in specially made ships that can hold up to 8000 tons of CO_2 at these conditions. The onshore storage conditions lie between 13 and 18 bar (g) with a temperature between -30 and -26 °C. The subsequent transport to the injection well takes place at an elevated pressure to ensure single-phase liquid transport in the uninsulated pipeline [27]. The pipeline is designed for a maximum annual capacity of 5 Mt CO_2 while the compressor station allows for 1.5 Mt per year, allowing future scale increase like for the Northern Endurance project.

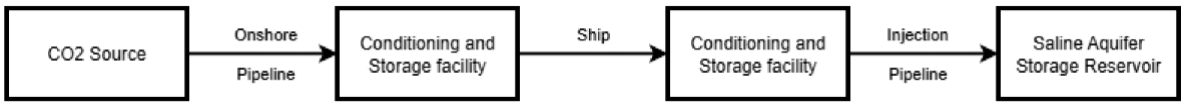

Figure 2.6: Block diagram of Northern Lights project logistics which consists of transporting CO_2 through an onshore pipeline to a condition and storage facility before the CO_2 is subsequently transported with a ship to a conditioning and storage facility at another location from which the CO_2 is injected into a saline aquifer storage reservoir.

2.2.4. Stream Specifications

All three selected projects provide strict stream specifications so that the CO_2-rich streams show the desired phase behavior during transport and storage. Furthermore, certain impurities are also restricted to prevent corrosion and blockage issues or, in the case of toxic compounds, to comply with the relevant regulations. Table 2.8 compares the different quality requirements per project. Furthermore, the operational and safety considerations for each component are listed. It can be noted that Porthos and Northern Endurance have set similar requirements but Northern Lights has significantly stricter requirements. This difference comes from the transportation conditions as CO_2 needs to be liquefied at lower pressures for ship transport. Sections 2.6.1 and 2.6.2 explain more about these transport methods.

2.2.5. Summary of Selected CCS Projects

Table 2.7 shows a summary of the three projects which are discussed in this section. It compares a number of important points like the total volume capacity that can be stored, the yearly maximum pipeline capacity based on pipeline diameter and yearly maximum capacity of the pump and compressor station. Furthermore, the storage and transportation methods are compared in combination with the pressure and temperature ranges during pipeline or ship transport.

Table 2.7: Overview of transport conditions, capacity, CO_2 sources and location for the Porthos, Northern Endurance and Northern Lights CCS projects, as discussed in Section 2.2.

	Porthos [21]	**Northern Endurance [24] [25]**	**Northern Lights [27]**
Location	Rotterdam, NL	Teesside, UK	Øygarden, NO
Transport	Pipeline	Pipeline	Ship and Pipeline
Storage	Depleted Gas Field	Saline Aquifer	Saline Aquifer
Volume capacity	37.6 Mt CO_2	450 Mt CO_2	> 100 Mt CO_2
Max. pipeline capacity	9.3 Mt/y CO_2	10 Mt/y CO_2	5 Mt/y CO_2
Max. pump capacity	9.3 Mt/y CO_2	4 Mt/y CO_2	1.5 Mt/y CO_2
Pipeline Pressure	24 to 135 bar (g)	110 to 195 bar (g)	> Critical Pressure
Pipeline Temperature	-	40 °C to 10 °C	-
Ship Storage Pressure	-	-	15 bar (g)
Ship Storage Temperature	-	-	-26 °C
CO_2 Sources	SMR Plants	Gas-fired power plant SMR Plants	Biomass power plant Fertilizer plant Cement plant

2.3. Impurity Sources and Considerations

It is important to understand why certain restrictions are placed on the impurities present in received CO_2 streams and which impurities could be present based on the CO_2 source. Table 2.9 gives an overview of impurities that could be present based on the CO_2 source, it also gives a summary of possible effects these impurities have on gas treatment. The identified sources are combustion off-gas, waste or biomass power plants, hydrogen or ammonia production plants and coal gasification, respectively [31]. Furthermore, this table also compares the possible effects which each component can have if the volume levels are too high. The effects can be divided into separate liquid phase formation, solid formation, phase behavior impact, corrosion issues and toxicity. The formation of a separate liquid or solid phase can damage equipment [32]. Furthermore, like in the case of H_2O, corrosion can occur when certain components get absorbed into the separate liquid water phase. Lastly, toxicity can also be an issue. It can occur in certain cases that equipment should be vented, toxic components could then harm surrounding people or the environment and should therefore also be limited to safe levels [33].

Table 2.8: Maximum allowable impurity content and minimum CO_2 volume percentage for the Porthos, Northern Endurance and Northern Lights project, grouped as in [28].

Component	Porthos [23]	Northern Endurance [29]	Northern Lights [30]
CO_2	$\geq$ 95 vol%	$\geq$ 95.14 vol%	> 99.81 vol%
H_2O	$\leq$ 70 ppm	$\leq$ 50 ppm	$\leq$ 30 ppm
Inerts			
H_2	$\leq$ 0.75 vol%	$\leq$ 0.75 vol%	$\leq$ 50 ppm
N_2	$\leq$ 2.4 vol%	Comb. $\leq$ 4 vol%	$\leq$ 50 ppm
Ar	$\leq$ 0.4 vol%	Comb. $\leq$ 4 vol%	$\leq$ 100 ppm
CH_4	$\leq$ 1 vol%	Comb. $\leq$ 4 vol%	$\leq$ 100 ppm
C_2H_6	–	Comb. $\leq$ 4 vol%	$\leq$ 75 ppm
O_2	$\leq$ 40 ppm	$\leq$ 10 ppm	$\leq$ 10 ppm
CO	$\leq$ 750 ppm	$\leq$ 1000 ppm	$\leq$ 100 ppm
Sulfur and acid gases			
S compounds	$\leq$ 20 ppm	$\leq$ 10 ppm	$\leq$ 10 ppm
H_2S	$\leq$ 5 ppm	$\leq$ 5 ppm	$\leq$ 9 ppm
NO_x	$\leq$ 5 ppm	$\leq$ 5 ppm	$\leq$ 1.5 ppm
COOH/amide compounds	$\leq$ 1 ppm	–	–
Volatile organic components			
Amines	$\leq$ 1 ppm	$\leq$ 1 ppm	$\leq$ 10 ppm
VOC [i]	$\leq$ 10 ppm	–	$\leq$ 10 ppm
Aldehydes	$\leq$ 10 ppm	Formald. $\leq$ 20 ppm Acetald. $\leq$ 20 ppm	Formald. $\leq$ 20 ppm Acetald. $\leq$ 20 ppm
Ethanol	$\leq$ 20 ppm	–	$\leq$ 30 ppm
Methanol	$\leq$ 620 ppm	–	$\leq$ 30 ppm
HCN	$\leq$ 2 ppm	–	$\leq$ 1 ppm
NH_3	$\leq$ 3 ppm	$\leq$ 10 ppm	$\leq$ 10 ppm
P compounds	$\leq$ 1 ppm	–	–
Heavies			
Glycols	Dew point spec.	$\leq$ 1 ppm	MEG $\leq$ 0.005 ppm TEG not allowed
Aliphatic HC (C_{2+})	$\leq$ 1200 ppm	–	$\leq$ 1100 ppm
BTEX	$\leq$ 0.1 ppm	–	$\leq$ 0.5 ppm
Heavy metals			
Hg	–	$\leq$ 0.0025 ppm	$\leq$ 0.0003 ppm
Cd	–	$\leq$ 0.005 ppm	Comb. $\leq$ 0.03 ppm
Tl	–	$\leq$ 0.012 ppm	Comb. $\leq$ 0.03 ppm
Solids			
Solids	–	–	$\leq$ 1 μm
Note i: Excluding methane, aliphatic hydrocarbons, methanol, ethanol and aldehydes.			

2.4. Thermodynamic Models

A thermodynamic model for predicting phase equilibrium, density, thermal properties, hydrate formation and transport properties is necessary to design and size CCS equipment [38]. Correctly predicting phase equilibria, water dropout and hydrate formation is vital for preventing equipment damage. Other parameters like density, thermal and transport properties are needed to correctly size equipment and estimate energy requirements. The applicability of different thermodynamic models needs to be identified to produce reliable estimations. Table 2.10 compares cubic, GERG-2008 and PC-SAFT EoS applicability for different impurities in CO_2 streams. Section 2.4.1, 2.4.2 and 2.4.3 explain the differences between these models.

Table 2.9: Overview of possible effects and sources of components specified in the stream specifications of Table 2.8. CO_2 sources A to D correspond to combustion, waste or biomass power plant, hydrogen or ammonia plant and coal gasification plant respectively. $\surd$ means impurity is present in source, X means no presence and - indicates no mention in the source.

Components	**Presence [31]**				**Possible effects**
	A	B	C	D	
H_2O	-	-	-	-	Liquid or solid formation [32]
Inerts					
H_2	-	-	-	-	Phase behavior [32]
N_2	-	-	-	-	Phase behavior [32]
Ar	-	-	-	-	Phase behavior [32]
CH_4	-	-	-	-	Phase behavior [32]
C_2H_6	-	-	-	-	Phase behavior [32]
O_2	-	-	-	-	Phase behavior [32]
CO	$\surd$	$\surd$	$\surd$	$\surd$	Toxicity and stress corrosion cracking [34] [32]
Sulfur and acid gases					
S compounds	$\surd$	$\surd$	$\surd$	$\surd$	Corrosion [35]
H_2S	$\surd$	$\surd$	$\surd$	$\surd$	Corrosion and toxicity[36]
NO_x	$\surd$	$\surd$	$\surd$	$\surd$	Corrosion [35]
COOH and amide compounds	-	-	-	-	Corrosion [35]
Volatile organic components					
Amines	$\surd$	X	$\surd$	X	Separate phase formation [37]
VOC	$\surd$	$\surd$	$\surd$	$\surd$	Toxicity and phase behavior [33]
Aldehydes	$\surd$	$\surd$	$\surd$	$\surd$	Corrosion [34]
Ethanol	$\surd$	$\surd$	$\surd$	$\surd$	Water dropout [34]
Methanol	$\surd$	$\surd$	X	$\surd$	Water dropout [34]
HCN	$\surd$	X	X	$\surd$	Toxicity [33]
NH_3	-	-	-	-	Corrosion and can form solids with CO_2 [34]
P compounds	X	X	$\surd$	$\surd$	Toxicity [33]
Heavies					
Glycols	-	-	-	-	Water dropout [34]
Aliphatic HC (C_{2+})	$\surd$	$\surd$	$\surd$	$\surd$	Phase behavior [32]
BTEX	$\surd$	$\surd$	$\surd$	$\surd$	Toxicity and phase behavior [33] [32]
Heavy metals					
Hg	$\surd$	X	X	$\surd$	Toxicity and equipment damage [33]
Cd	-	-	-	-	Toxicity [33]
Tl	-	-	-	-	Toxicity [33]
Solids					
Solids	-	-	-	-	Equipment damage and blockage [33]

2.4.1. Cubic Equation of State

Cubic Equations of State (EoS) like the Van der Waals equation are an improvement on the ideal gas law [40]. The Van der Waals equation is an historically significant equation which improved the ideal gas law by removing two assumptions. The first removed assumption was that molecules occupy a negligible volume compared to the total gas volume, the second one is that these molecules experience negligible attractive and repelling forces. Removing these assumptions introduced the additions shown in Equation 2.2. The Van der Waals equation was historically significant but was later improved through the addition of mixing rules in the Redlich-Kwong EoS [39]. These mixing rules use Binary Interaction Parameters (BIPs) which can be tuned to experimental data, ensuring a good fit between the models prediction and experimental measurements. This model is also further improved through various iterations to overcome inherent inaccuracies stemming from non-ideal systems. Two such improved EoS models that are frequently used in industrial applications are the Soave-Redlich-Kwong (SRK) and Peng-Robinson (PR) EoS.

Table 2.10: EoS capability in the modeling range of impurities. Y means yes, N means no and IN means insufficient data. C means caution as low accuracies, absolute average deviation larger than 5% for phase prediction, thermophysical properties or both, have been noted in literature [39].

Main Impurity	**Cubic EoS**	**GERG-2008**	**PC-SAFT**
H_2O	C	Y	C
H_2S	Y	Y	Y
SO_2	Y	N	IN
O_2	C	C	C
H_2	C	C	C
N_2	C	Y	C
Ar	Y	Y	C
CO	Y	C	C
NO_x (NO and NO_2)	IN	N	IN
Methane, Ethane, Propane	C	Y	C
Benzene, Toluene, Ethyl Benzene, Xylene	C	N	C
Minor Impurity			
Amines (e.g., MDEA, Piperazine, MEA, DEA)	C	N	IN
Methanol/Ethanol	C	N	IN
MEG/TEG	C	N	IN
NH_3	C	N	IN
Trace Impurity			
Hg	C	N	IN
HCN	C	N	IN
COS	C	N	IN
Nitrosamines	C	N	IN

Cubic EoS are good at predicting close to ideal mixtures at relatively low computation requirements but do not handle chemical associations and polar components well. This is a problem since the CO_2-rich mixtures coming from the steel industry include polar components like water, carbon monoxide and NO_x gases. The Cubic Plus Association (CPA) EoS manages polar components through the use of association theories.

$$p = \frac{R \cdot T}{V_m} \tag{2.1}$$

$$p = \frac{R \cdot T}{V_m - b} - \frac{a}{V_m^2} \tag{2.2}$$

2.4.2. Helmholtz Energy Approximation Equation of State

An alternative to cubic EoS are Helmholtz energy approximation models like GERG-2008. This model uses reference equations for pure components and combines these with Binary Interaction Parameters, BIPs, to determine the behavior of mixtures with high accuracy [39]. The BIPs in the GERG-2008 model are tuned for each combination of the 21 included components. The model is specifically designed for natural gas mixtures and therefore has a high accuracy for these fluids, but it does not perform well for mixtures that include water. It has been reported that the approximated solubility of CO_2 can be off as much as 50% [41].

2.4.3. Statistical Models

Statistical Associating Fluid Theory (SAFT) based models like PC-SAFT are an alternative to the aforementioned analytical models. These are complex equations, which describe the behavior of the system based on the repulsion, dispersion, association and solvation of molecules [38]. The models assume the molecules to be chains of hard spheres, each molecule can then be described by the number of segments, or hard spheres, the diameter of these segments and the energy per segment. These variables are regressed on experimental data so the applicability for CO_2-rich mixtures depends on available experimental data. Furthermore, the reliance on experimental data causes these models to be unsuitable beyond the used data range. It was also found that SAFT models are unable to accurately predict the critical point of CO_2 mixtures. In one study the critical point was estimated to be 5 K and 5 bar higher than predicted by a reliable EoS for a mixture with 3 vol% methane [42].

2.4.4. Molecular Simulation

In addition to the models mentioned in Table 2.10, phase predictions and thermophysical properties can also be determined through molecular simulations like Molecular Dynamics (MD) or Monte Carlo (MC) simulations [43]. Molecular Dynamics simulations are used to simulate the motion of a number of molecules within a certain volume [44]. This method can be used to determine physical properties both in equilibrium and nonequilibrium by simulating how the molecules move and interact with each other. Monte Carlo simulations on the other hand are mainly used to simulate equilibrium situations because the MC method does not use equations of motion. The MC method is a statistical sampling method where random trial moves are made and selected based on probability, creating averages. In Raju et al. [43], a study into CCS mixtures, MC is used to determine phase equilibria and thermodynamic properties such as density, isothermal compressibility, thermal expansion coefficient, heat capacities, Joule-Thomson coefficient and speed of sound. MD, on the other hand, was used to determine the viscosity of different mixtures but also densities to check with MC.

2.5. Phase Behavior of CO_2-rich Mixtures

2.5.1. Phase Diagram of Pure Carbon Dioxide

Figure 2.7 shows the phase diagram of pure carbon dioxide. This figure illustrates five different phases at which carbon dioxide can exist. Namely as a solid, liquid, gas, dense or supercritical fluid [45]. The lines between these phases are characterized by the triple and critical points. The triple point marks the temperature and pressure at which the solid, liquid and gas phases meet, it is found at 5.2 bar (a) and 217 K for pure CO_2 [46]. The high triple point pressure of 5.2 bar (a) signifies that CO_2 does not exist as a liquid at atmospheric pressure. The triple point is also of significance to understand at which temperature liquid CO_2 will freeze. It is important to accurately predict this behavior since solid CO_2 can damage equipment. The critical point can also be identified in the figure, this point marks the temperature and pressure from where the fluid becomes supercritical. There is no distinction between the liquid and gaseous phase in this region. That means the fluid in this region has the volumetric density of a liquid, but the viscosity of a gas. The critical point for pure CO_2 is at 7.38 MPa and 304 K. The dense phase is the region above the critical pressure but below the critical temperature. The fluid will have the volumetric density of a liquid but a viscosity comparable to that of the gaseous phase, just like a supercritical phase. The difference is that the dense phase is a highly compressed fluid while the supercritical phase is a distinct state of matter.

2.5.2. Effects of Impurities

In practice, streams of captured CO_2 are not pure but contain various impurities depending on the CO_2 source and gas treatment steps. As mentioned in Section 2.2.4, certain restrictions are placed on the maximum content of these impurities. This could be due to transport and storage efficiency, operational considerations or health and safety issues [32]. The transport efficiency could for example be affected by non-condensable components like nitrogen and oxygen. Figure 2.8a and 2.8b show the effects of nitrogen and oxygen, the bubble point line will significantly increase due to these impurities. Therefore, the transport pressure needs to be increased to stay in the favorable liquid phase, this higher pressure will increase equipment and energy costs and therefore needs to be limited.

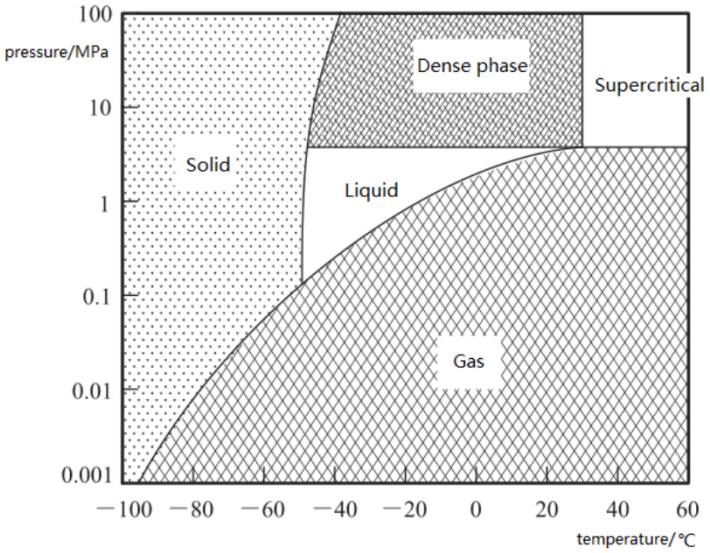

Figure 2.7: Phase diagram of pure carbon dioxide showing the solid, liquid, gas, dense and supercritical phase regions at a pressure range from 0.001 to 100 MPa and temperature range from 173 to 333 K. Reproduced from Wang, H., Chen, J. & Li, Q. (2019). A Review of Pipeline Transportation Technology of carbon dioxide, IOP Conference Series: Earth and Environmental Science, 310(3), 032033 [47]. © The Authors. Licensed under CC BY 3.0.

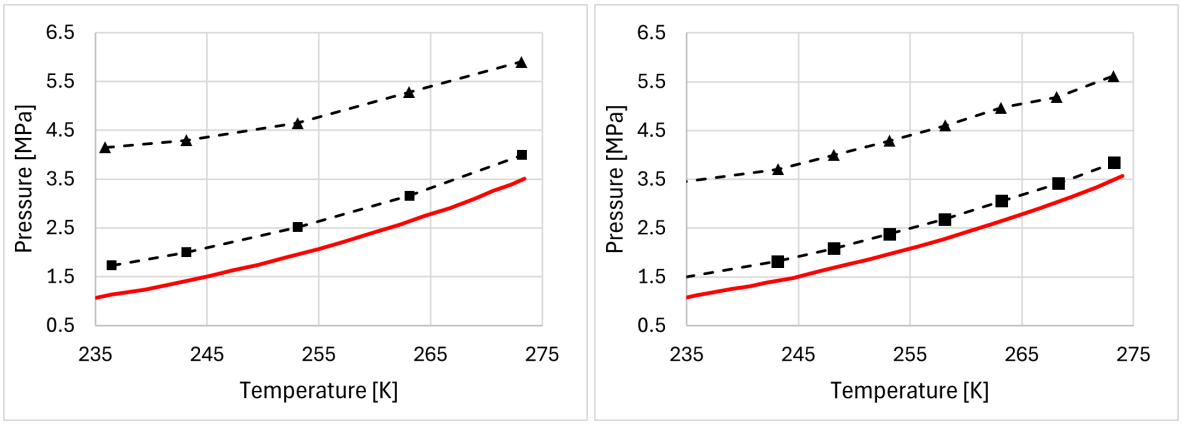

(a) Nitrogen **(b)** Oxygen

Figure 2.8: Effects of nitrogen, left, and oxygen, right, volume fraction on the bubble point line of a CO_2-rich mixture. The red line represent the bubble-point line for 100 vol% CO_2 determined with an equation of state. Square and triangular markers represents experimental data for 99 and 95 vol% CO_2 respectively. Recreated from [48].

Another issue could be H_2O content, Figure 2.9 shows the different phases that can occur when pure CO_2 is in contact with water. The separate water phase can occur as ice, liquid or hydrate, denoted as I, L_w and H respectively in this pressure and temperature range. CO_2 hydrates are crystalline H_2O structures which can trap CO_2 molecules, the hydrates can form problems at lower temperatures or during depressurization as the solids can damage equipment or plug pipelines [32]. The water can also be present as ice in the lower pressure and temperature range, which can cause the same operational problems as hydrates. The water will remain in the liquid phase at higher temperatures but this can lead to corrosion problems. This liquid phase can be highly corrosive by dissolved gas impurities like NO_2, SO_2 and H_2S or it can lead to sweet corrosion due to dissolved CO_2 [35]. This leads to higher equipment cost and operational cost due to a need for more frequent maintenance. Therefore both the content of water and these acid gases should be kept to a minimum. Figure 2.10 gives an illustration of the maximum water content before water dropout or hydrate formation occurs for a range of temperatures.

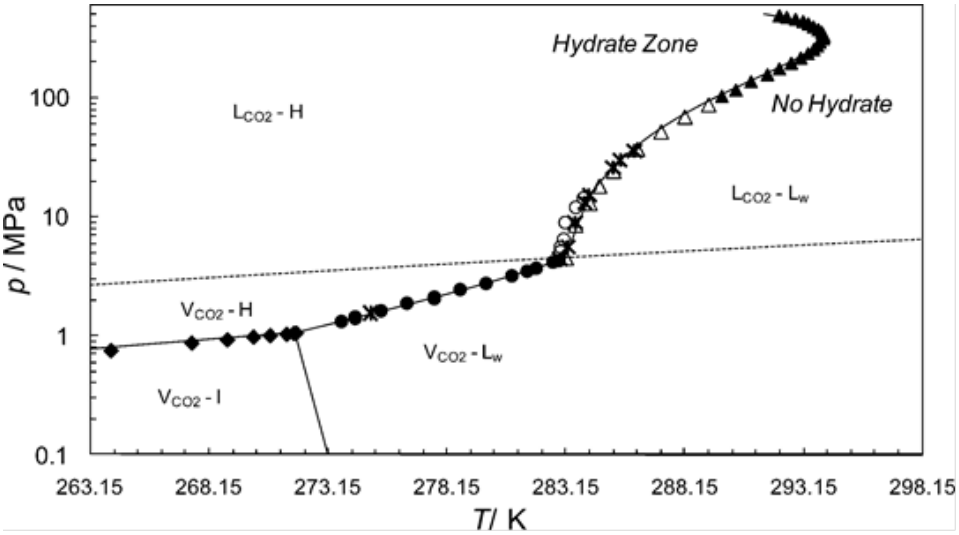

Figure 2.9: Pressure temperature diagram of CO_2 and water displaying the hydrate stability zone at a pressure range of 0.1 to 150 MPa and temperature range of 263 to 298 K. The black curve represents model predictions with the icons represent experimental data and the dashed line represents the bubble line of pure CO_2. The water is present as ice, I, liquid, L_w, or hydrate, H and the CO_2 is present as vapor V_{CO_2} or liquid L_{CO_2}. Reproduced with permission from [49]. Copyright 2014 American Chemical Society.

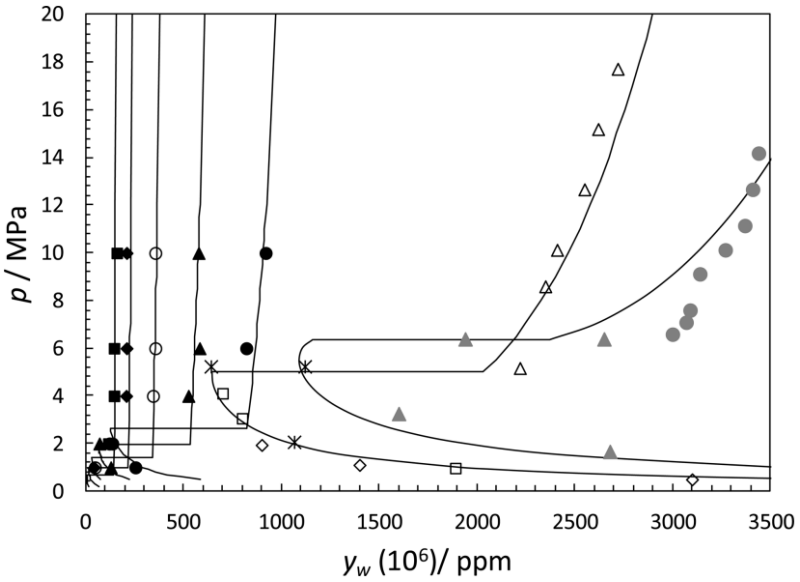

Figure 2.10: Water content in the vapor and liquid phases of carbon dioxide in equilibrium with hydrates or liquid water at 223, 233, 243, 253, 263, 288, and 298 K from left to right respectively. Solid black lines represent model predictions and symbols represent experimental data. Reproduced with permission from [49]. Copyright 2014 American Chemical Society.

2.6. Transportation Methods

CO_2 can either be transported through pipelines or by various transportation vehicles [50]. Liquefied CO_2 can be transported from inland industrial sites with trains, trucks or barges. These vehicles can either be specially built for CO_2 transport or loaded with ISO tank containers filled with liquid CO_2. These vehicles can be used to directly transport the CO_2 to a storage location or the CO_2 can be subsequently be transferred to a ship which transports it further by sea which can increase the transportation scale. Section 2.6.1 will further explore CO_2 liquefaction for ship transport. This mode of transport is especially interesting for Tata Steel Netherlands since has its own port with an open connection to the north sea. In addition, Section 2.6.2 will identify pipeline operations to compare this mode of transportation to ship transport.

2.6.1. Liquefaction for Ship transport

CO_2 is liquefied before ship transport to maximize the capacity of the ships since gaseous CO_2 takes up roughly five hundred times more volume than liquid CO_2 [51]. CO_2 shipping is typical done at pressures below 20 bar (g). Higher shipping pressures are considered to be economically impractical since the heavier pressure vessels will significantly increase the cost of the CO_2 transport ships [52]. CO_2 liquefaction by only increasing the pressure is therefore not possible since CO_2 at ambient temperatures and 20 bar (g) cannot exist in the liquid phase, as shown in the phase diagram of Figure 2.7 in Section 2.5. This section will identify different processes to liquefy the CO_2 in this low pressure range.

Closed System

A closed liquefying system uses a refrigeration cycle that is separate from the CO_2 stream [51]. This refrigeration cycle cools the CO_2 stream through a heat exchanger to the desired transportation temperature at which the stream will liquefy. The stream needs to be pressurized to the desired liquefaction pressure before this step since the pressure is not significantly changed over this process step. The stream should be cooled to ambient temperatures after the compression step to save on refrigeration energy requirements, Figure 2.11 shows an overview of the whole process. The efficiency of a closed liquefaction system is dependent on the compressor efficiency and the Coefficient Of Performance, COP, of the refrigeration system. The refrigeration system can be optimized by selecting the optimal refrigerant and refrigeration cycle. The system shown in Figure 2.11 for example utilizes a three-stage refrigeration cycle to increase the COP but this also complicates the system and increases CAPEX cost [51].

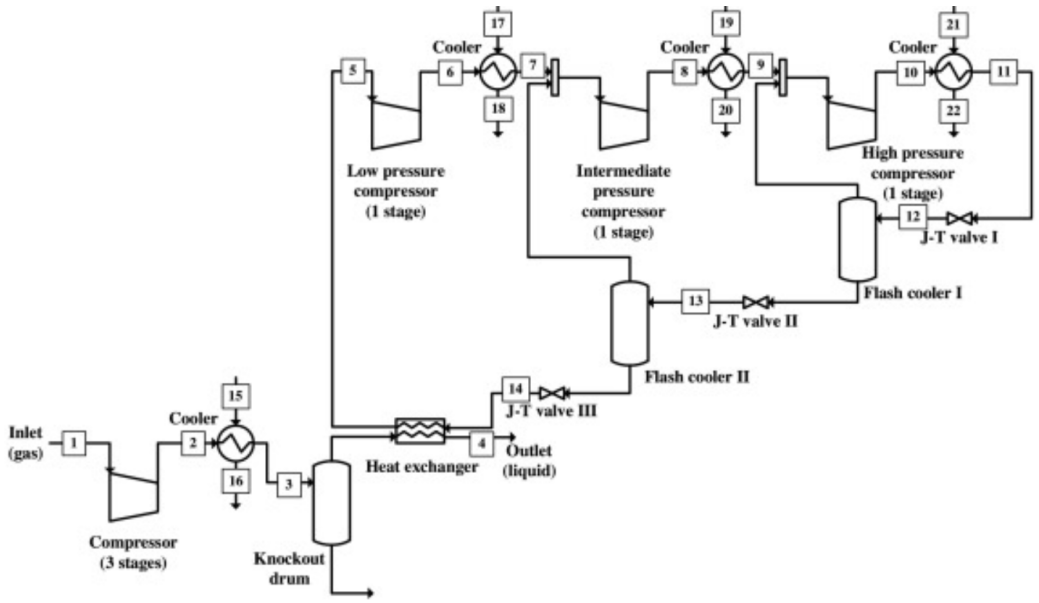

Figure 2.11: Closed liquefaction system with three-stage intercooled compression and external refrigeration cycle with three-stage intercooled compression. Reprinted from International Journal of Greenhouse Gas Control, Vol 35, Youngkyun Seoa; Hwalong Youa; Sanghyuk Leea; Cheol Huhb; Daejun Chang, Evaluation of CO2 liquefaction processes for ship-based carbon capture and storage (CCS) in terms of life cycle cost (LCC) considering availability, pages 1-12, Copyright 2015, with permission from Elsevier [51].

Open System

Open liquefaction systems are classified based on the fact that the stream itself is compressed and then expanded to a lower temperature through a Joule-Thomson valve. The stream can then be separated into a liquid and gaseous phase to obtain the desired liquid stream. The gaseous stream can be connected back to the compressor through a heat exchanger that cools the stream leading into the Joule-Thomson valve to increase the efficiency and close the loop. An alternative is to purge this gaseous stream to remove impurities from the system. This configuration is called a Linde-Hampson system. The efficiency can be further increased by designing a dual pressure Linde-Hampson system

which uses two compressor steps, as shown in Figure 2.12. This systems depends on the Joule-Thomson effect. However, this effect does not always produces a negative temperature change with a temperature drop [53]. The temperature change could also be positive and is dependent on the Joule-Thomson coefficient that can be evaluated with Equation 2.3, the sign of this coefficient defines the temperature change. The Joule-Thomson is dependent on both pressure and temperature, as can be concluded from Equation 2.3. When equaling this equation to zero a inversion temperature, the temperature at which the sign changes, can be evaluated for a certain pressure. This can produce a graph like Figure 2.13 when evaluated over a pressure range. A figure like this is useful to determine the operating ranges of a open liquefaction system for a certain fluid.

$$\mu_{\mathrm{JT}} = (\frac{\partial T}{\partial p})_h \tag{2.3}$$

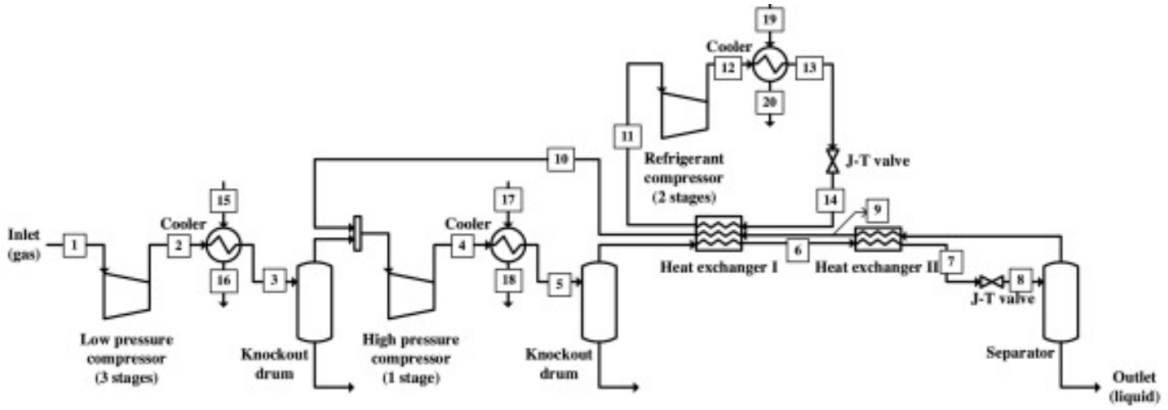

Figure 2.12: Linde-Hampson liquefaction system with two-stage intercooled compression. The system has an external refrigerant cycle with two-stage intercooled compression to precool the gas stream and subsequently cools the stream to liquefaction temperature through a pressure drop over a Joule-Thomson valve. Reprinted from International Journal of Greenhouse Gas Control, Vol 35, Youngkyun Seoa; Hwalong Youa; Sanghyuk Leea; Cheol Huhb; Daejun Chang, Evaluation of CO2 liquefaction processes for ship-based carbon capture and storage (CCS) in terms of life cycle cost (LCC) considering availability, pages 1-12, Copyright 2015, with permission from Elsevier [51].

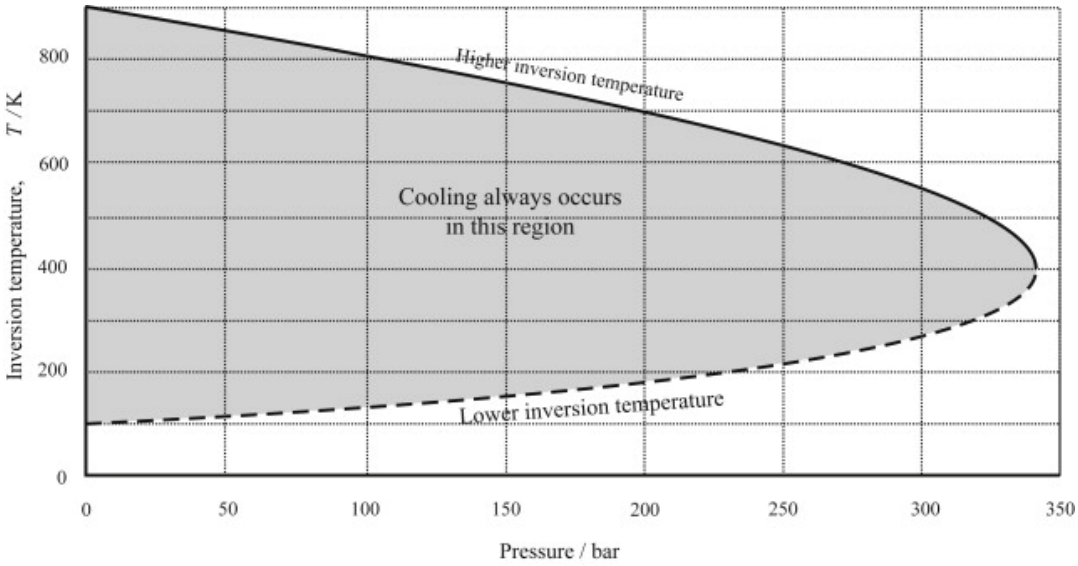

Figure 2.13: Higher and lower Joule-Thomson inversion temperatures for air in the pressure range of 0 to 35 MPa, displaying the region wherein cooling due to the Joule-Thomson effect occurs. Reprinted from Advanced Thermodynamics for Engineers (Second Edition), Chapter 18, by D. Winterbone and A. Turan, 2020, Elsevier Butterworth-Heinemann, page 435, Copyright 2015, with permission from Elsevier [53].

Cryogenic Liquefaction

An alternative to the previously mentioned processes is cryogenic liquefaction [54]. A cryogenic process also needs an open or closed refrigeration system to cool the CO_2 stream but the system is designed so that cryogenic temperatures are reached. When the cryogenic stream is then fed into a distillation column it can be used to separate the CO_2 from non-condensable components to purify the stream. This process requires a large energy investment but the advantage is the combination of CO_2 separation and liquefaction into one system.

2.6.2. Pipeline Transport

Another transportation method for CO_2 is through a pipeline, like introduced in Section 2.6. This means of transport is often considered as the most economically efficient option [55]. Long range transport pipelines are usually operated at a supercritical pressure, this is advantageous due to the higher volumetric density and lower viscosity. A higher volumetric density allows a smaller pipeline diameter to transport a certain mass flow rate and a smaller pipeline diameter will lead to a lower investment cost. A lower viscosity will lower the pressure drop across the pipeline, this will allow a lower entry pressure which leads to lower energy requirements in the compression step. The temperature of the stream will be strongly dependent on the environment since the pipelines are usually uninsulated. This means the stream will be at an elevated temperature due to heat from compression and then cools down to the environment temperature. Therefore, CO_2 transport at supercritical pressure usually takes place in the dense phase since, in most cases, the environmental temperature is lower than 304 K, which is the critical temperature of pure CO_2 [46].

Figure 2.14 gives an overview of a possible transport method as reported in [56]. It is assumed that the CO_2 stream leaves the source in the gaseous phase. A compressor is used to elevate the pressure to the critical pressure. The stream cools down after the compressor stage so that it transitions into the dense phase. A pump is placed after the compression step to further increase the pressure to the desired inlet pressure so the stream stays in the dense phase regardless of the pressure drop in the pipeline. This unit has to be a pump since the liquid and dense phase are incompressible. Alternatively, the stream could be compressed to the desired inlet pressure where it will transition into a supercritical fluid and can then transition into the dense phase through cooling but this process route uses more energy [55]. Depending on the pipeline length, a booster pump could be used to increase the pressure to keep the stream in the dense phase and provide the right injection pressure.

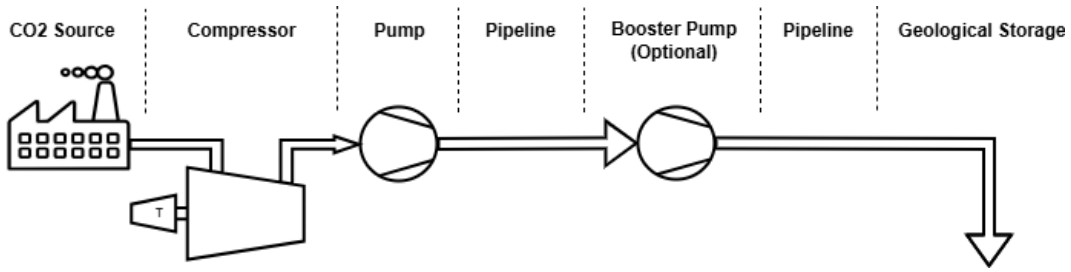

Figure 2.14: Schematic of CO_2 transportation through an pipeline to an offshore geological storage location. The CO_2 is first compressed and subsequently pumped into a pipeline with optional booster pumpers before being injected into a geological storage site. Recreated based on [56].

2.7. Summary

2.7.1. Research Gaps

The literature review was carried out to find the latest technical insights about transportation of CO_2-rich mixtures from steelwork off-gases but a number of research gaps were found. Different gas compositions of steelwork off-gases were identified but these ranges are quite large in some cases. Reported ranges are not always representative of those found at the Tata Steel IJmuiden site since the actual gas compositions are largely depend on the resources used in the specific processes. Therefore most of these reported gas compositions can only be used as indications of the actual composition. The compositions for the HIsarna reactor and ENERGIRON DR plant are however representative for a possible installation within Tata Steel.

The references used for the identification of CCS projects were less scientific. Most sources that were found are documentation meant for companies that will connect to these CCS projects. More detailed technical information about the used infrastructure could not be found. Based on the identified stream specifications, further research was done to find the reasoning behind these limitations but the available sources for this were quite brief on the reasoning behind the limits. Research about the behavior of these streams with all trace impurities was not found in a CCS context.

From the identified EoS, a rather positive image was given for cubic EoS since these kinds of equations can be fitted to experimental data of mixtures. But this means these Binary Interaction Parameters need to be identified for the mixtures of interest. Section 2.5 dives deeper in the phase behavior of certain mixtures but these were binary mixtures so the actual phase behavior found in multi-component systems could potentially significantly differ from the found behaviors.

Section 2.6.1 identifies different liquefaction processes, this is purely to provide an overview of possible options and based on the actual process limitations certain adaptions on the shown processes could be needed. Likewise for Section 2.6.2 where pipeline transport is discussed, this gives an overview of the logistics and operating conditions but technical details about the system are dependent on the actual application.

2.7.2. Research Questions

As introduced in Section 1.2, the objective of this thesis is answering the following main research question.

> What are the energy requirements and costs of transporting CO_2-rich mixtures derived from steelworks off-gases?

Based on the reviewed literature and resulting research gaps, a few sub research questions are recommended to be worked out to answer the main research question. These questions can be formulated as the following points.

- What is the stream composition and water content of the analyzed off-gas after pretreatment?
- What are the thermodynamic properties of the analyzed CO_2-rich streams?
- What are the energy requirements for liquefaction to shipping conditions of the researched CO_2 mixtures?
- What are the capital and operational costs of the different analyzed processes?

3

Methodology

3.1. Process Logistics

3.1.1. Transportation Method Selection

Chapter 2 explored both pipeline and ship transport options. Pipeline transport is reported as the most economically efficient option in most situations [55]. A potential drawback of pipeline transport is the difficulty of obtaining planning permits for a dedicated CO_2 pipeline, like in the case of the Porthos project, where delays occurred even with accelerated permitting procedures [57]. It is therefore not ideal to construct a CO_2 transportation pipeline when comparing the potential delays associated with permitting procedures and the ambition to implement CCS within the relatively short time frame presented in the Environmental Effect Report from Tata Steel Netherlands [7]. A more suitable solution is ship-based transportation, which adds flexibility in project scale and timeframe. Additionally, a company like Northern Lights provides ship-based transport as a service and could therefore be implemented within a shorter time frame [26]. The focus of this thesis will therefore be on CO_2 liquefaction for subsequent ship-based transport.

3.1.2. Transport Conditions Selection

Section 2.5.2 identified that the bubble pressure will increase with impurity content [48]. Section 2.6.1 mentioned that shipping liquid CO_2 above 20 bar (g) is considered to be economically impractical because of the increase in pressure vessel and therefore weight [52]. Therefore, the shipping pressure will need to be kept as low as possible and vary with the stream composition. The bubble pressure also varies with stream temperature. Therefore, the shipping pressure cannot be selected before a shipping temperature is selected. Section 2.6.1 identified that the Joule-Thomson inversion temperature needs to be analyzed to make sure an open liquefaction system is able to reach the desired liquefaction temperature. Additionally, the refrigerant selection will influence the temperatures that can be reached in the closed liquefaction system. Therefore, these factors should first be determined before suitable transport conditions can be selected.

3.1.3. System Boundary

The system boundary for the ship transport of liquefied CO_2 is set as that for a CO_2 transportation and storage project like the Northern Lights project. A company like Northern Lights provides CO_2 storage as a service where the CO_2-producing company is only responsible for the CO_2 capture, purification, buffer storage and ship loading facilities [26]. Northern Lights operates its own CO_2 transport ships and storage facilities, the CO_2 producing company only pays for the delivered CO_2. CO_2 capture and purification is not modeled in this research, the stream composition of a treated CO_2-rich stream is taken as input for the liquefaction system instead. This produces the system boundary shown in Figure 3.1

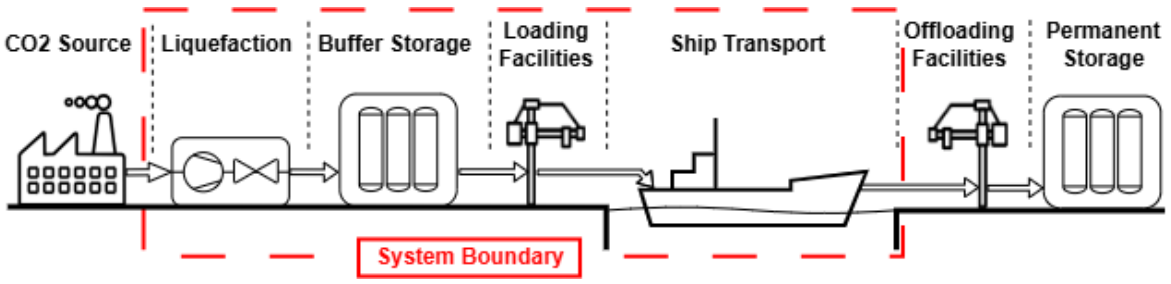

Figure 3.1: System boundary of this research consisting of liquefaction, buffer storage, loading facilities and ship transport. Therefore it excludes gas treatment at the CO_2 source, offloading facilities and permanent storage.

3.2. Off-gas Compositions

3.2.1. Gas Preprocessing

Table 3.1 presents the predicted off-gas composition of an industrial-scale HIsarna plant as described in Section 2.1.4. While the CO_2 content is higher than that of traditional blast furnace gas, it is still too low for efficient transport. Therefore, the CO_2 content needs to be increased. One process investigated at Tata Steel is Pressure Swing Adsorption (PSA) [12]. The referenced study developed an Aspen Adsorption model capable of predicting the CO_2-rich stream generated by the process. This model was adapted in subsequent research to predict the CO_2-rich stream composition when the HIsarna off-gas composition from Table 3.1 is used as input. Table 3.2 presents the results for three selected CO_2 volume fractions, which are discussed in more detail later in this thesis. The CO_2 fractions after PSA are based on the CO_2 purity requirements described in Section 2.2.4. These gases do not contain trace impurities like NO_x and SO_x or solid dust particles, it is assumed these components are removed, to a negligible amount for this study, from the off-gas during gas preprocessing and purification.

Table 3.1: Predicted gas composition of an industrial-scale HIsarna plant excluding H_2O [17].

Component	Dry volume Percentage
CO_2 [vol%]	64.5
H_2O [vol%]	0.0
N_2 [vol%]	13.2
CO [vol%]	20.1
H_2 [vol%]	2.2

Table 3.2: Stream composition of HIsarna off-gas after purifying to 95.5, 97.5 and 99.5 vol% CO_2 through PSA.

Component	Volume Percentage		
CO_2 [vol%]	95.50	97.50	99.50
N_2 [vol%]	3.00	1.70	0.24
CO [vol%]	1.48	0.79	0.26
H_2 [vol%]	0.02	0.01	0.00

The CO and H_2 can also be removed by burning it in a heat recovery unit. It is assumed that the CO and H_2 are burned off with an excess oxygen of 1.6 relative to the stoichiometric requirement [58]. The resulting dried stream composition is shown in Table 3.3. Using these compositions as input, the PSA model predicts the compositions shown in Table 3.4.

Table 3.3: Dry HIsarna off-gas composition after the CO and H_2 is combusted with an excess oxygen ratio of 1.6 to simulate a heat recovery step.

Component	Dry Volume Percentage
CO_2 [vol%]	80.9
N_2 [vol%]	12.6
O_2 [vol%]	6.4

Table 3.4: Dry HIsarna off-gas composition after purifying to 95.5, 97.5 and 99.5 vol% CO_2 through PSA and the CO and H_2 is combusted with an excess oxygen ratio of 1.6 to simulate a heat recovery step.

Component	Volume Percentage		
CO_2 [vol%]	95.50	97.50	99.50
N_2 [vol%]	3.82	2.14	0.45
O_2 [vol%]	0.68	0.36	0.05

3.2.2. Water content

The stream compositions do not contain water, this is based on the use of PSA for the purifying step. The adsorbents used in this process exhibit high selectivity for H_2O [59]. Therefore the H_2O is typically removed as much as possible to process the gas stream in a efficient way. Furthermore, any remaining H_2O will get trapped in the adsorbent due to the competitive adsorption. Consequently, the product stream from the PSA unit is assumed to contain a negligible amount of H_2O and is therefore not included.

3.3. Processes Simulation Software

Aspen HYSYS version 12 is used for the process simulation. This commercial software facilitates the simulation and design of chemical processes. It is widely used in industry due to its accuracy in simulation of oil and gas production, gas processing, chemical processing and air separation [60]. The software contains physical and thermodynamic properties for a large selection of chemicals and supports a range of thermodynamic models. Furthermore, it supports equipment sizing and techno-economic analyses. The selection of this software will also support the availability for further research within Tata Steel Netherlands since Aspen software is already in use within the company [12].

3.4. Thermodynamic Properties

3.4.1. Thermodynamic Properties Reference Software

The NIST REFPROP database is used to generate vapor-liquid equilibrium diagrams, Joule-Thomson inversion temperature diagrams and as a reference to validate results obtained from Aspen HYSYS [46]. The objective of the software is to incorporate the most accurate available models into a tool capable of calculating the thermodynamic properties of industrially important fluids [61]. The database is developed to be near, or within, the uncertainty limits of experimental data and can therefore be regarded as a reliable reference.

3.4.2. EoS selection

Selecting an appropriate EoS is an essential part of creating reliable results in Aspen HYSYS. Four EoS are selected in Aspen HYSYS and compared on applicability to maximize reliability, the selected EoS are PC-SAFT, GERG-2008, CPA and PR. The selection is based on the models identified in Section 2.4 and their availability in Aspen HYSYS. The bubble point pressure was chosen as the primary comparison parameter, as the liquefaction process will be designed around this value. NIST REFPROP is chosen as a reliable reference, like explained in Section 3.4. The bubble point pressure is predicted for each stream composition at temperatures of 223, 243, 263 and 283 K. The Mean Absolute Error (MAE) is subsequently calculated with Equation 3.1 to identify the EoS that most closely matches the NIST REFPROP version 10 database.

$$\text{MAE} = \frac{1}{n}\sum_{i=1}^{n_{tot}} |y_i - x_i| \tag{3.1}$$

The ASME Steam fluid package was selected is selected for the cooling water streams, in accordance to the recommendations provided in the internal Aspen HYSYS version 12 documentation. This fluid package is valid for pressures below 103 MPa and temperatures between 273 and 1089 K [62]. The fluid package is therefore valid as the cooling water streams will not exceed these limitations.

The REFPROP fluid package is used for the ammonia streams in the refrigeration cycles, also in accordance with recommendations in the internal Aspen HYSYS version 12 documentation. Preliminary results indicate that this fluid package does not reproduce the same results as the NIST REFPROP version 10 database for the analyzed CO_2-rich streams. Instead, it produces results identical to those obtained using the GERG-2008 fluid package for these streams. Therefore, the REFPROP fluid package in Aspen HYSYS version 12 is exclusively used for refrigerant streams and is excluded from the EoS selection of the CO_2-rich streams. The pressure limit of this fluid package, for ammonia, is 1000 MPa and the allowable temperature range is between 196 and 700 Kelvin, which will not be exceeded.

3.5. Closed System Liquefaction Model

3.5.1. Process Configuration

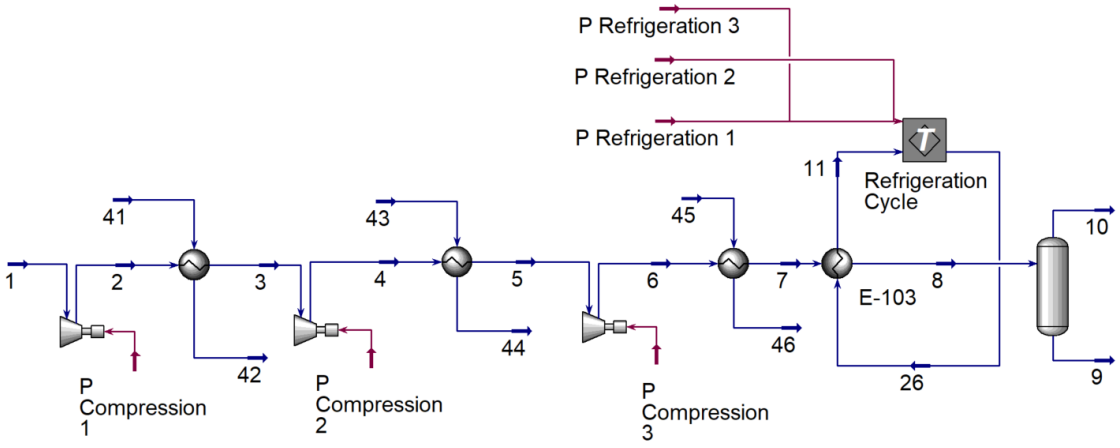

Figure 3.2: Aspen HYSYS model of the closed liquefaction system with an external refrigeration cycle. The stream is compressed in a three-step configuration with intercooling before passing through a heat exchanger connected to the external refrigeration cycle. The stream is separated into a gaseous and liquid stream as final step.

A closed liquefaction system uses an external refrigeration cycle to cool the process stream until it liquefies, as described in Section 2.6.1. Figure 3.2 shows the developed model in Aspen HYSYS according to the reference discussed in Section 2.6.1 [51]. The compression is carried out in three stages, with intercooling to an ambient temperature after each compression step. Subsequently, the stream passes through a heat exchanger connected to an external refrigeration cycle to liquefy the stream. After liquefaction, the stream is transported to a buffer storage.

3.5.2. Refrigeration Cycle

The efficiency of a closed system liquefaction system is based on the Coefficient Of Performance (COP) of the refrigeration cycle. The COP dependents on both the refrigeration cycle configuration and the refrigerant fluid. Based on comparable literature, ammonia is identified as the most suitable refrigerant for a CO_2 liquefaction system [63] [51]. The selection of a natural refrigerant also make this research more future proof, as EU legalization will phase out hydrofluorcarbon refrigerants completely by 2050 [64]. The operating points of the refrigerant cycle are based on a condenser outlet temperature of 308 K and an evaporator inlet temperature of 4 K below the desired liquefied product stream temperature, consistent with literature [51]. The outlet pressure of the final compressor step is set at 1.4 MPa and the evaporator outlet is set at 0.1 MPa, also in agreement with literature values.

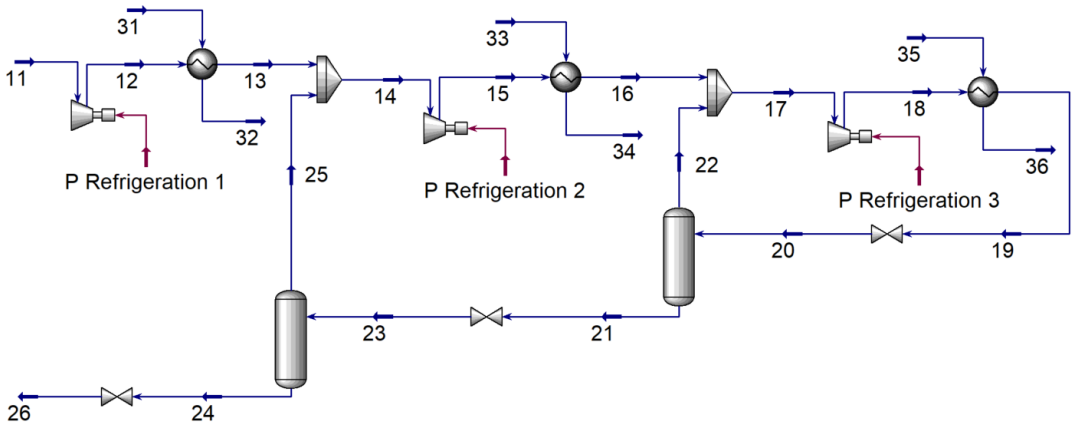

Figure 3.3: Refrigeration cycle of the closed system liquefaction model consisting of three-stage compression with intercooling and three Joule-Thomson valves with separators in between which recycle the gaseous stream.

3.6. Open System Liquefaction Model

An open liquefaction system utilizes the Joule-Thomson effect to liquefy the CO_2 stream, as discussed in Section 2.6.1. The reference used in Section 2.6.1 identifies a precooled Linde Hampson system as the most efficient option among from the evaluated options [51]. This system is recreated in Aspen HYSYS with the modification that vapor stream separated in the flash tank is purged rather than recycled, like utilized in a similar study that considered a CO_2 stream with impurities [63]. This approach improves the purity of the liquefied stream, as the vapor stream contains a higher fraction of non-condensable impurities compared than the liquid stream. The model is further characterized by three-step compression with intercooling to ambient temperature, followed by an external refrigeration cycle to precool the CO_2 prior to expansion through the Joule-Thomson valve. The combination of multistage compression and precooling increases the overall efficiency of the system. As discussed in Section 3.5.2, ammonia is selected as the refrigerant due to its favorable COP in this configuration [63] [51]. A simpler refrigeration cycle is utilized due to the the lower refrigeration duty compared to the closed liquefaction system. This refrigeration cycle consists of two-stage compression with intercooling, a condenser, a throttling valve and a heat exchanger.

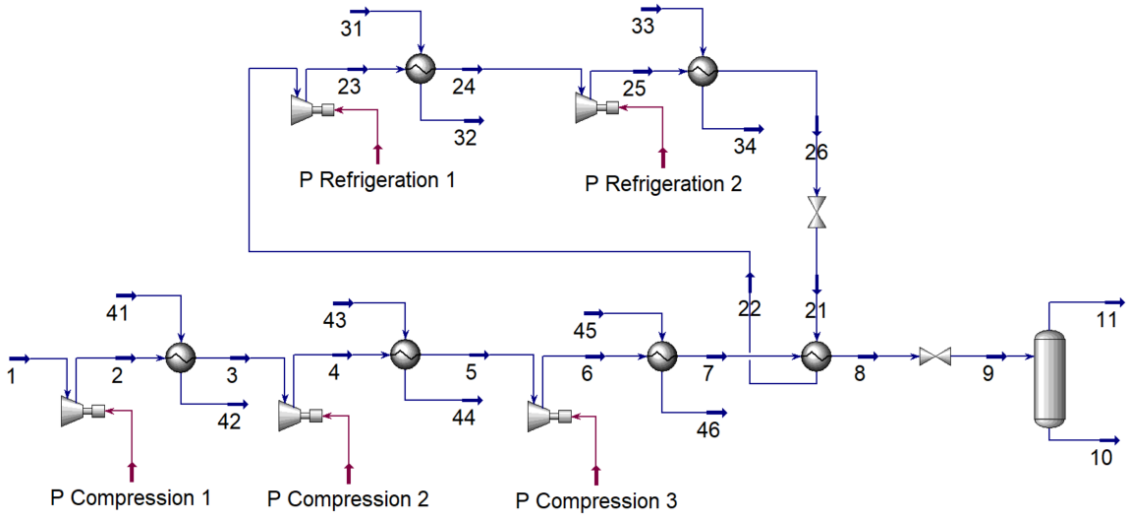

Figure 3.4: Aspen HYSYS model of the open liquefaction system. Consisting of a three-stage compression configuration with intercooling. The stream passes through a heat exchanger connected to an external refrigeration cycle after compression before being throttled through a Joule-Thomson valve. The stream is separated into a gaseous and liquid stream as a final step.

3.7. Techno-Economic Analysis

3.7.1. Process Scale

The process scale is selected to represent a pilot scale, an intermediate scale and an upscaled case in order to analyze cost increase. The annual liquefaction capacities representing these cases are assumed to be 100, 200 and 400 kt liquefied product per year, based on the annual capacities and number of supplying companies of the CCS projects summarized in Section 2.2.5. In this context, liquefied product refers to the total mass that is transported to the storage location and therefore also includes the mass of impurities. This should not be confused with the total annual stored mass of pure CO_2 which will be smaller due to the presence of impurities.

3.7.2. Liquefaction Equipment

The equipment costs for the liquefaction system are calculated using cost correlations from the book Chemical Engineering Design [65]. These correlations estimate capital expenditure (CAPEX) based on equipment size or power. The correlations are based on equipment costs for the United States Gulf Coast in January of 2010, represented as $C_{2010,USGC}$ and it corresponds to a Chemical Engineering Plant Cost Index (CEPCI) value of 532.9. The costs are updated to more recent values using a CEPCI value of 800, corresponding to the value of 2024 [66]. The CAPEX is furthermore adjusted to represent equipment cost in the Netherlands by applying a location factor, LF_{NL}. A location factor of 1.19 is used for the Netherlands [65]. These adjustments produce the equipment CAPEX for the Netherlands in 2024, expressed as $C_{2024,NL}$ in Equation 3.2.

$$C_{2024,NL} = C_{2010,USGC} \cdot \frac{CEPCI_{2024}}{CEPCI_{2010}} \cdot LF_{NL} \tag{3.2}$$

The correlation for the various pieces of equipment are all in the form of Equation 3.3, with C_e as the capital cost of the equipment, S as size parameter and with dimensionless variables a, b and n. Table 3.5 summarizes every correlation which is used in this techno-economic analysis. All compressors are assumed to be centrifugal compressors, the CAPEX is based on driver power which is extracted from the Aspen models. The heat exchangers are all assumed to be U-tube shell and tube heat exchangers, hereby the cost is dependent on the heat transfer area. The heat transfer area is also extracted from the Aspen models, the sizing is determined with the Aspen Process Economic Analyzer (APEA). The CAPEX of phase separators, with or without Joule-Thomson valve, are calculated with the correlation for vertical carbon steel pressure vessels. The shell mass of the pressure vessel is the unit for size in this correlation. The dimensions of the pressure vessel are determined in the the Aspen models using the APEA, the mass is subsequently calculated using Equation 3.4 with diameter d, height h wall thickness t_{wall} and carbon steel density ρ_{cs}. The wall thickness t_{wall} is dependent of the internal pressure $p_{separator}$, internal diameter d and maximum allowable stress S_{cs}, it can be calculated with Equation 3.5. This equation is however only valid if the calculated value is larger than the minimum wall thickness needed to support it owns construction, this minimum value depends on the vessels diameter and is shown in Table 3.6. This minimum wall thickness value also includes a corrosion allowance.

$$C_{Equipment} = a + b \cdot S^n \tag{3.3}$$

$$m_{Pressure\ Vessel} = (\frac{1}{2} \cdot \pi \cdot d^2 + \pi \cdot d \cdot h) \cdot t_{wall} \cdot \rho_{cs} \tag{3.4}$$

$$t_{wall} = \frac{p_{separator} \cdot d}{2 \cdot S_{cs} - p_{separator}} \tag{3.5}$$

Table 3.5: Variables used in the correlations to determine the CAPEX of compressors, heat exchangers and vertical carbon steel pressure vessels [65].

Equipment	Unit for size, S	a	b	n
Compressor	Driver power, kW	580,000	20,000	0.6
Heat exchanger	Area, m^2	28,000	54	1.2
Vertical carbon steel pressure vessel	Shell mass, kg	11,600	34	0.85

Table 3.6: Minimum wall thickness for a carbon steel pressure vessel to support its own weight dependent on internal diameter [65].

Vessel Diameter [m]	Minimum Thickness [mm]
Up to 1.0	5
1.0 to 2.0	7
2.0 to 2.5	9
2.5 to 3.0	10
3.0 to 3.5	12

The operational expenditure (OPEX) of the liquefaction system is based on the various compressors throughout the system which are all electrically driven. Other OPEX contributes, such as maintenance and cooling water, are neglected as the analysis focuses on a high-level cost comparison. Equation 3.6 is used to determine the total annual electricity cost based on the total compressor power requirements, P_{total}, extracted from the Aspen models and industrial electricity cost c_{el}.

$$O_{Equipment} = P_{total} \cdot 8760 \cdot c_{el} \tag{3.6}$$

3.7.3. Transport Infrastructure

Section 3.1.3 showcased the system boundaries which also apply to the transport infrastructure that is accounted for in this techno-economic analysis. The analyzed transport infrastructure consists of the buffer storage and loading facilities at the CO_2 producing site as well as the shipping fuel cost and OPEX adjusted to yearly use. The buffer storage costs are based on the required volume V_{buffer} and absolute shipping pressure $p_{shipping}$, Equation 3.7 is used for the CAPEX while Equation 3.8 is used for the OPEX [52]. The buffer storage is assumed to be 1.5 times the ship volume to account for processes disruptions. The loading facilitates costs are based on the required annual capacity M_{annual} in kt per year, Equation 3.9 is used for the CAPEX and Equation 3.10 is used for the OPEX.

$$C_{Buffer} = (\frac{920 - 550}{1600 - 800} \cdot p_{shipping} + 226.5) \cdot V_{Buffer} \tag{3.7}$$

$$O_{Buffer} = 0.06 \cdot C_{Buffer} \tag{3.8}$$

$$C_{Loading\ Facilities} = 7.9 \cdot 10^6 \cdot \frac{M_{annual}}{3000} \tag{3.9}$$

$$O_{Loading\ Facilities} = 0.02 \cdot C_{Loading\ Facilities} \tag{3.10}$$

Shipping cost is based on the same reference which includes CAPEX, OPEX and fuel cost based on the ship capacity in kt CO_2 and shipping pressure [52]. The data is available for a shipping pressure of 0.8 or 1.6 MPa and capacities ranging from 2.5 to 100 kt CO_2. This research will assume a CO_2 transport ship with a capacity of 8.25 kt CO_2, corresponding to reported ship capacity of the Northern Lights project [67]. The fuel usage is only considered to be dependent on the ship capacity by the reference. Equation 3.11 is used to calculate the fuel cost based on shipping distance s, ship capacity M_{ship}, fuel usage per km per ton of ship capacity f and fuel cost c_{fuel}. Equation 3.12 is used to calculate the ship CAPEX, it is an linearly extrapolated formula based on the available data for 0.8 and 1.6 MPa shipping. The ship CAPEX can subsequently be used to calculate the OPEX using Equation 3.13 which is adjusted to the annual usage in days, D_{annual}. D_{annual} is evaluated based on ship speed v, one-way shipping distance s, off- and on-loading time $D_{loading}$ and the round trips per year evaluated with dividing the annual shipping capacity by the ship capacity.

$$O_{Shipping\ Fuel} = s \cdot M_{ship} \cdot f \cdot c_{fuel} \tag{3.11}$$

$$C_{Ship} = \frac{64 - 30.7}{1600 - 800} \cdot p_{shipping} + 1.6 \tag{3.12}$$

$$O_{Ship} = 0.05 \cdot \frac{D_{annual}}{365} \cdot C_{Ship} \tag{3.13}$$

$$D_{annual} = (\frac{2 \cdot s}{24 \cdot v} + D_{loading}) \cdot \frac{M_{annual}}{M_{ship}} \tag{3.14}$$

3.7.4. Fixed Variables

Various variables used in the equations for the techno-economic analysis have fixed values in this research, they are summarized in Table 3.7.

Table 3.7: Values, units and references of fixed variables used in equations of the techno-economic analysis.

Variable	Symbol	Value	Unit	Reference
Density carbon steel	ρ_{cs}	7900	[kg·m^{-3}]	[65]
Industrial electricity cost	c_{el}	0.095	[€ ·kWh^{-1}]	[68]
Shipping distance (one-way)	s	900	[km]	[69]
Ship mass capacity	M_{ship}	8250	[t]	[67]
Specific fuel consumption	f	6.84	[g ·t^{-1} ·km^{-1}]	[52]
Fuel cost	c_{fuel}	325.00	[€ ·t^{-1}]	[52]
Ship speed	v	26	[km·h^{-1}]	[70]
Off- and on-loading time	$D_{loading}$	1.0	[days]	[70]

3.7.5. Techno-Economic Analysis Scope

The scope of this techno-economic analysis is a high-level cost comparison between different process scales and CO_2 input purities. The accuracy of the correlations used to estimate the costs of liquefaction equipment reflects this choice as these are reported to be applicable for preliminary estimates. These preliminary, or class 4, estimates are reported to have an accuracy of $\pm$ 30% and are recommended to make coarse choices between design alternatives [65]. The liquefaction equipment OPEX only accounts for the electricity costs of the various electrically driven compressors and neglects costs coming from sources such as maintenance or the cooling water system. All CAPEX costs are treated as a one-time investment as the focus is on a high-level system comparison. Therefore, the operational lifetime of the systems, and consequently the annualized CAPEX and discounting, are not taken into consideration.

3.8. Summary

The methodology chapter started with defining the process logistics in Section 3.1. It was determined that ship-based transport of liquefied CO_2 is the preferred transportation method because of the increased flexibility and shorter implementation time frame. The transportation conditions for these ships cannot be determined yet, it was noted that the Joule-Thomson inversion temperature and the phase behavior of the different mixtures should first be analyzed. A corresponding shipping temperature and pressure can then be determined per mixture based on these results. Section 3.1 finishes by detailing the system boundaries, this research will not model off-gas processing but assumes a range of pretreated CO_2-rich mixtures that will be taken as input for a liquefaction process model. The subsequent buffer storage, loading facilities and ship transport of the CO_2 is also considered in the techno-economic analysis. This means the offloading facilities and permanent storage are excluded since a construction like the Northern Lights project is considered where these final steps are offered as a service.

Section 3.2.1 specifies the various pretreated gas streams are considered for liquefaction and transport. Six synthetic gas streams are defined in this section. These streams can be divided into two impurity cases or three CO_2 purity levels. The first impurity case assumes that the HIsarna off-gas is directly purified, after standard gas treatment such as NO_x and SO_x removal, to 95.5, 97.5 and 99.5 vol% CO_2 through a Pressure Swing Adsorption, PSA, unit. This first case therefore includes N_2, CO and H_2 impurities and neglects trace impurities such as NO_x and SO_x. The second impurity case assumes the CO_2 is first processed through a heat recovery unit, in which the CO and H_2 is combusted with an excess O_2 ratio of 1.6, and subsequently purified to 95.5, 97.5 and 99.5 vol% CO_2. This second case

therefore only includes N_2 and O_2 impurities. These different stream compositions allow the effects of impurity type and CO_2 purity to be evaluated independently. The water content for all six synthetic gas compositions is assumed to be negligible since the gases must be dried before the PSA step and the PSA unit will likely absorb a significant amount of any remaining water.

Aspen HYSYS version 12 is selected in Section 3.3 as the process simulation software because of its utilization within Tata Steel Netherlands and accuracy. NIST REFPROP version 10 is selected in Section 3.4 as the thermodynamic property reference software because of its reported high accuracy. Section 3.4 further specifies the method in which an appropriate EoS will be selected for the CO_2-rich streams. PC-SAFT, GERG-2008, CPA and PR will be compared to NIST REFPROP version 10 on bubble line pressure for four temperatures ranging from 223 K to 283 K. The accuracy of the models is then determined by calculating the MAE of these results. ASME steam and REFPROP fluid packages are selected for the cooling water and refrigerant respectively in this section based on recommendations from the internal Aspen HYSYS version 12 documentation.

Section 3.5 explains the Aspen HYSYS model that was constructed for the closed liquefaction system. It consists of three compression stages with intercooling and a subsequent external refrigerant cycle to cool to the desired shipping temperature at which the gas and liquid streams are separated. The refrigerant cycle also utilizes three compression stages with intercooling and the selected refrigerant is ammonia. Ammonia is reported to have a favorable COP at CO_2 liquefaction operating conditions and since it is a natural refrigerant will also be more future proof than hydrofluorcarbon refrigerants.

The open liquefaction system model is specified in Section 3.6, it also utilizes a three-step compression configuration with intercooling. The stream is precooled after compression before the gas is expanded and therefore cooled through a Joule-Thomson valve to the shipping temperature. As a final step the stream is separated in a liquid and gaseous stream to further purify the stream.

The methodology concludes with Section 3.7 detailing the method for the techno-economic analysis. The process scale for this analysis is determined at 100, 200 and 400 kt liquefied product per year to represent a pilot scale, intermediate scale and a scale up. Section 3.7.2 give the various equations that are utilized to determine the CAPEX and OPEX of the liquefaction equipment. The method of determining the CAPEX and OPEX for the buffer storage, loading facilities and subsequent ship transport are specified in Section 3.7.3.

4

Results and Discussion

4.1. EoS Selection Results

The bubble pressure is calculated with different fluid packages in Aspen HYSYS version 12 and compared to REFPROP version 10. The MAE is subsequently calculated with Equation 3.1 which was presented in Section 3.4.2. PC-SAFT is identified to be the most accurate EoS for the CO_2-rich mixtures with N_2 and O_2, based on the results as shown in Figure 4.1. CPA was found to be a slightly more accurate EoS in the case of a CO_2-rich mixture with N_2, CO and H_2, as shown in Figure 4.2. Therefore the PC-SAFT EoS will be selected to calculate the model with the CO_2-rich mixture with N_2 and O_2 and the CPA EoS will be selected in the model with N_2, CO and H_2. Table 2.10 warned that PC-SAFT could produce deviations larger than 5 percent for various parameters when dealing with N_2 and O_2 impurities but based on the smaller MAE it can be concluded that the Aspen model is correctly fitted based on these results. Table 2.10 also flagged cubic EoS for potentially large deviations when handling N_2, CO and H_2 impurities but Figure 4.2 shows a small MAE for CPA and PR. CPA shows the smallest error, probably since this EoS handles polar components, such as H_2, better [39]. PC-SAFT produced a Mean Absolute Percentage Error (MAPE) of 2.2 percent, as shown in Appendix A, for the 95.5 vol% CO_2 with N_2 and O_2 impurities case. CPA produced a maximum MAPE of 1.7 percent for the 95.5 vol% CO_2 with N_2, CO and H_2 impurities case.

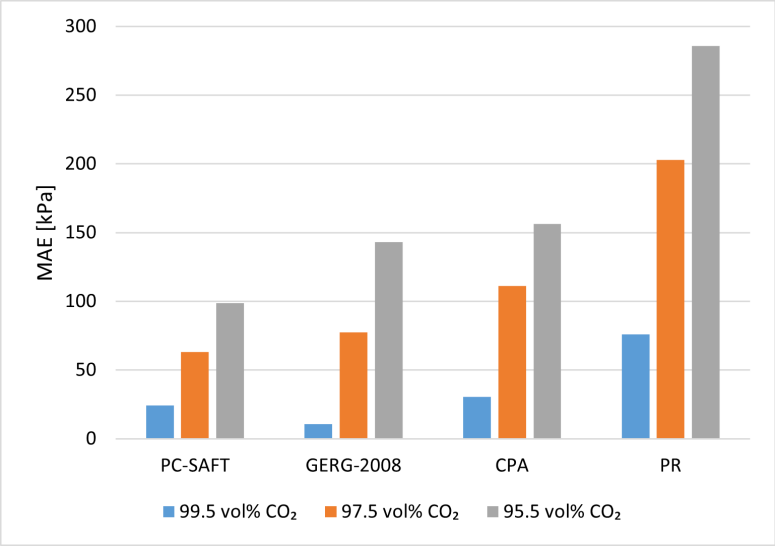

Figure 4.1: MAE of the bubble point pressure for CO_2-rich mixtures with N_2 and O_2, averaged over results for the temperatures of 223, 243, 263 and 283 K. The bubble point pressure was predicted with PC-SAFT, GERG-2008, CPA and PR Fluid Packages in Aspen HYSYS version 12, the error is subsequently based on the difference with REFPROP version 10 predictions.

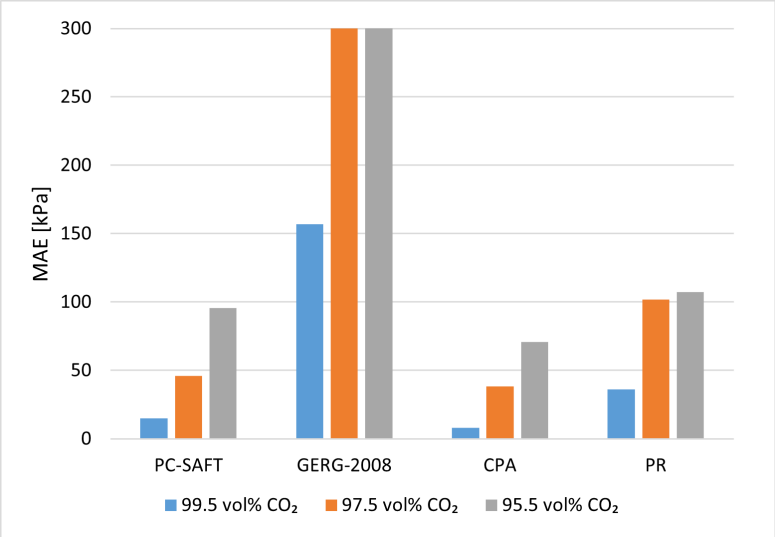

Figure 4.2: MAE of the bubble point pressure for CO_2-rich mixtures with N_2, CO and H_2, averaged over results for the temperatures of 223, 243, 263 and 283 K. The bubble point pressure was predicted with PC-SAFT, GERG-2008, CPA and PR Fluid Packages in Aspen HYSYS version 12, the error is subsequently based on the difference with REFPROP version 10 predictions. The MAE for the GERG-2008 model are cutoff at 300 kPa.

4.2. Joule-Thomson Coefficient Inversion Temperature

Figure 4.3 is created using NIST REFPROP version 10, it depicts the inversion temperature of the Joule-Thomson coefficient based on pressure and stream composition. It can be noted that the 0.955 volume fraction CO_2 exhibits the most restrictive inversion temperature graph for liquefaction through Joule-Thomson cooling. Figure 4.4 provides a more detailed view of the differences between of inversion temperature between the different impurity cases, it can be noted that the differences are relatively small. Furthermore, it also provides a more detailed view of the inversion temperature around 2 MPa, the range of possibly interesting shipping pressures. It can be noted that the inversion temperature in this pressure range lays in the range of possible shipping temperatures identified in Section 2.2.5. This has consequences for the allowable shipping temperature of higher purity stream liquefied with the open liquefaction system. Care should be taken to select a shipping temperature that remains above the inversion temperature to ensure proper cooling.

4.3. System Operating Conditions

The results found for the Joule-Thomson inversion temperatures limit the liquefaction temperature for streams with a 0.995 CO_2 volume fraction in an open liquefaction system to roughly 243 to 244 K in the pressure range typically used for CO_2 transport by ship. Additionally, the selected refrigerant, ammonia, has a evaporation temperature of 240 K at atmospheric pressure. This produces a minimum liquefaction temperature of 245 K for closed liquefaction system, assuming a evaporator pressure of 0.1 MPa is selected and a minimum temperature difference between the liquefaction and refrigerant stream of 5 K is chosen. Furthermore, reference research used for identifying various liquefaction systems also utilized a liquefaction temperature of 245 K. These points led to the decision to set the shipping temperature at 245 K for all mixtures and systems in this research.

The pressure drop needed for Joule-Thomson cooling influenced the selection of shipping pressure. A higher inlet pressure allows for a higher outlet pressure which will allow for a lower CO_2 purity needed for liquefaction. However, a Joule-Thomson does not work properly if the incoming fluid stream is an subcooled liquid. Since the inlet temperature is fixed by the precooling refrigeration cycle at 258 K, the pressure will influence the vapor fraction of the inlet stream. The inlet vapor fraction is set at 1 percent, to ensure the Joule-Thomson valve receives a predominately gaseous input, which will produce different inlet pressure based on the stream composition. Table 4.1 summarizes the different shipping pressures that are produced by these criteria.

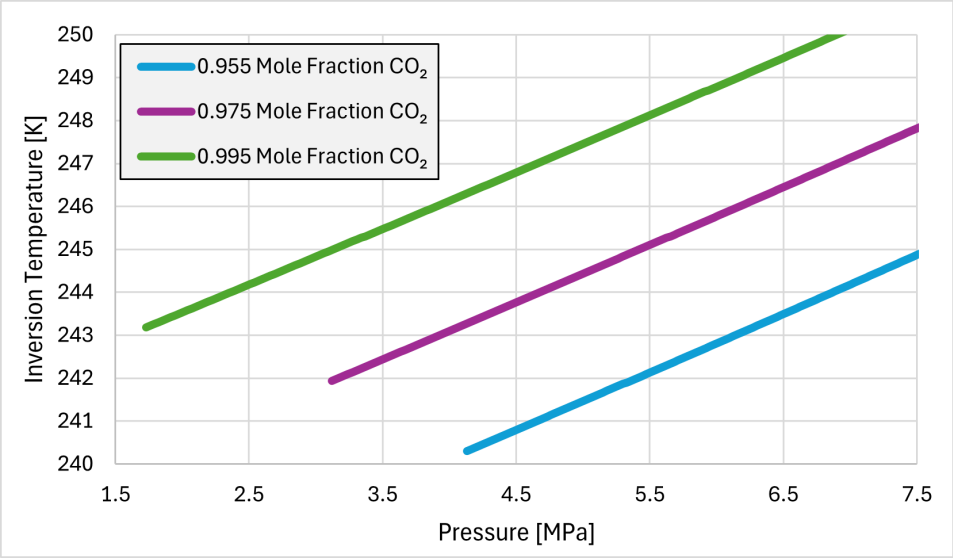

Figure 4.3: Joule-Thomson coefficient inversion temperature at a pressure range of 1.5 to 7.5 MPa for synthetic HIsarna off-gas mixtures with 0.955, 0.975 and 0.995 volume fractions CO_2 in combination with N_2, CO and H_2 impurities. Evaluated with NIST REFPROP version 10 [46].

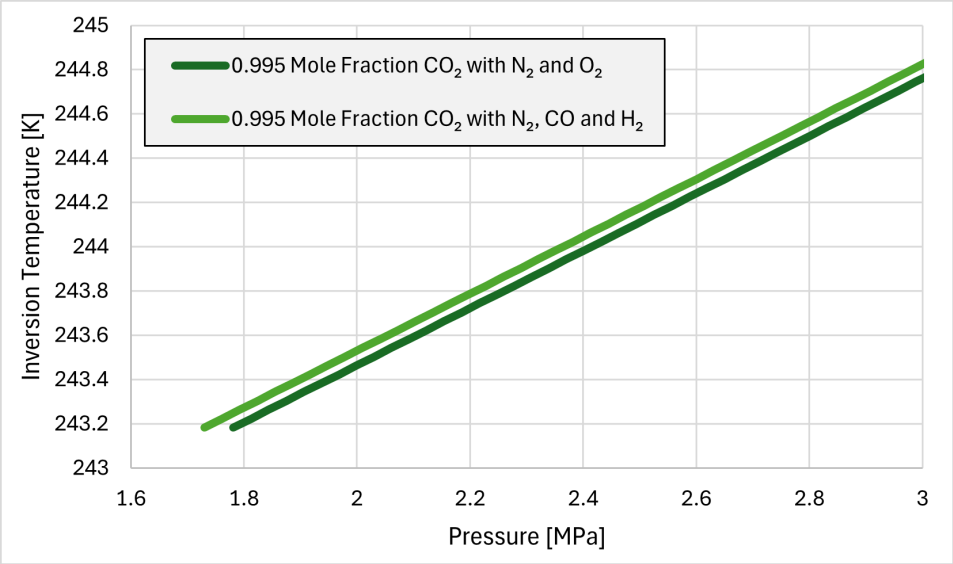

Figure 4.4: Joule-Thomson coefficient inversion temperature at a pressure range of 1.6 to 3.0 MPa for synthetic HIsarna off-gas mixtures of 0.995 volume fraction CO_2 with N_2 and O_2 or N_2, CO and H_2 impurities. Evaluated with NIST REFPROP version 10 [46].

Table 4.1: Shipping conditions varying with CO_2 volume percentage and impurity components

Component	Only PSA			PSA and heat recovery		
CO_2 volume percentage [vol%]	95.50	97.50	99.50	95.50	97.5	99.50
Shipping pressure [kPa]	2166	1882	1596	2174	1888	1599
Shipping temperature [K]	245	245	245	245	245	245

4.4. VLE Diagrams of Synthetic HIsarna Off-gas Mixtures

Vapor liquid equilibrium diagrams were constructed of all synthetic mixtures covered in Section 3.2.1. Table 4.2 summarizes these mixtures to create a clear overview.

Table 4.2: Gas composition of analyzed synthetic mixtures with 95.5, 97.5 and 99.5 vol% CO_2 for the only PSA case, containing N_2, CO and H_2 impurities, and the PSA with heat recovery case, containing N_2 and O_2 impurities. As covered in Section 3.2.1.

Component	Untreated	Only PSA			PSA and heat recovery		
Volume percentage CO_2 [vol%]	64.5	95.50	97.50	99.50	95.50	97.50	99.50
Volume percentage N_2 [vol%]	13.2	3.00	1.70	0.24	3.82	2.14	0.45
Volume percentage O_2 [vol%]	-	-	-	-	0.68	0.36	0.05
Volume percentage CO [vol%]	20.1	1.48	0.79	0.26	-	-	-
Volume percentage H_2 [vol%]	2.2	0.02	0.01	0.00	-	-	-

4.4.1. VLE Diagram of a Synthetic Untreated HIsarna Off-gas Mixture

Figure 4.5 depicts the VLE diagram of an untreated synthetic HIsarna off-gas mixture. The dashed line represents the bubble point line and the solid line represents the dew point line, the critical point is located at the point where these two lines meet. It can be noted that this mixture experiences a large two phase region due to the large volume fraction of impurities. Furthermore, the critical pressure is significantly higher than that of pure CO_2 and the bubble pressure does not decrease with a temperature decrease but instead increases. Therefore it is not possible to aid liquefaction with cooling but a liquefaction process for this mixture should instead rely on a pressure increase alone.

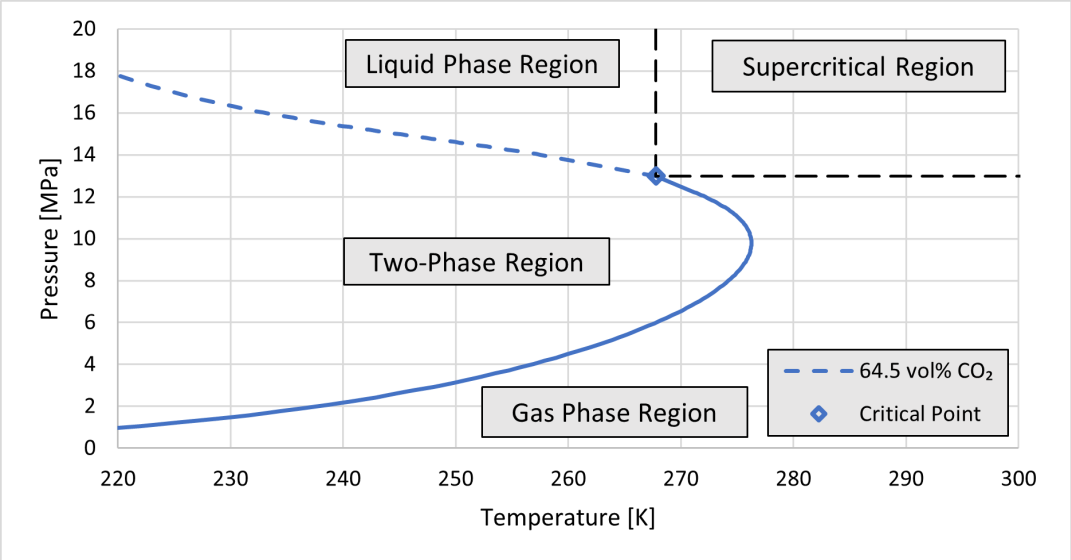

Figure 4.5: VLE diagram for the phase envelope of a synthetic HIsarna off-gas mixture with a volume fraction of 0.645 CO_2, 0.132 N_2, 0.201 CO and 0.022 H_2. The figure displays the gas, two-phase, liquid and supercritical region. Evaluated with NIST REFPROP version 10 [46].

4.4.2. VLE Diagram of Synthetic HIsarna Off-gas Mixtures After PSA

Figure 4.6 depicts the VLE diagrams of synthetic HIsarna off-gas mixtures that are purified to 95.5, 97.5 and 99.5 volume percent through PSA, this means the impurities consist of N_2, CO and H_2. The dashed line represents the bubble point line and the solid line represents the dew line and the critical point is located at the point where these lines meet, like Figure 4.5. It can be noted that size of the two-phase region is decreased with a decreasing volume fraction of impurities. Furthermore, the critical pressures experience a less significant increase and the bubble pressure decrease with temperature.

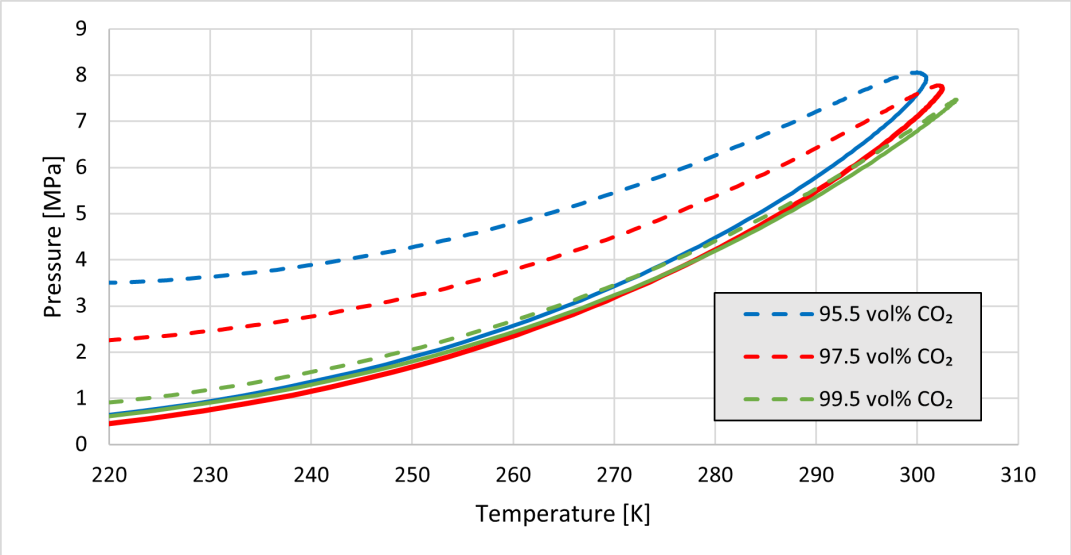

Figure 4.6: VLE diagram at the pressure range of 0 to 9 MPa and temperature range of 220 to 310 K for synthetic HIsarna off-gas mixtures purified through PSA to 0.955, 0.975 and 0.995 volume fraction CO_2 with N_2, CO and H_2 impurities. Evaluated with NIST REFPROP version 10 [46].

Figure 4.7 produces a detailed view around the proposed liquefaction temperature of 245 K. This figure depicts how the bubble pressure increases with impurity content. This figure additionally identifies that only the 99.5 vol% CO_2 is fully liquefied under a pressure of 2 MPa, this illustrates that the additional purification is a necessary part of a liquefaction system for the 95.5 and 97.5 vol% CO_2 streams.

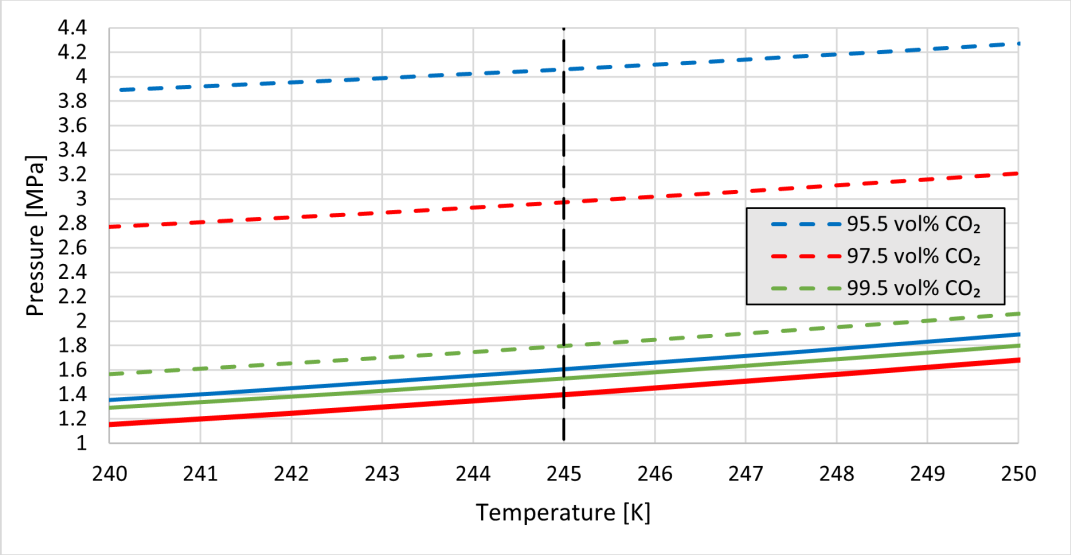

Figure 4.7: VLE diagram at the pressure range of 1.0 to 4.4 MPa and temperature range of 240 to 250 K for synthetic HIsarna off-gas mixtures purified through PSA to 0.955, 0.975 and 0.995 volume fraction CO_2 with N_2, CO and H_2 impurities. Evaluated with NIST REFPROP version 10 [46].

4.4.3. VLE Diagram of Synthetic HIsarna Off-gas Mixtures After PSA and Heat Recovery

Figure 4.8 depicts the VLE diagrams of the synthetic HIsarna off-gas mixtures that have the combustible components burned off with an excess oxygen ratio of 1.6 and is subsequently purified to 95.5, 97.5 and 99.5 volume percent through PSA. The impurities consist of N_2 and O_2. It can be noted that the difference of impurity components does not significantly influence the phase behavior of the mixture compared to Figure 4.6. When comparing these VLE diagrams in detail it can however be noticed that the nitrogen and oxygen impurity combination does increase the bubble and critical pressure slightly.

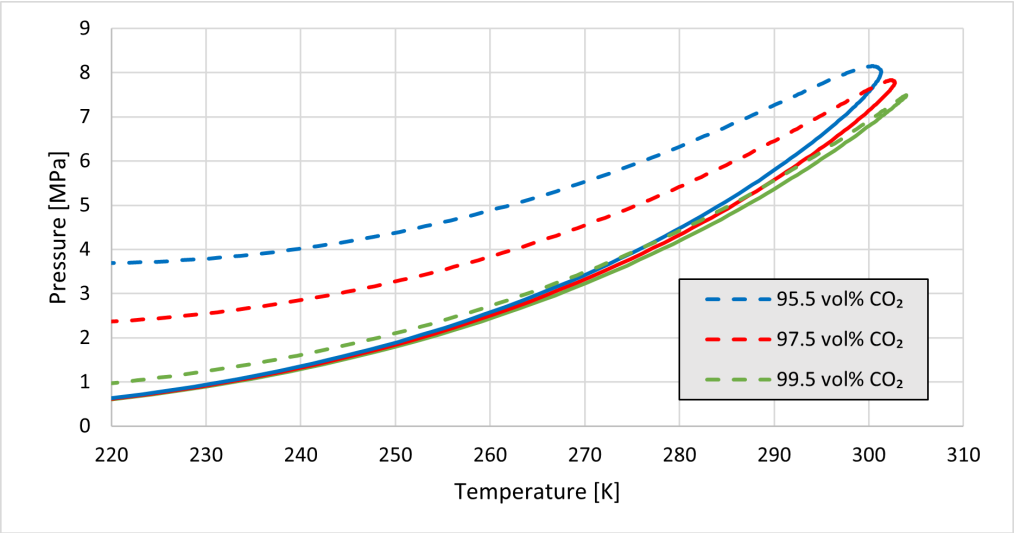

Figure 4.8: VLE diagram at the pressure range of 0 to 9 MPa and temperature range of 220 to 310 K for synthetic HIsarna off-gas mixtures purified through PSA to 0.955, 0.975 and 0.995 volume fraction CO_2 with N_2 and O_2 impurities. Evaluated with NIST REFPROP version 10 [46].

Figure 4.9 produces a detailed view around the proposed liquefaction temperature of 245 K. It can be noted that only the 99.5 vol% CO_2 stream has a bubble pressure under 2 MPa, like the case with N_2, CO and H_2. Furthermore, when comparing this figure with Figure 4.7, the increased bubble pressure is more visible.

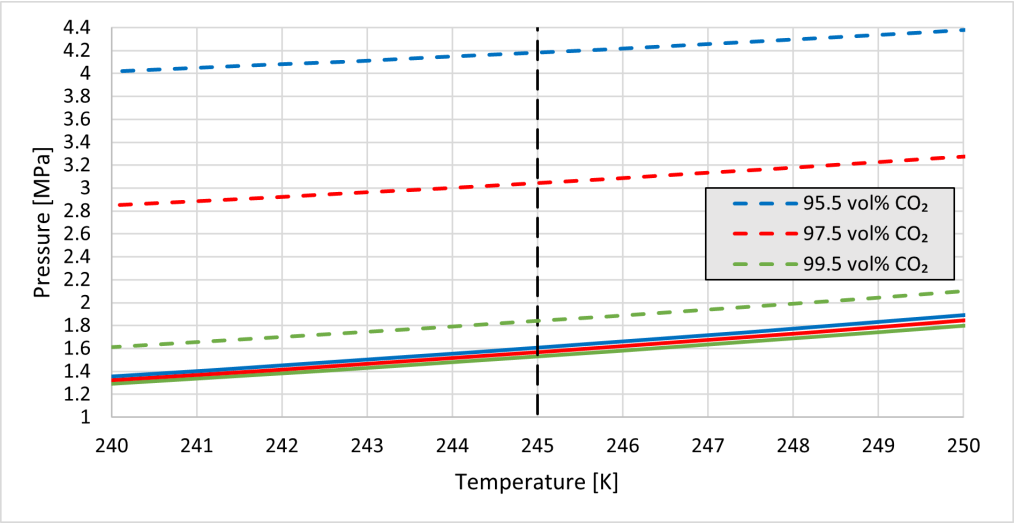

Figure 4.9: VLE diagram at the pressure range of 1.0 to 4.4 MPa and temperature range of 240 to 250 K for synthetic HIsarna off-gas mixtures purified through PSA to 0.955, 0.975 and 0.995 volume fraction CO_2 with N_2 and O_2 impurities. Evaluated with NIST REFPROP version 10 [46].

4.5. Open Liquefaction System

Figure 4.10 shows the Aspen HYSYS model, as detailed in Section 3.6 that was used to create the results for this section. The stream numbers specified in tables 4.3 through 4.8 corresponds to the numbering in this Figure 4.10.

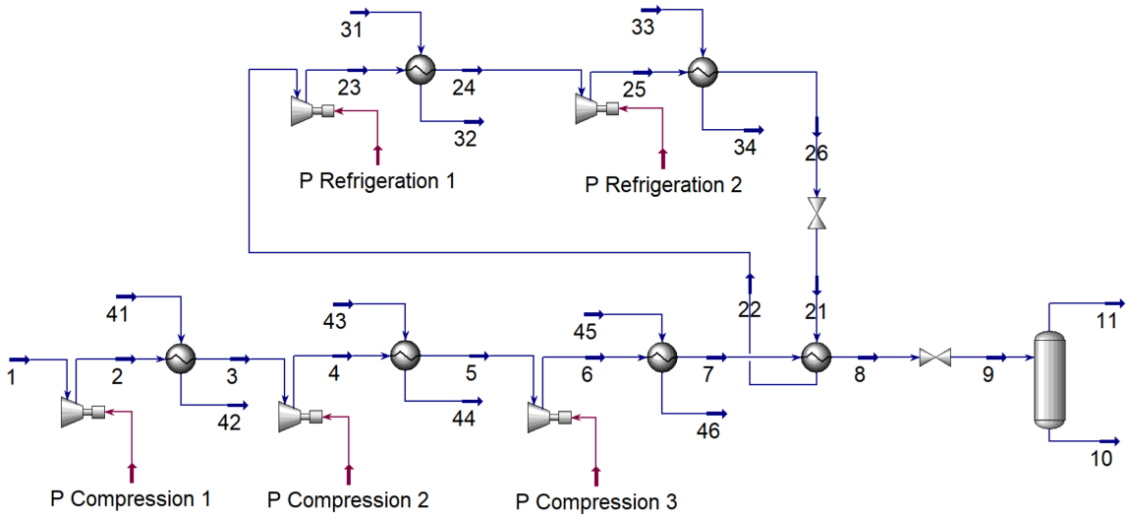

Figure 4.10: Aspen HYSYS model of the open liquefaction system displaying the various stream numbers as referenced in the tables of Section 4.5.

4.5.1. Open system with N_2, CO and H_2 impurities

The open liquefaction model as specified in Section 3.6 was used to evaluate the liquefaction energy for 95.5, 97.5 and 99.5 vol% CO_2 mixtures with N_2, CO and H_2 impurities. The models were evaluated with the operating conditions specified in Section 4.3 to produce the results shown in tables 4.3, 4.4 and 4.5 for the 95.5, 97.5 and 99.5 vol% CO_2 mixture respectively. Figure 4.11 gives an overview of the energy requirements per system component, this consists of the three compressor stages and two refrigeration cycle compressors for the open liquefaction system.

Table 4.3: Stream properties, as numbered in Figure 4.10, of the open liquefaction system evaluated with an input stream of 95.5 vol% CO_2 with N_2, CO and H_2 impurities.

Stream Number	1	3	5	7	8	10	11	21	22
Vapor Fraction [-]	1.00	1.00	1.00	1.00	0.01	0.00	1.00	0.19	1.00
Temperature [K]	30	35	35	35	-15	-28	-28	-20	-20
Pressure [kPa]	100	357	1274	4545	4545	2167	2167	190	190
Mass Flow [kg · s^{-1}]	3.64	3.64	3.64	3.64	3.64	3.17	0.47	1.01	1.01

Table 4.4: Stream properties, as numbered in Figure 4.10, of the open liquefaction system evaluated with an input stream of 97.5 vol% CO_2 with N_2, CO and H_2 impurities.

Stream Number	1	3	5	7	8	10	11	21	22
Vapor Fraction	1.00	1.00	1.00	1.00	0.01	0.00	1.00	0.19	1.00
Temperature [K]	30	35	35	35	-15	-28	-28	-20	-20
Pressure [kPa]	100	328	1076	3530	3530	1882	1882	190	190
Mass Flow [kg · s^{-1}]	3.59	3.59	3.59	3.59	3.59	3.17	0.41	1.05	1.05

Table 4.5: Stream properties, as numbered in Figure 4.10, of the open liquefaction system evaluated with an input stream of 99.5 vol% CO_2 with N_2, CO and H_2 impurities.

Stream Number	1	3	5	7	8	10	11	21	22
Vapor Fraction [-]	1.00	1.00	1.00	1.00	0.01	0.00	1.00	0.19	1.00
Temperature [K]	30	35	35	35	-15	-28	-28	-20	-20
Pressure [kPa]	100	293	860	2522	2522	1596	1596	190	190
Mass Flow [kg · s^{-1}]	3.54	3.54	3.54	3.54	3.54	3.17	0.36	1.08	1.08

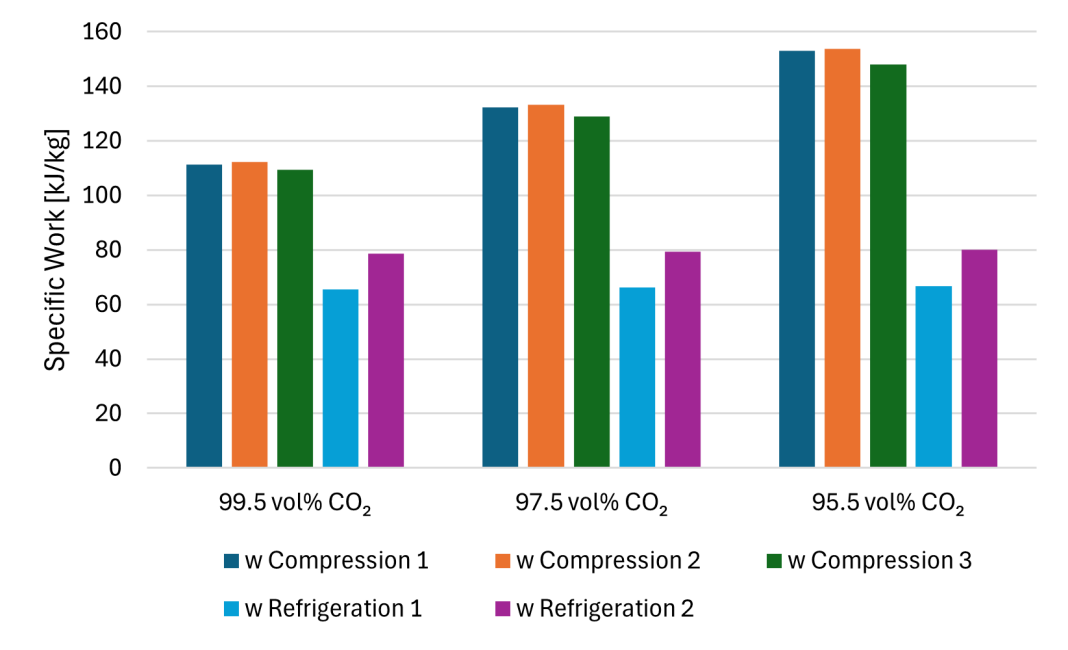

Figure 4.11: Energy requirements per compression and refrigeration compressor expressed in kJ per liquefied kilogram for an open liquefaction system which utilizes a feed-stream of 95.5, 97.5 and 99.5 vol% CO_2 with N_2, CO and H_2 impurities. Evaluated with Aspen HYSYS version 12.

4.5.2. Open system with N_2 and O_2 impurities

The open liquefaction model as specified in Section 3.6 was used to evaluate the liquefaction energy for 95.5, 97.5 and 99.5 vol% CO_2 mixtures with N_2 and O_2 impurities. The models were evaluated with the operating conditions specified in Section 4.3 to produce the results shown in tables 4.6, 4.7 and 4.8 for the 95.5, 97.5 and 99.5 vol% CO_2 mixture respectively. Figure 4.12 gives an overview of the energy requirements per system component, this consists of the three compressor stages and two refrigeration cycle compressors for the open liquefaction system.

Table 4.6: Stream properties, as numbered in Figure 4.10, of the open liquefaction system evaluated with an input stream of 95.5 vol% CO_2 with N_2 and O_2 impurities.

Stream Number	1	3	5	7	8	10	11	21	22
Vapor Fraction [-]	1.00	1.00	1.00	1.00	0.01	0.00	1.00	0.19	1.00
Temperature [K]	30	35	35	35	-15	-28	-28	-20	-20
Pressure [kPa]	100	359	1288	4625	4625	2174	2174	190	190
Mass Flow [kg · s^{-1}]	3.65	3.65	3.65	3.65	3.65	3.17	0.48	0.99	0.99

Table 4.7: Stream properties, as numbered in Figure 4.10, of the open liquefaction system evaluated with an input stream of 97.5 vol% CO_2 with N_2 and O_2 impurities.

Stream Number	1	3	5	7	8	10	11	21	22
Vapor Fraction [-]	1.00	1.00	1.00	1.00	0.01	0.00	1.00	0.19	1.00
Temperature [K]	30	35	35	35	-15	-28	-28	-20	-20
Pressure [kPa]	100	329	1084	3568	3568	1888	1888	190	190
Mass Flow [kg · s^{-1}]	3.59	3.59	3.59	3.59	3.59	3.17	0.42	1.03	1.03

Table 4.8: Stream properties, as numbered in Figure 4.10, of the open liquefaction system evaluated with an input stream of 99.5 vol% CO_2 with N_2 and O_2 impurities.

Stream Number	1	3	5	7	8	10	11	21	22
Vapor Fraction [-]	1.00	1.00	1.00	1.00	0.01	0.00	1.00	0.19	1.00
Temperature [K]	30	35	35	35	-15	-28	-28	-20	-20
Pressure [kPa]	100	294	864	2540	2540	1599	1599	190	190
Mass Flow [kg · s^{-1}]	3.53	3.53	3.53	3.53	3.53	3.17	0.36	1.07	1.07

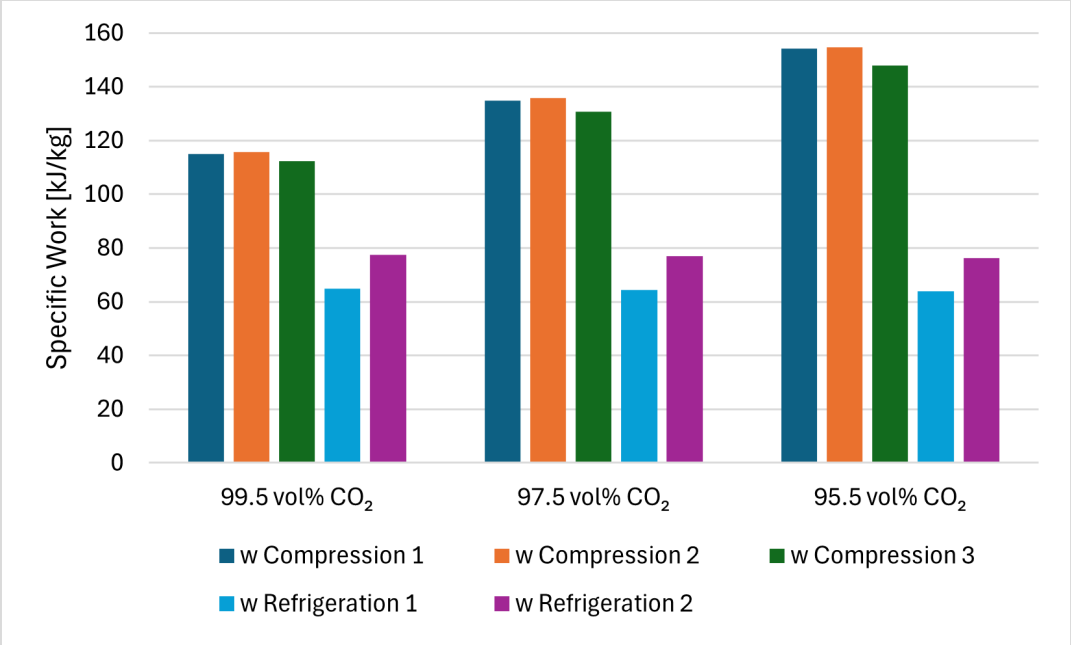

Figure 4.12: Energy requirements per compression and refrigeration compressor expressed in kJ per liquefied kilogram for an open liquefaction system which utilizes a feed-stream of 95.5, 97.5 and 99.5 vol% CO_2 with N_2 and O_2 impurities. Evaluated with Aspen HYSYS version 12.

4.6. Closed Liquefaction System

Figure 4.13 shows the Aspen HYSYS model, as detailed in Section 3.5 that was used to create the results for this section. The stream numbers specified in tables 4.9 and 4.14 corresponds to the numbering in this figure.

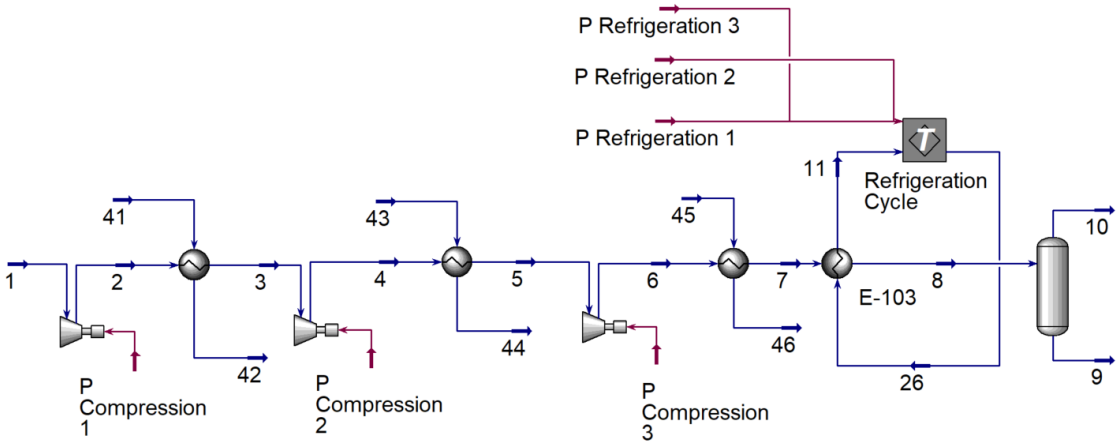

Figure 4.13: Aspen HYSYS model of the closed liquefaction system displaying the various stream numbers as referenced in the tables of Section 4.5.

4.6.1. Closed system with N_2, CO and H_2 impurities

The closed liquefaction model as specified in Section 3.5 was used to evaluate the liquefaction energy for 95.5, 97.5 and 99.5 vol% CO_2 mixtures with N_2, CO and H_2 impurities. The models were evaluated with the operating conditions specified in Section 4.3 to produce the results shown in tables 4.9, 4.10 and 4.11 for the 95.5, 97.5 and 99.5 vol% CO_2 mixture respectively. Figure 4.14 gives an overview of the energy requirements per system component, this consists of the three compressor stages and three refrigeration cycle compressors for the closed liquefaction system.

Table 4.9: Stream properties, as numbered in Figure 4.13, of the closed liquefaction system evaluated with an input stream of 95.5 vol% CO_2 with N_2, CO and H_2 impurities.

Stream Number	1	3	5	7	8	9	10	11	26
Vapor Fraction [-]	1.00	1.00	1.00	1.00	0.14	0.00	1.00	1.00	0.06
Temperature [K]	30	35	35	35	-28	-28	-28	-33	-33
Pressure [kPa]	100	279	779	2174	2174	2174	2174	103	103
Mass Flow [$kg \cdot s^{-1}$]	3.64	3.64	3.64	3.64	3.64	3.17	0.47	0.91	0.91

Table 4.10: Stream properties, as numbered in Figure 4.13, of the closed liquefaction system evaluated with an input stream of 97.5 vol% CO_2 with N_2, CO and H_2 impurities.

Stream Number	1	3	5	7	8	9	10	11	26
Vapor Fraction [-]	1.00	1.00	1.00	1.00	0.12	0.00	1.00	1.00	0.06
Temperature [K]	30	35	35	35	-28	-28	-28	-33	-33
Pressure [kPa]	100	266	709	1888	1888	1888	1888	103	103
Mass Flow [$kg \cdot s^{-1}$]	3.58	3.58	3.58	3.58	3.58	3.17	0.41	0.92	0.92

Table 4.11: Stream properties, as numbered in Figure 4.13, of the closed liquefaction system evaluated with an input stream of 99.5 vol% CO_2 with N_2, CO and H_2 impurities.

Stream Number	1	3	5	7	8	9	10	11	26
Vapor Fraction [-]	1.00	1.00	1.00	1.00	0.1	0.00	1.00	1.00	0.06
Temperature [K]	30	35	35	35	-28	-28	-28	-33	-33
Pressure [kPa]	100	251	635	1599	1599	1599	1599	103	103
Mass Flow [$kg \cdot s^{-1}$]	3.51	3.51	3.51	3.51	3.51	3.17	0.34	0.92	0.92

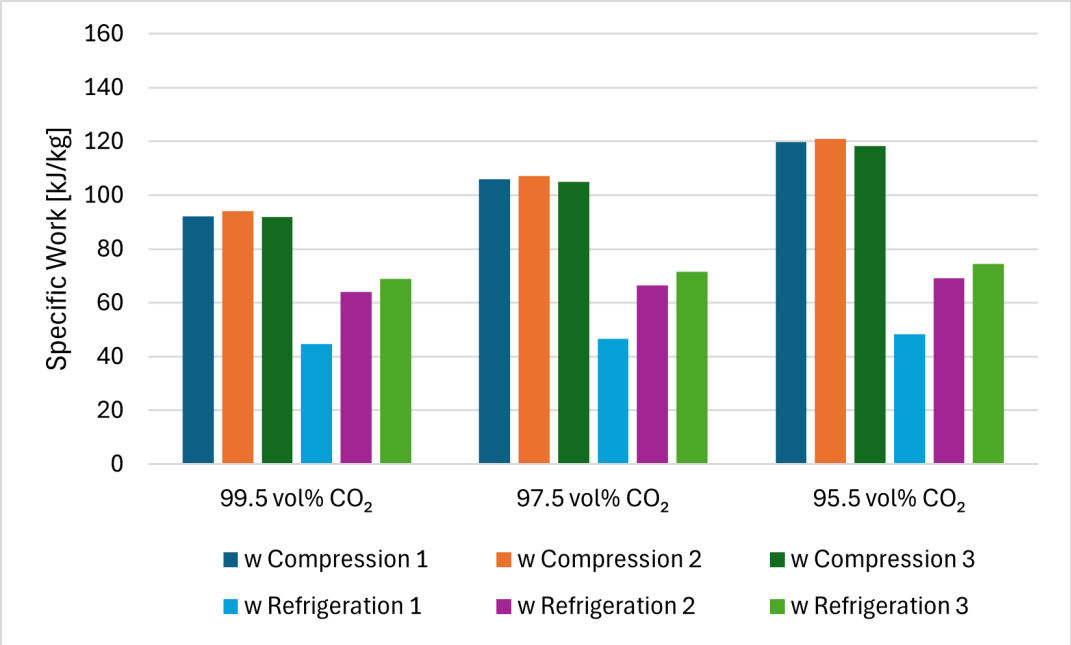

Figure 4.14: Energy requirements per compression and refrigeration compressor expressed in kJ per liquefied kilogram for a closed liquefaction system which utilizes a feed-stream of 95.5, 97.5 and 99.5 vol% CO_2 with N_2, CO and H_2 impurities. Evaluated with Aspen HYSYS version 12.

4.6.2. Closed system with N_2 and H_2 impurities

The closed liquefaction model as specified in Section 3.5 was used to evaluate the liquefaction energy for 95.5, 97.5 and 99.5 vol% CO_2 mixtures with N_2 and O_2 impurities. The models were evaluated with the operating conditions specified in Section 4.3 to produce the results shown in tables 4.12, 4.13 and 4.14 for the 95.5, 97.5 and 99.5 vol% CO_2 mixture respectively. Figure 4.14 gives an overview of the energy requirements per system component, this consists of the three compressor stages and three refrigeration cycle compressors for the closed liquefaction system.

Table 4.12: Stream properties, as numbered in Figure 4.13, of the closed liquefaction system evaluated with an input stream of 95.5 vol% CO_2 with N_2 and O_2 impurities.

Stream Number	1	3	5	7	8	9	10	11	26
Vapor Fraction	1.00	1.00	1.00	1.00	0.14	0.00	1.00	1.00	0.06
Temperature [K]	30	35	35	35	-28	-28	-28	-33	-33
Pressure [kPa]	100	279	779	2174	2174	2174	2174	103	103
Mass Flow [kg · s^{-1}]	3.65	3.65	3.65	3.65	3.65	3.17	0.48	0.9	0.9

Table 4.13: Stream properties, as numbered in Figure 4.13, of the closed liquefaction system evaluated with an input stream of 97.5 vol% CO_2 with N_2 and O_2 impurities.

Stream Number	1	3	5	7	8	9	10	11	26
Vapor Fraction	1.00	1.00	1.00	1.00	0.12	0.00	1.00	1.00	0.06
Temperature [K]	30	35	35	35	-28	-28	-28	-33	-33
Pressure [kPa]	100	266	709	1888	1888	1888	1888	103	103
Mass Flow [kg · s^{-1}]	3.59	3.59	3.59	3.59	3.59	3.17	0.42	0.91	0.91

Table 4.14: Stream properties, as numbered in Figure 4.13, of the closed liquefaction system evaluated with an input stream of 99.5 vol% CO_2 with N_2 and O_2 impurities.

Stream Number	1	3	5	7	8	9	10	11	26
Vapor Fraction	1.00	1.00	1.00	1.00	0.1	0.00	1.00	1.00	0.06
Temperature [K]	30	35	35	35	-28	-28	-28	-33	-33
Pressure [kPa]	100	251	635	1599	1599	1599	1599	103	103
Mass Flow [kg · s^{-1}]	3.53	3.53	3.53	3.53	3.53	3.17	0.36	0.91	0.91

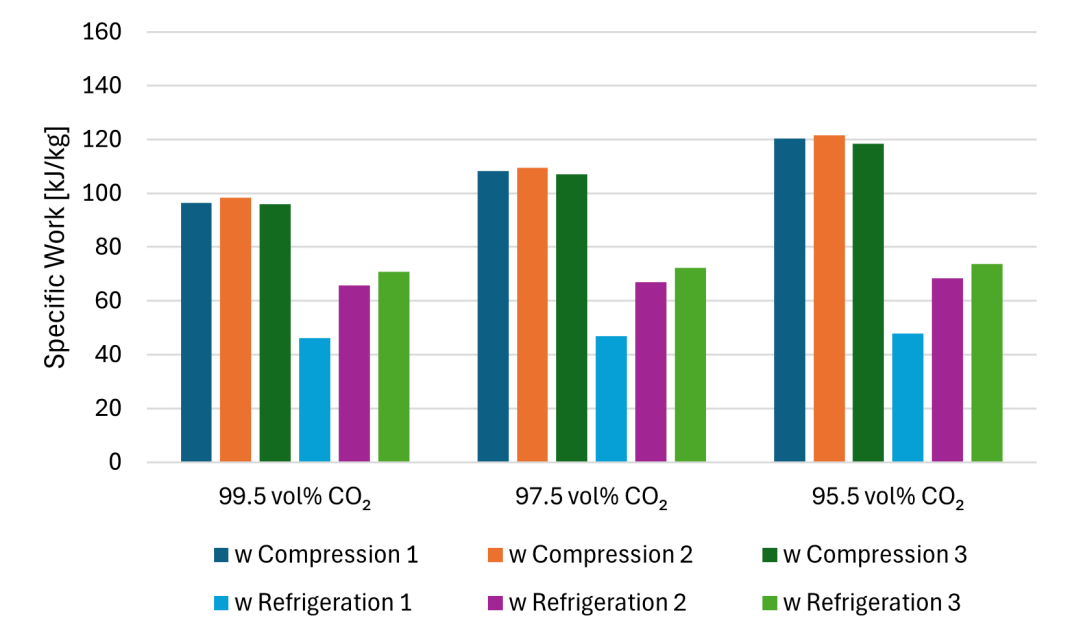

Figure 4.15: Energy requirements per compression and refrigeration compressor expressed in kJ per liquefied kilogram for an closed liquefaction system which utilizes a feed-stream of 95.5, 97.5 and 99.5 vol% CO_2 with N_2 and O_2 impurities. Evaluated with Aspen HYSYS version 12.

4.7. Liquefaction Systems Comparison

Section 4.5 and 4.6 presented the results obtained for the open closed liquefaction systems respectively with the energy requirements per equipment unit depending on input stream composition. These systems produce different output stream compositions based on the input stream. The output stream composition does not vary between closed or open liquefaction systems because the output conditions are kept equal between these systems. Table 4.15 presents the results for the output stream compositions based on input stream compositions.

Table 4.15: Stream composition after liquefaction for input mixtures of 95.5, 97.5 and 99.5 vol% CO_2 for the only PSA case, containing N_2, CO and H_2 impurities, and the PSA with heat recovery case, containing N_2 and O_2 impurities.

Component	Only PSA			PSA and heat recovery		
Input volume percentage CO_2 [vol%]	95.50	97.50	99.50	95.50	97.50	99.50
Output volume percentage CO_2 [vol%]	98.92	99.40	99.88	98.87	99.37	99.87
Volume percentage N_2 [vol%]	0.92	0.52	0.11	0.71	0.40	0.06
Volume percentage O_2 [vol%]	0.17	0.09	0.01	-	-	-
Volume percentage CO [vol%]	-	-	-	0.42	0.22	0.07
Volume percentage H_2 [vol%]	0.00	0.00	0.00	-	-	-

Figure 4.16 is produced to more accurately compare the energy requirements of different liquefaction systems varying with input stream composition. The closed liquefaction system is more energy efficient than the open liquefaction system across all CO_2 purities. Furthermore, the CO_2-rich stream that has gone through a heat recovery step, so with N_2 and O_2 impurities instead of N_2, CO and H_2, is slightly more energy efficient to liquefy. However, this difference is negligible compared to the increase of liquefaction energy resulting from higher CO_2 purity in the feed stream.

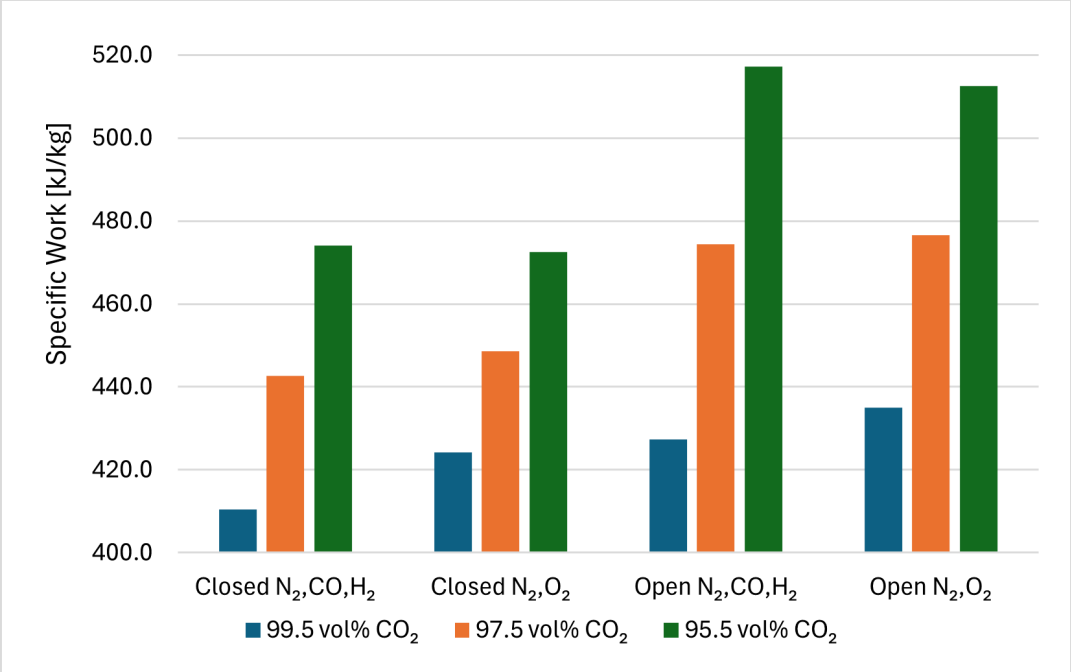

Figure 4.16: Liquefaction energy expressed in kJ per kg of product stream for open and closed liquefaction system with 95.5, 97.5 and 99.5 vol% CO_2 with N_2 and O_2 or N_2, CO and H_2 impurities.

4.8. Results and Discussion Summary

This chapter started with Section 4.1 presenting the a comparison of the different analyzed thermodynamic models for two impurity cases. Out of PC-SAFT, GERG-2008, CPA and PR EoS's it was found that PC-SAFT performed the best for the case of CO_2 with N_2 and O_2 impurities. CPA was found to be the most accurate option for the case with N_2, CO and H_2 impurities. This could be explained due to the H_2 impurity which is a polar component and the fact that CPA is an EoS which is developed to model mixtures with polar components. Section 4.2 subsequently explores the Joule-Thomson inversion temperature for the different analyzed mixtures in this research. It was found that the difference between the two impurity cases is relatively small compared to the difference originating from varying the CO_2 volume fraction. A decrease of volume fraction of impurities produces an increase of inversion temperature. Therefore the minimum liquefying temperature that can be reached through a Joule-Thomson valve in a open liquefaction system is determined by the 99.5 vol% CO_2 case. Section 4.3 determined the operating conditions per stream composition. The shipping temperature was set to 245 K for all streams based on the results found for the Joule-Thomson inversion temperature and the selection of ammonia as a refrigerant. The shipping pressures are determined with the open liquefaction system since this system is more restricting than the closed liquefaction system due to the Joule-Thomson valve's maximum inlet pressure which varies per stream composition. The shipping pressures were set to be 2166, 1882 and 1596 kPa respectively for the 95.5, 97.5 and 99.5 vol% CO_2 streams respectively in the case of N_2, CO and H_2 impurities. The shipping pressures were determined to be slightly higher in the case of N_2 and O_2 case, namely 2174, 1888 and 1599 kPa.

Section 4.4 showed the VLE diagrams which were constructed for the different gas compositions. The first mixture that was analyzed was untreated HIsarna off-gas with 64.5 vol% CO_2 and N_2, CO and H_2 impurities. It was identified that this mixture does not have a bubble point line pressure that decreases with temperature and therefore can only be liquefied with a pressure increase till above the critical point of this mixture. This results showed that the HIsarna off-gas needs to be purified before ship transport is possible. Section 4.4.2 produced VLE diagrams of the full two-phase region and a detailed view around the shipping conditions for 95.5, 97.5 and 99.5 vol% CO_2 mixtures with N_2, CO and H_2 impurities. It was found that after a purification step that the 99.5 vol% CO_2 mixture is the only mixture that has a bubble point pressure below 2 MPa at 245 K, which is reported as a maximum economically viable shipping pressure. Section 4.4.3 produced the same diagrams for 95.5, 97.5 and 99.5 vol% CO_2 mixtures with N_2 and O_2 impurities. These results showed a slightly increased bubble point line pressure for all mixtures but the 99.5 vol% CO_2 mixture still has a bubble point pressure under 2 MPa at 245 K. Sections 4.5 and 4.6 presented the results of the Aspen HYSYS models for the open and closed liquefaction systems respectively. These sections analyzed the six input mixtures consisting of 95.5, 97.5 and 99.5 vol% CO_2 mixtures with N_2, CO H_2 or N_2 and O_2 impurities for both systems. The sections provide tables with vapor fraction, temperature, pressure and mass flows for certain selected streams of the Aspen HYSYS models. Furthermore they also provide graphs which show the energy requirements per kilogram of liquefied product for the different input mixtures. These graphs show that this energy requirements decrease with an increase of the input CO_2 volume fraction for all impurity an system variations. Section 4.7 presents an overview graph to accurately compare these results. It shows that an open liquefaction system is more energy intensive than a closed liquefaction system. Furthermore, the cases with N_2 and O_2 impurities show a slightly lower energy requirement but this is negligible compared to the difference between liquefaction systems. Section 4.7 also compare the stream compositions of the liquefied product, the liquefied product has a higher volume fraction CO_2 than the input stream due to the separation step at the system outlet. The noncondensable impurities make up a larger volume fraction in the gaseous purge stream which therefore increases the CO_2 volume fraction in the liquefied outlet. Table 4.15 shows that the 95.5 vol% stream is purified to 98.9 vol%, the 97.5 vol% stream increases to 99.4 vol% and the 99.5 vol% stream increases to 99.9 vol%.

5

Techno-Economic Analysis

5.1. Liquefaction System Costs

This section presents the results for the techno-economic analysis of the liquefaction systems based on the equations specified in Section 3.7. The costs were analyzed for the 100, 200 and 400 kt annual liquefaction capacity, as specified in Section 3.7.1. Instead of analyzing all gas composition variations, the decision was made to only analyze the 95.5 and 99.5 vol% CO_2 with N_2, CO and H_2 cases. The energy requirements and shipping pressure were found to not vary significantly between the two impurity variations in Chapter 4. It is assumed that the cost results will also not significantly vary since the energy requirements and shipping pressure largely influence the economic calculations. The N_2 and O_2 impurity case is therefore omitted, as the the differences are expected to be negligible. This keeps the analysis concise and clear.

5.1.1. Closed Liquefaction System

Figure 5.1 and 5.2 show the OPEX and CAPEX for the closed liquefaction system respectively. It can be noted that both the OPEX and CAPEX do not vary significantly between the 95.5 and 99.5 vol% cases but do increase with scale. While the OPEX increases linearly with scale, the CAPEX increases sublinearly with scale indicating economies of scale.

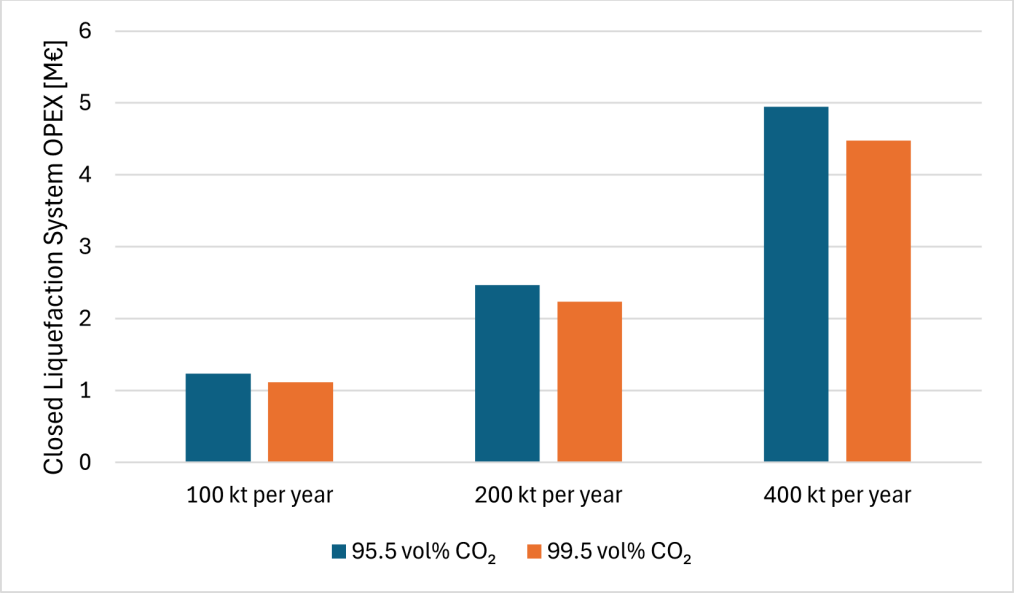

Figure 5.1: Annual OPEX in million € for a closed liquefaction system producing 100, 200 or 400 kt CO_2-rich liquid per year based on a input stream of 95.5 or 99.5 vol% CO_2 with N_2, CO and H_2 impurities.

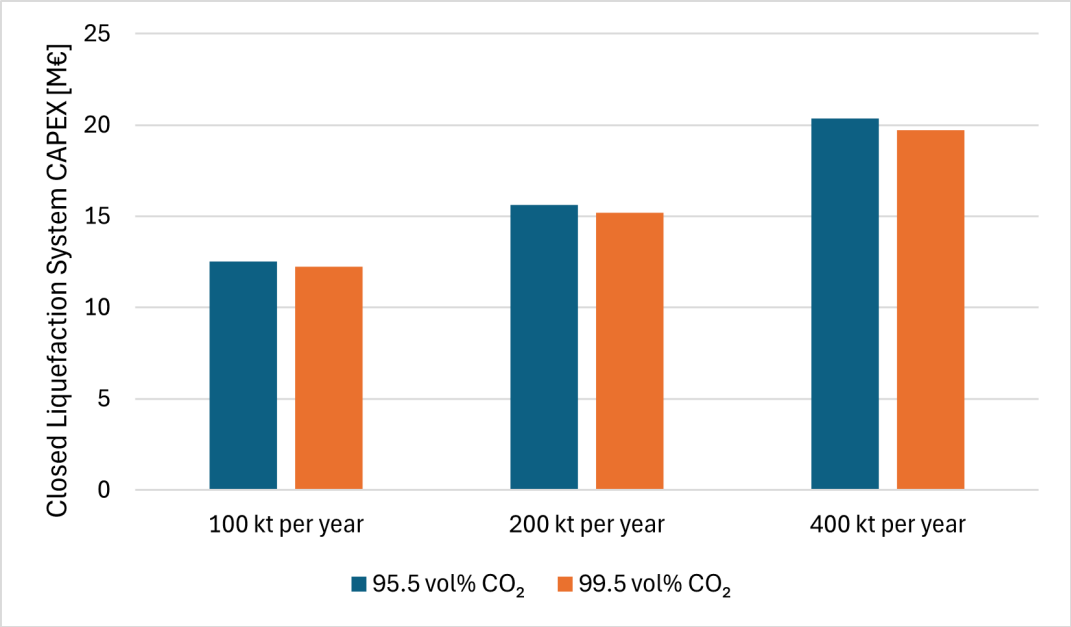

Figure 5.2: CAPEX in million € for a closed liquefaction system producing 100, 200 or 400 kt CO_2-rich liquid per year based on a input stream of 95.5 or 99.5 vol% CO_2 with N_2, CO and H_2 impurities.

5.1.2. Open Liquefaction System

Figure 5.3 and 5.5 show the OPEX and CAPEX for the open liquefaction system respectively. It can be noted that both the OPEX and CAPEX do not vary significantly between the 95.5 and 99.5 vol% cases but do increase with scale, like the closed liquefaction system. For this system the OPEX also increases linearly with scale and the CAPEX increases sublinearly.

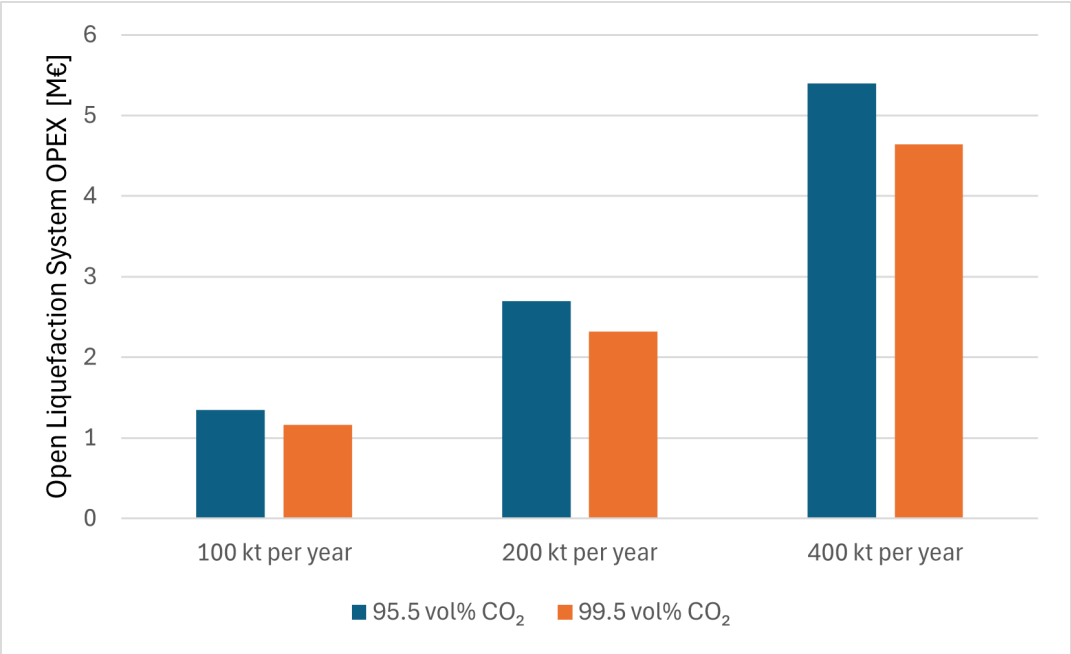

Figure 5.3: Annual OPEX in million € for an open liquefaction system producing 100, 200 or 400 kt CO_2-rich liquid per year based on a input stream of 95.5 or 99.5 vol% CO_2 with N_2, CO and H_2 impurities.

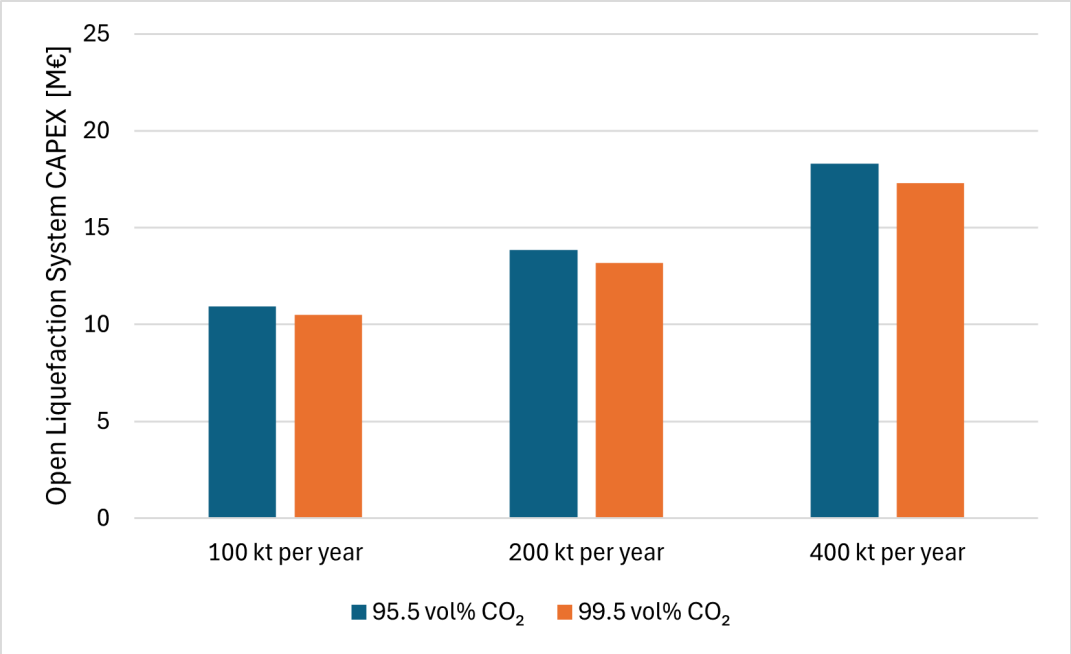

Figure 5.4: CAPEX in million € for an open liquefaction system producing 100, 200 or 400 kt CO_2-rich liquid per year based on a input stream of 95.5 or 99.5 vol% CO_2 with N_2, CO and H_2 impurities.

5.2. Transportation Costs

Figure 5.5 and 5.6 show the OPEX and CAPEX of the transportation as specified in Section 3.7.3. It can be noted that the OPEX scales slightly sublinear with process scale and the 99.5 vol% CO_2 case is more economically favorable than the 95.5 vol% CO_2 case due to the lower shipping pressure. The CAPEX stays fairly constant with scale, this is due to the fact that the CAPEX is dominated by the buffer storage cost which is dependent on ship size and not the number of ships. For the CAPEX it can also be noted that the 99.5 vol% CO_2 case is more economically favorable than the 95.5 vol% CO_2 case, resulting from the lower shipping pressure such as for the OPEX.

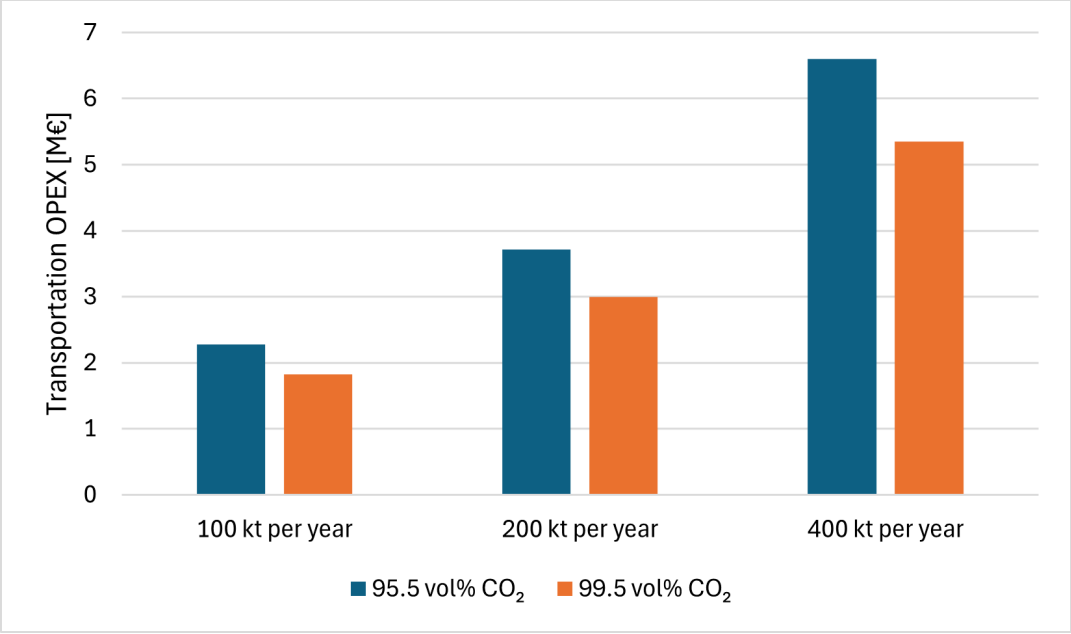

Figure 5.5: Annual OPEX in million € for shipping and transport infrastructure processing 100, 200 or 400 kt CO_2-rich liquid per year based on a input stream of 95.5 or 99.5 vol% CO_2 with N_2, CO and H_2 impurities.

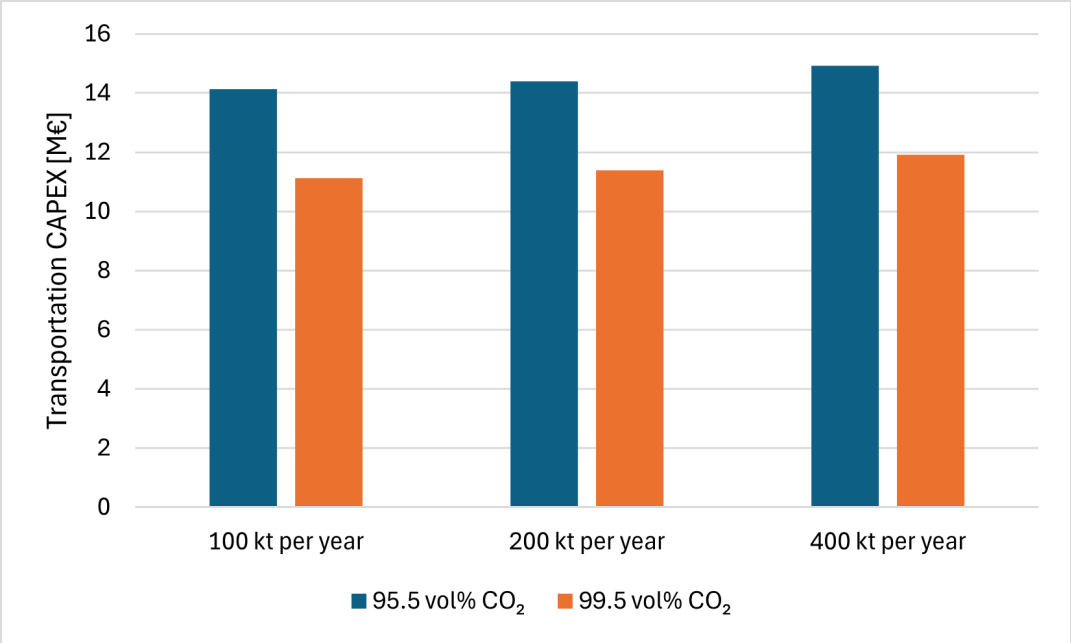

Figure 5.6: CAPEX in million € for shipping and transport infrastructure processing 100, 200 or 400 kt CO_2-rich liquid per year based on a input stream of 95.5 or 99.5 vol% CO_2 with N_2, CO and H_2 impurities.

5.3. Total Cost

Figure 5.7 and 5.8 show the total OPEX and CAPEX respectively that are identified in this chapter. It can be noted that the closed system has a slightly lower OPEX but also a slightly higher CAPEX compared to the open system. The difference between the 95.5 vol% and 99.5 vol% CO_2 cases is also visible in these figures, as identified earlier in this chapter. The 99.5 vol% case has a lower OPEX and CAPEX for both system variations.

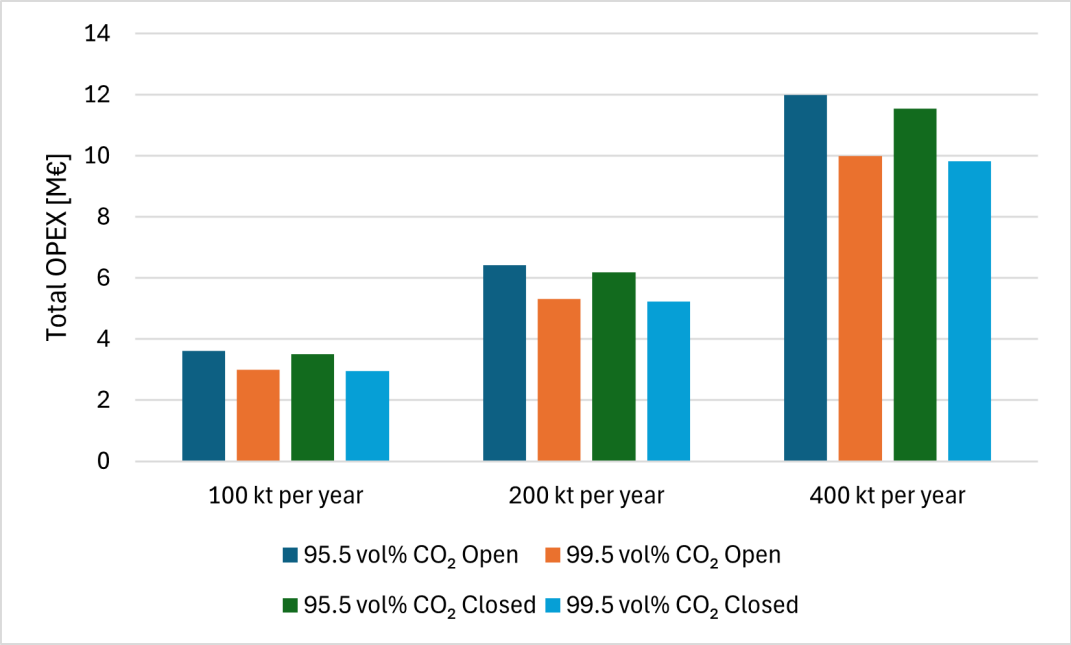

Figure 5.7: Total OPEX in million € for transportation infrastructure and liquefaction equipment processing 100, 200 or 400 kt CO_2-rich liquid per year based on a input stream of 95.5 or 99.5 vol% CO_2 with N_2, CO and H_2 impurities.

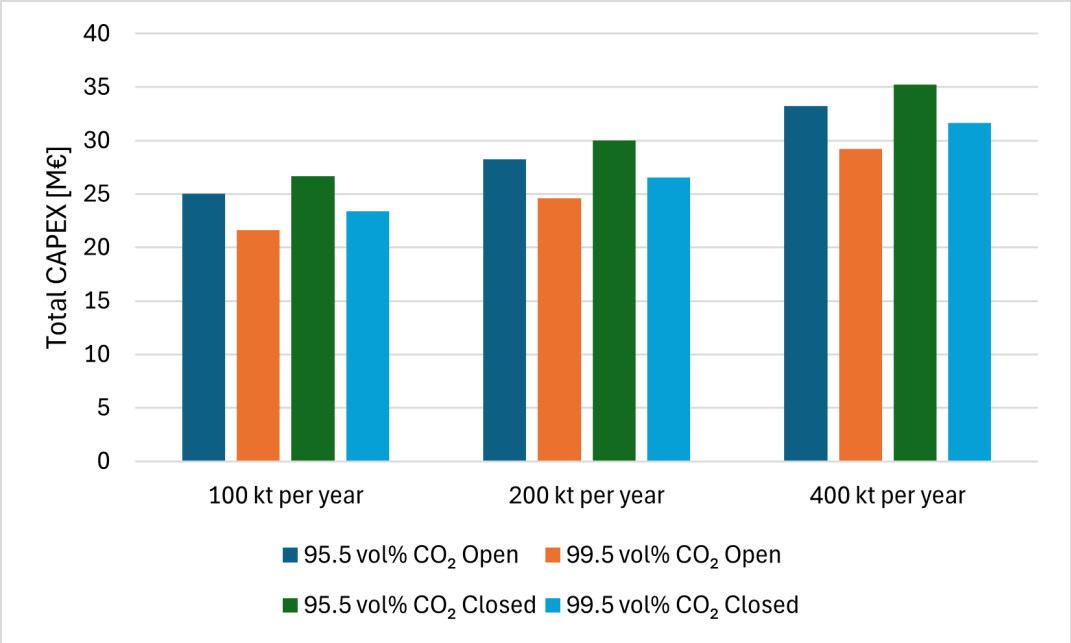

Figure 5.8: Total CAPEX in million € for transportation infrastructure and liquefaction equipment processing 100, 200 or 400 kt CO_2-rich liquid per year based on a input stream of 95.5 or 99.5 vol% CO_2 with N_2, CO and H_2 impurities.

5.4. Techno-Economic Analysis Summary

This chapter presented the results of the techno-economic analysis. The analysis was executed for 95.5 and 99.5 vol% CO_2 gas streams with N_2, CO and H_2 impurities. The 95.5 and 99.5 vol% CO_2 gas streams were evaluated for closed and open liquefaction systems in Section 5.1.1 and 5.1.2 respectively. These cases were evaluated at a scale of 100, 200 and 400 kt/y scales producing a total of twelve cases. The cases with N_2 and O_2 were not analyzed to not further increase the number of cases. Chapter 4 found that energy requirements differences between both impurity components cases are relatively small, therefore it was assumed that the costs will also not differ significantly. Section 5.1.1 and 5.1.2 present the OPEX and CAPEX for the described cases, these results found that the OPEX scales linearly and CAPEX scales sublinearly with process scale for both closed and open liquefaction systems. Both systems furthermore displayed an increased OPEX and CAPEX for the 95.5 vol$ CO_2 cases. This increase cost can be explained due to the higher operating pressure in combination with the larger purge stream. The larger purge stream increases the input mass flow to produce the same liquefied output mass flow. This higher mass flow increases the work needed to be done by the compressors and increases equipment size, therefore both OPEX and CAPEX increase. Section 5.2 focused on the transportation costs which consists of buffer storage, loading facilities and ship transport. It found that OPEX scales linearly but the OPEX only increases slightly with process scale. CAPEX is dominated by the buffer storage cost, this cost is determined by the buffer storage capacity. The capacity is determined by the capacity of the CO_2 transporting ship and therefore was kept constant between the process scales. The slight increase comes from the loading facilities which do scale with yearly capacity. Furthermore, it was identified that the 95.5 vol% CO_2 case has a higher OPEX and CAPEX, this can be explained due to the higher transport pressure. This higher transport pressure increases the OPEX and OPEX of the buffer storage as well as for the transport ship which produce the increased costs. Section 5.3 concludes by giving a graph which compares the total OPEX and CAPEX for all twelve cases. This comparison makes clear that a closed liquefaction system has a smaller OPEX but higher CAPEX compared to an open liquefaction system. Furthermore, the total costs show that the OPEX increases almost linear but the CAPEX increases sublinear. This indicates that these systems benefit from economies of scale.

6

Conclusions and Recommendations

This work aimed to determine the energy requirements and costs of transporting CO_2-rich mixtures derived from steelwork off-gases. The stream composition and water content of the off-gas after pretreatment was first identified to answer this research question. The focus was put on HIsarna off-gas which has a CO_2 volume percentage of 65 after drying. It was found that this is too low for ship transport due to the high bubble line pressure at this composition. Therefore the off-gas needs to be pretreated, three synthetic mixtures of 95.5, 97.5 and 99.5 volume percent CO_2, evaluated with a PSA model, were selected. It furthermore distinguished between two cases were the HIsarna off-gas is treated without intermediate step or were the off-gas combustible components were combusted for heat recovery with excess oxygen. These cases therefore included N_2, CO and H_2 or N_2 and O_2 impurities. The water content of these mixtures were found to be negligible due to the PSA step were the gas needs to be dried before this process and any remaining moisture gets trapped in this unit.

Pressure temperature diagrams of the phase behavior were constructed for the six synthetic mixtures. Based on these diagrams it can be concluded that only the 99.5 volume percentage CO_2 mixture, for both impurities cases, can be liquefied below a pressure of 2 MPa at 245 K. The literature review concluded that a pressure significantly higher than 2 MPa is not economically feasible for liquid CO_2 transport by ship. Therefore it was concluded that the design of a liquefaction system should include an additional purification step to use the 95.5 and 97.7 volume percentage CO_2 gas streams as input.

Two liquefaction systems were modeled based on the liquefaction systems identified in the literature review. The models were altered based on the requirement of an additional purification step. The two liquefaction systems are distinguished based on the open or closed liquefaction method. These two models were used to analyze the energy requirements to liquefy the 6 synthetic mixtures. A few conclusions can be drawn when comparing the energy requirements of these models for the six synthetic mixtures. It was found that the specific work increased with impurity content and that the open liquefaction system is the most energy intensive. Furthermore, it could be concluded that the synthetic mixtures of 99.5 and 97.5 volume percent CO_2 are slightly more energy intensive in the case with N_2 and O_2 impurities when compared to the cases with N_2, CO and H_2 impurities for both the open and closed liquefaction. The cases with N_2 and O_2 impurities were however found to be slightly more efficient for both open and closed liquefaction systems at 95.5 volume percent CO_2. Despite these findings it should be noted that the difference in energy requirements due to different impurity components is negligible to the differences produced by varying the CO_2 volume percentage and liquefaction system variant.

Furthermore, the capital and operational costs of these systems were calculated for a scale of 100, 200 and 400 kt liquefied product per year. The operational cost is based on the specific work that was calculated with the various Aspen HYSYS models combined with various correlations for the buffer storage and transport storage operational costs. The energy costs and other cost correlations are assessed for a location based in northwestern Europe. It was found that operational costs scaled linearly with scale. It was concluded that a closed liquefaction system is slightly more economically efficient, although the difference is almost negligible. These results furthermore showed that a higher purity input stream also reduces the operational costs by a more significant amount. These conclusions are in agreement with the calculated specific work per process. The capital costs were also calculated with

correlations for a location based in northwestern Europe, these results showed a sublinearly increase of costs with scale. Therefore it can be concluded that economies of scale are applicable to these systems. It was furthermore concluded that the open liquefaction system is favorable in terms of capital costs, in contradiction to the operational costs and specific work. The results for the capital costs did however show a preference for a higher input stream CO_2 volume fraction, in agreement with the conclusions for the operational costs and specific work.

A set of recommendations can be made based on this research and these conclusions. The first recommendation is to identify the operational and capital cost of the pretreatment steps that are necessary to create the mixtures that were selected as input gas stream. These results can then be be compared with the results from this research to identify which liquefaction system and input gas composition gives the most economically preferable combination.

It is further recommended to perform a more thorough analysis of the selected liquefaction system and input gas composition to provide more accuracy in the results. This more thorough result could be done by analyzing more gas compositions with smaller CO_2 volume fraction increments to find an optimum. Furthermore the Aspen HYSYS models can be further optimized to the selected operational conditions to increase the accuracy compared to a final design. The techno-economic analysis can also be further expanded when a preferred case is selected, expansions could include plant construction and design costs or account for service and maintenance on liquefaction equipment.

Another recommendation is to further analyze effects of trace impurities which could impose operational considerations such as corrosion or equipment damage, like identified in the literature review. The different components and amounts of these trace impurities are however dependent on the gas pretreatment and are therefore dependent on a full-scale analysis.

A

EoS Comparison Data

Tables A.2 and A.2 give an overview of the results obtained with the various evaluated fluid packages from Aspen HYSYS version 12 and NIST Refprop version 10 for the bubble point pressure at 223, 243, 263 and 283 K. Furthermore the MAE value is given for these results which is used to compare these fluid packages in Figures 4.1 and 4.2. The tables also show the MAPE which was not used as a selection criteria but ensures the chosen fluid packages do not exceed a MAPE of 5 %. The MAPE was calculated with Equation A.1.

$$\text{MAPE} = \frac{100}{n} \sum_{i=1}^{n_{tot}} \left| \frac{y_i - x_i}{y_i} \right| \tag{A.1}$$

Table A.1: Bubble point pressures, at 223, 243, 263 and 283 K, evaluated with various fluid packages in Aspen HYSYS version 12 for 95.5, 97.5 and 99.5 vol% CO_2 mixtures with N_2 and O_2 impurities. Aspen HYSYS results are compared to NIST Refprop version 10 bubble point pressure predictions by calculating the MAE and MAPE.

Fluid package	**PC-SAFT**	**GERG-2008**	**RefProp** (Aspen)	**CPA**	**PR**	**Refprop** (NIST)
99.5 vol% CO_2						
MAE [kPa]	24	11	7	30	76	-
MAPE [%]	1.6	0.7	0.3	1.8	4.3	-
$p_{\text{Bubble point}}$ (223K) [kPa]	1001	1061	1045	997	955	1045
$p_{\text{Bubble point}}$ (243K) [kPa]	1730	1765	1765	1726	1671	1753
$p_{\text{Bubble point}}$ (263K) [kPa]	2936	2952	2952	2923	2866	2943
$p_{\text{Bubble point}}$ (283K) [kPa]	4783	4766	4766	4734	4705	4760
97.5 vol% CO_2						
MAE [kPa]	63	77	77	111	203	-
MAPE [%]	2.2	2.5	2.5	3.8	6.4	-
$p_{\text{Bubble point}}$ (223K) [kPa]	2257	2527	2527	2190	2110	2412
$p_{\text{Bubble point}}$ (243K) [kPa]	2921	3055	3055	2866	2773	2969
$p_{\text{Bubble point}}$ (263K) [kPa]	4046	4106	4106	3981	3879	4041
$p_{\text{Bubble point}}$ (283K) [kPa]	5769	5767	5767	5663	5573	5724
95.5 vol% CO_2						
MAE [kPa]	98	143	143	156	286	-
MAPE [%]	2.2	3.3	3.3	3.8	6.5	-
$p_{\text{Bubble point}}$ (223K) [kPa]	3501	3921	3921	3357	3251	3709
$p_{\text{Bubble point}}$ (243K) [kPa]	4091	4279	4279	3973	3851	4118
$p_{\text{Bubble point}}$ (263K) [kPa]	5125	5189	5189	5000	4861	5069
$p_{\text{Bubble point}}$ (283K) [kPa]	6711	6687	6687	6548	6397	6608

Table A.2: Bubble point pressures, at 223, 243, 263 and 283 K, evaluated with various fluid packages in Aspen HYSYS version 12 for 95.5, 97.5 and 99.5 vol% CO_2 mixtures with N_2, CO and H_2 impurities. Aspen HYSYS results are compared to NIST Refprop version 10 bubble point pressure predictions by calculating the MAE and MAPE.

Fluid package	**PC-SAFT**	**GERG-2008**	**RefProp** (Aspen)	**CPA**	**PR**	**Refprop** (NIST)
99.5 vol% CO_2						
MAE [kPa]	15	157	157	8	36	-
MAPE [%]	0.5	10.5	10.5	0.6	2	-
$p_{Bubble\ point}$ (223K) [kPa]	981	1242	1242	966	950	985
$p_{Bubble\ point}$ (243K) [kPa]	1714	1885	1885	1706	1670	1708
$p_{Bubble\ point}$ (263K) [kPa]	2923	3029	3029	2912	2867	2909
$p_{Bubble\ point}$ (283K) [kPa]	4774	4811	4811	4729	4708	4737
97.5 vol% CO_2						
MAE [kPa]	46	474	474	38	102	-
MAPE [%]	1.3	16.3	16.3	1.6	3.3	-
$p_{Bubble\ point}$ (223K) [kPa]	2264	3097	3097	2188	2149	2310
$p_{Bubble\ point}$ (243K) [kPa]	2915	3431	3431	2878	2811	2895
$p_{Bubble\ point}$ (263K) [kPa]	4034	4345	4345	4001	3914	3988
$p_{Bubble\ point}$ (283K) [kPa]	5757	5904	5904	5686	5599	5686
95.5 vol% CO_2						
MAE [kPa]	95	880	880	71	107	-
MAPE [%]	1.9	21.5	21.5	1.7	2.5	-
$p_{Bubble\ point}$ (223K) [kPa]	3515	5007	5007	3353	3325	3529
$p_{Bubble\ point}$ (243K) [kPa]	4084	4982	4982	3996	3923	3992
$p_{Bubble\ point}$ (263K) [kPa]	5107	5635	5635	5038	4924	4979
$p_{Bubble\ point}$ (283K) [kPa]	6691	6940	6940	6588	6442	6544

B

Stream Conditions of the Open Liquefaction Aspen HYSYS Models

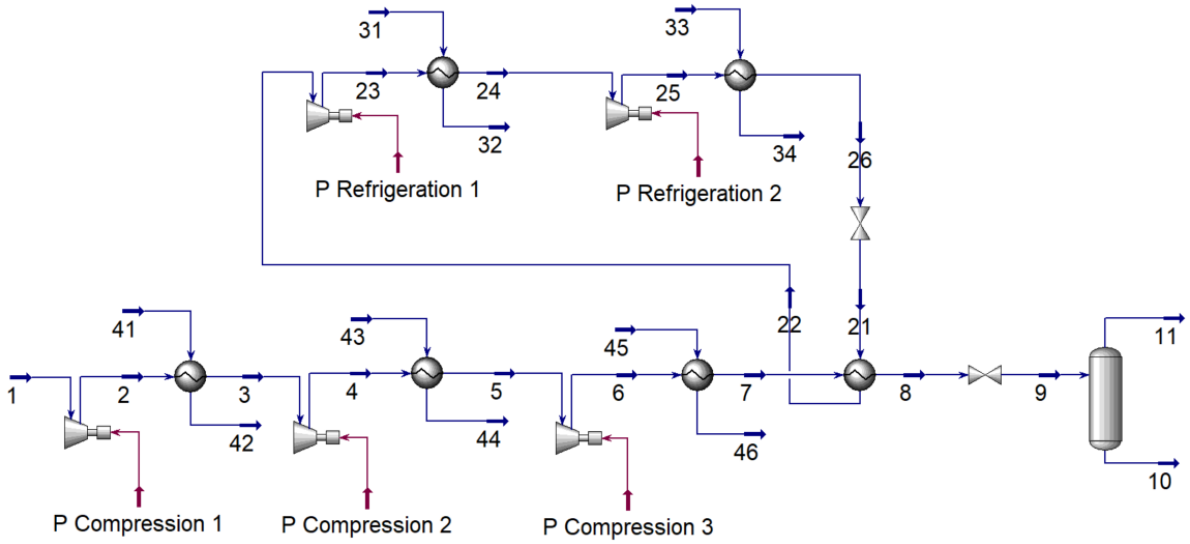

Figure B.1: Aspen HYSYS model of the open liquefaction system. Consisting of a three-stage compression configuration with intercooling. The stream passes through a heat exchanger connected to an external refrigeration cycle after compression before being throttled through a Joule-Thomson valve. The stream is separated into a gaseous and liquid stream as a final step. As first shown in Figure 3.4.

B.1. Open liquefaction model with 95.5 vol% CO_2 input stream and N_2, CO and H_2 impurities

Tables B.1 through B.3 show the vapor fraction, temperature, pressure and mass flow of all streams, as shown and numbered in Figure B.1, for the open liquefaction aspen model with an input stream of 95.5 vol% CO_2 with N_2, CO and H_2 impurities.

B.2. Open liquefaction model with 97.5 vol% CO_2 input stream and N_2, CO and H_2 impurities

Tables B.4 through B.6 show the vapor fraction, temperature, pressure and mass flow of all streams, as shown and numbered in Figure B.1, for the open liquefaction aspen model with an input stream of 97.5 vol% CO_2 with N_2, CO and H_2 impurities.

Table B.1: Properties of stream 1 through 9, as referenced in Figure B.1, of the open liquefaction system, modeled with an input stream of 95.5 vol% CO_2 with N_2, CO and H_2 impurities.

Stream Number	1	2	3	4	5	6	7	8	9
Vapor Fraction	1.00	1.00	1.00	1.00	1.00	1.00	1.00	0.01	0.14
Temperature [K]	30	153,7	35	160,8	35	162,8	35	-15	-28
Pressure [kpa]	100	357	357	1274	1274	4545	4545	4545	2167
Mass Flow [kg · s^{-1}]	3,64	3,64	3,64	3,64	3,64	3,64	3,64	3,64	3,64

Table B.2: Properties of stream 10 through 31, as referenced in Figure B.1, of the open liquefaction system, modeled with an input stream of 95.5 vol% CO_2 with N_2, CO and H_2 impurities.

Stream Number	10	11	21	22	23	24	25	26	31
Vapor Fraction	0.00	1.00	0,19	1.00	1.00	1.00	1.00	0.00	0.00
Temperature [K]	-28	-28	-20	-20	64,3	35	134,2	35	30
Pressure [kpa]	2167	2167	190	190	516	516	1400	1400	100
Mass Flow [kg · s^{-1}]	3,17	0,47	1,01	1,01	1,01	1,01	1,01	1,01	3,4

Table B.3: Properties of stream 32 through 46, as referenced in Figure B.1, of the open liquefaction system, modeled with an input stream of 95.5 vol% CO_2 with N_2, CO and H_2 impurities.

Stream Number	32	33	34	41	42	43	44	45	46
Vapor Fraction	0.00	0.00	0.00	0.00	0.00	0.00	0.00	0.00	0.00
Temperature [K]	35	30	35	30	35	30	35	30	35
Pressure [kpa]	100	100	100	100	100	100	100	100	100
Mass Flow [kg · s^{-1}]	3,4	67,37	67,37	19,29	19,29	21,11	21,11	24,61	24,61

Table B.4: Properties of stream 1 through 9, as referenced in Figure B.1, of the open liquefaction system, modeled with an input stream of 97.5 vol% CO_2 with N_2, CO and H_2 impurities.

Stream Number	1	2	3	4	5	6	7	8	9
Vapor Fraction	1.00	1.00	1.00	1.00	1.00	1.00	1.00	0.01	0.12
Temperature [K]	30	144.1	35	151	35	152.6	35	-15	-28
Pressure [kpa]	100	328	328	1076	1076	3530	3530	3530	1882
Mass Flow [kg · s^{-1}]	3.59	3.59	3.59	3.59	3.59	3.59	3.59	3.59	3.59

Table B.5: Properties of stream 10 through 31, as referenced in Figure B.1, of the open liquefaction system, modeled with an input stream of 97.5 vol% CO_2 with N_2, CO and H_2 impurities.

Stream Number	10	11	21	22	23	24	25	26	31
Vapor Fraction	0.00	1.00	0.19	1.00	1.00	1.00	1.00	0.00	0.00
Temperature [K]	-28	-28	-20	-20	64.3	35	134.2	35	30
Pressure [kpa]	1882	1882	190	190	516	516	1400	1400	100
Mass Flow [kg · s^{-1}]	3.17	0.41	1.05	1.05	1.05	1.05	1.05	1.05	3.52

Table B.6: Properties of stream 32 through 46, as referenced in Figure B.1, of the open liquefaction system, modeled with an input stream of 97.5 vol% CO_2 with N_2, CO and H_2 impurities.

Stream Number	32	33	34	41	42	43	44	45	46
Vapor Fraction	0.00	0.00	0.00	0.00	0.00	0.00	0.00	0.00	0.00
Temperature [K]	35	30	35	30	35	30	35	30	35
Pressure [kpa]	100	100	100	100	100	100	100	100	100
Mass Flow [kg · s^{-1}]	3.52	69.74	69.74	17.35	17.35	18.96	18.96	21.28	21.28

B.3. Open liquefaction model with 99.5 vol% CO_2 input stream and N_2, CO and H_2 impurities

Tables B.7 through B.9 show the vapor fraction, temperature, pressure and mass flow of all streams, as shown and numbered in Figure B.1, for the open liquefaction aspen model with an input stream of 99.5 vol% CO_2 with N_2, CO and H_2 impurities.

Table B.7: Properties of stream 1 through 9, as referenced in Figure B.1, of the open liquefaction system, modeled with an input stream of 99.5 vol% CO_2 with N_2, CO and H_2 impurities.

Stream Number	1	2	3	4	5	6	7	8	9
Vapor Fraction	1.00	1.00	1.00	1.00	1.00	1.00	1.00	0.01	0.10
Temperature [K]	30	131.8	35	138.6	35	139.6	35	-15	-28
Pressure [kpa]	100	293	293	860	860	2522	2522	2522	1596
Mass Flow [kg · s^{-1}]	3.54	3.54	3.54	3.54	3.54	3.54	3.54	3.54	3.54

Table B.8: Properties of stream 10 through 31, as referenced in Figure B.1, of the open liquefaction system, modeled with an input stream of 99.5 vol% CO_2 with N_2, CO and H_2 impurities.

Stream Number	10	11	21	22	23	24	25	26	31
Vapor Fraction	0.00	1.00	0.19	1.00	1.00	1.00	1.00	0.00	0.00
Temperature [K]	-28	-28	-20	-20	64.3	35	134.2	35	30
Pressure [kpa]	1596	1596	190	190	516	516	1400	1400	100
Mass Flow [kg · s^{-1}]	3.17	0.36	1.08	1.08	1.08	1.08	1.08	1.08	3.63

Table B.9: Properties of stream 32 through 46, as referenced in Figure B.1, of the open liquefaction system, modeled with an input stream of 99.5 vol% CO_2 with N_2, CO and H_2 impurities.

Stream Number	32	33	34	41	42	43	44	45	46
Vapor Fraction	0.00	0.00	0.00	0.00	0.00	0.00	0.00	0.00	0.00
Temperature [K]	35	30	35	30	35	30	35	30	35
Pressure [kpa]	100	100	100	100	100	100	100	100	100
Mass Flow [kg · s^{-1}]	3.63	71.92	71.92	15.07	15.07	16.49	16.49	17.83	17.83

B.4. Open liquefaction model with 95.5 vol% CO_2 input stream and N_2 and O_2 impurities

Tables B.10 through B.12 show the vapor fraction, temperature, pressure and mass flow of all streams, as shown and numbered in Figure B.1, for the open liquefaction aspen model with an input stream of 95.5 vol% CO_2 with N_2 and O_2 impurities.

Table B.10: Properties of stream 1 through 9, as referenced in Figure B.1, of the open liquefaction system, modeled with an input stream of 95.5 vol% CO_2 with N_2 and O_2 impurities.

Stream Number	1	2	3	4	5	6	7	8	9
Vapor Fraction [-]	1.00	1.00	1.00	1.00	1.00	1.00	1.00	0.01	0.12
Temperature [K]	30	144.9	35	151.7	35	153.2	35	-15	-28
Pressure [kpa]	100	329	329	1084	1084	3568	3568	3568	1888
Mass Flow [kg · s^{-1}]	3.59	3.59	3.59	3.59	3.59	3.59	3.59	3.59	3.59

Table B.11: Properties of stream 10 through 31, as referenced in Figure B.1, of the open liquefaction system, modeled with an input stream of 95.5 vol% CO_2 with N_2 and O_2 impurities.

Stream Number	10	11	21	22	23	24	25	26	31
Vapor Fraction [-]	0.00	1.00	0.19	1.00	1.00	1.00	1.00	0.00	0.00
Temperature [K]	-28	-28	-20	-20	64.3	35	134.2	35	30
Pressure [kpa]	1888	1888	190	190	516	516	1400	1400	100
Mass Flow [kg · s^{-1}]	3.17	0.42	1.03	1.03	1.03	1.03	1.03	1.03	3.47

Table B.12: Properties of stream 32 through 46, as referenced in Figure B.1, of the open liquefaction system, modeled with an input stream of 95.5 vol% CO_2 with N_2 and O_2 impurities.

Stream Number	32	33	34	41	42	43	44	45	46
Vapor Fraction [-]	0.00	0.00	0.00	0.00	0.00	0.00	0.00	0.00	0.00
Temperature [K]	35	30	35	30	35	30	35	30	35
Pressure [kpa]	100	100	100	100	100	100	100	100	100
Mass Flow [kg · s^{-1}]	3.47	68.72	68.72	17.44	17.44	19.05	19.05	21.34	21.34

B.5. Open liquefaction model with 97.5 vol% CO_2 input stream and N_2 and O_2 impurities

Tables B.13 through B.15 show the vapor fraction, temperature, pressure and mass flow of all streams, as shown and numbered in Figure B.1, for the open liquefaction aspen model with an input stream of 97.5 vol% CO_2 with N_2 and O_2 impurities.

Table B.13: Properties of stream 1 through 9, as referenced in Figure B.1, of the open liquefaction system, modeled with an input stream of 97.5 vol% CO_2 with N_2 and O_2 impurities.

Stream Number	1	2	3	4	5	6	7	8	9
Vapor Fraction [-]	1.00	1.00	1.00	1.00	1.00	1.00	1.00	0.01	0.12
Temperature [K]	30	144.9	35	151.7	35	153.2	35	-15	-28
Pressure [kpa]	100	329	329	1084	1084	3568	3568	3568	1888
Mass Flow [kg · s^{-1}]	3.59	3.59	3.59	3.59	3.59	3.59	3.59	3.59	3.59

Table B.14: Properties of stream 10 through 31, as referenced in Figure B.1, of the open liquefaction system, modeled with an input stream of 97.5 vol% CO_2 with N_2 and O_2 impurities.

Stream Number	10	11	21	22	23	24	25	26	31
Vapor Fraction [-]	0.00	1.00	0.19	1.00	1.00	1.00	1.00	0.00	0.00
Temperature [K]	-28	-28	-20	-20	64.3	35	134.2	35	30
Pressure [kpa]	1888	1888	190	190	516	516	1400	1400	100
Mass Flow [kg · s^{-1}]	3.17	0.42	1.03	1.03	1.03	1.03	1.03	1.03	3.47

Table B.15: Properties of stream 32 through 46, as referenced in Figure B.1, of the open liquefaction system, modeled with an input stream of 97.5 vol% CO_2 with N_2 and O_2 impurities.

Stream Number	32	33	34	41	42	43	44	45	46
Vapor Fraction [-]	0.00	0.00	0.00	0.00	0.00	0.00	0.00	0.00	0.00
Temperature [K]	35	30	35	30	35	30	35	30	35
Pressure [kpa]	100	100	100	100	100	100	100	100	100
Mass Flow [kg · s^{-1}]	3.47	68.72	68.72	17.44	17.44	19.05	19.05	21.34	21.34

B.6. Open liquefaction model with 99.5 vol% CO_2 input stream and N_2 and O_2 impurities

Tables B.16 through B.18 show the vapor fraction, temperature, pressure and mass flow of all streams, as shown and numbered in Figure B.1, for the open liquefaction aspen model with an input stream of 99.5 vol% CO_2 with N_2 and O_2 impurities.

Table B.16: Properties of stream 1 through 9, as referenced in Figure B.1, of the open liquefaction system, modeled with an input stream of 99.5 vol% CO_2 with N_2 and O_2 impurities.

Stream Number	1	2	3	4	5	6	7	8	9
Vapor Fraction [-]	1.00	1.00	1.00	1.00	1.00	1.00	1.00	0.01	0.10
Temperature [K]	30	132.8	35	139.1	35	140.2	35	-15	-28
Pressure [kpa]	100	294	294	864	864	2540	2540	2540	1599
Mass Flow [kg $\cdot$ s^{-1}]	3.53	3.53	3.53	3.53	3.53	3.53	3.53	3.53	3.53

Table B.17: Properties of stream 10 through 31, as referenced in Figure B.1, of the open liquefaction system, modeled with an input stream of 99.5 vol% CO_2 with N_2 and O_2 impurities.

Stream Number	10	11	21	22	23	24	25	26	31
Vapor Fraction [-]	0.00	1.00	0.19	1.00	1.00	1.00	1.00	0.00	0.00
Temperature [K]	-28	-28	-20	-20	64.3	35	134.2	35	30
Pressure [kpa]	1599	1599	190	190	516	516	1400	1400	100
Mass Flow [kg $\cdot$ s^{-1}]	3.17	0.36	1.07	1.07	1.07	1.07	1.07	1.07	3.58

Table B.18: Properties of stream 32 through 46, as referenced in Figure B.1, of the open liquefaction system, modeled with an input stream of 99.5 vol% CO_2 with N_2 and O_2 impurities.

Stream Number	32	33	34	41	42	43	44	45	46
Vapor Fraction [-]	0.00	0.00	0.00	0.00	0.00	0.00	0.00	0.00	0.00
Temperature [K]	35	30	35	30	35	30	35	30	35
Pressure [kpa]	100	100	100	100	100	100	100	100	100
Mass Flow [kg $\cdot$ s^{-1}]	3.58	70.98	70.98	15.16	15.16	16.51	16.51	17.86	17.86

C

Stream Conditions of the Closed Liquefaction Aspen HYSYS Models

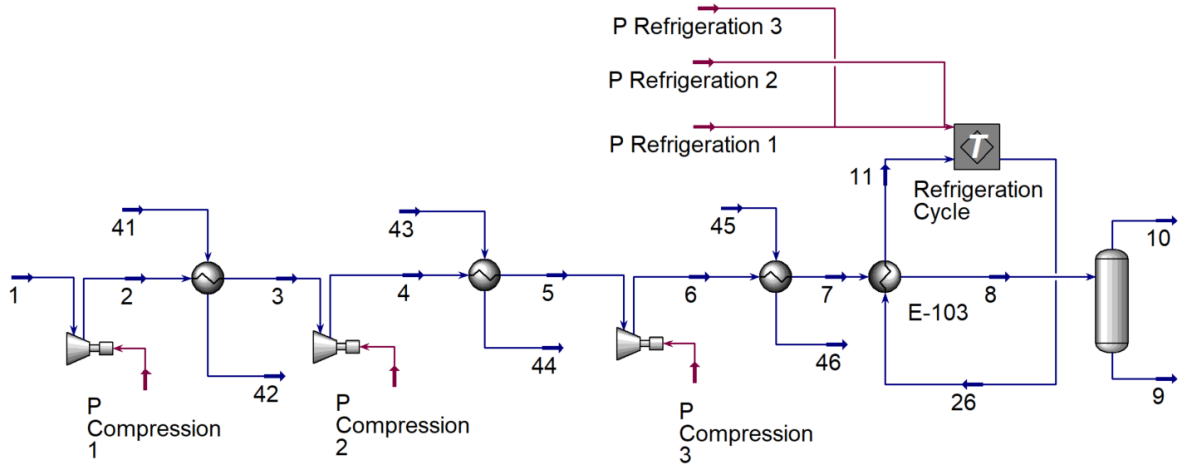

Figure C.1: Refrigeration cycle of the closed system liquefaction model consisting of three-stage compression with intercooling and three Joule-Thomson valves with separators in between which recycle the gaseous stream. As first shown in Figure 3.2.

C.1. Closed liquefaction model with 95.5 vol% CO_2 input stream and N_2, CO and H_2 impurities

Tables C.1 through C.2 show the vapor fraction, temperature, pressure and mass flow of all streams, as shown and numbered in Figure C.1, for the main model of the closed liquefaction system with an input stream of 95.5 vol% CO_2 with N_2, CO and H_2 impurities.

Table C.1: Properties of stream 1 through 9, as referenced in Figure C.1, of the closed liquefaction system, modeled with an input stream of 95.5 vol% CO_2 with N_2, CO and H_2 impurities.

Stream Number	1	2	3	4	5	6	7	8	9
Vapor Fraction	1.00	1.00	1.00	1.00	1.00	1.00	1.00	0.14	0.00
Temperature [K]	30	128	35	134.5	35	135.3	35	-28	-28
Pressure [kpa]	100	279	279	779	779	2174	2174	2174	2174
Mass Flow [kg·s^{-1}]	3.64	3.64	3.64	3.64	3.64	3.64	3.64	3.64	3.17

Table C.2: Properties of stream 10 through 46, as referenced in Figure C.1, of the closed liquefaction system, modeled with an input stream of 95.5 vol% CO_2 with N_2, CO and H_2 impurities.

Stream Number	10	11	26	41	42	43	44	45	46
Vapor Fraction	1.00	1.00	0.06	0.00	0.00	0.00	0.00	0.00	0.00
Temperature [K]	-28	-33	-33	30	35	30	35	30	35
Pressure [kpa]	2174	103	103	100	100	100	100	100	100
Mass Flow [kg·s^{-1}]	0.47	0.91	0.91	14.92	14.92	16.28	16.28	17.33	17.33

C.2. Closed liquefaction model with 97.5 vol% CO_2 input stream and N_2, CO and H_2 impurities

Tables C.3 through C.4 show the vapor fraction, temperature, pressure and mass flow of all streams, as shown and numbered in Figure C.1, for the main model of the closed liquefaction system with an input stream of 97.5 vol% CO_2 with N_2, CO and H_2 impurities.

Table C.3: Properties of stream 1 through 9, as referenced in Figure C.1, of the closed liquefaction system, modeled with an input stream of 97.5 vol% CO_2 with N_2, CO and H_2 impurities.

Stream Number	1	2	3	4	5	6	7	8	9
Vapor Fraction	1.00	1.00	1.00	1.00	1.00	1.00	1.00	0.12	0.00
Temperature [K]	30	122.6	35	129.1	35	129.8	35	-28	-28
Pressure [kpa]	100	266	266	709	709	1888	1888	1888	1888
Mass Flow [kg·s^{-1}]	3.58	3.58	3.58	3.58	3.58	3.58	3.58	3.58	3.17

Table C.4: Properties of stream 10 through 46, as referenced in Figure C.1, of the closed liquefaction system, modeled with an input stream of 97.5 vol% CO_2 with N_2, CO and H_2 impurities.

Stream Number	10	11	26	41	42	43	44	45	46
Vapor Fraction	1.00	1.00	0.06	0.00	0.00	0.00	0.00	0.00	0.00
Temperature [K]	-28	-33	-33	30	35	30	35	30	35
Pressure [kpa]	1888	103	103	100	100	100	100	100	100
Mass Flow [kg·s^{-1}]	0.41	0.92	0.92	13.76	13.76	15.06	15.06	15.89	15.89

C.3. Closed liquefaction model with 99.5 vol% CO_2 input stream and N_2, CO and H_2 impurities

Tables C.5 through C.6 show the vapor fraction, temperature, pressure and mass flow of all streams, as shown and numbered in Figure C.1, for the main model of the closed liquefaction system with an input stream of 99.5 vol% CO_2 with N_2, CO and H_2 impurities.

Table C.5: Properties of stream 1 through 9, as referenced in Figure C.1, of the closed liquefaction system, modeled with an input stream of 99.5 vol% CO_2 with N_2, CO and H_2 impurities.

Stream Number	1	2	3	4	5	6	7	8	9
Vapor Fraction	1.00	1.00	1.00	1.00	1.00	1.00	1.00	0.10	0.00
Temperature [K]	30	116.2	35	123.3	35	123.4	35	-28	-28
Pressure [kpa]	100	251	251	635	635	1599	1599	1599	1599
Mass Flow [kg·s^{-1}]	3.51	3.51	3.51	3.51	3.51	3.51	3.51	3.51	3.17

Table C.6: Properties of stream 10 through 46, as referenced in Figure C.1, of the closed liquefaction system, modeled with an input stream of 99.5 vol% CO_2 with N_2, CO and H_2 impurities.

Stream Number	10	11	26	41	42	43	44	45	46
Vapor Fraction	1.00	1.00	0.06	0.00	0.00	0.00	0.00	0.00	0.00
Temperature [K]	-28	-33	-33	30	35	30	35	30	35
Pressure [kpa]	1599	103	103	100	100	100	100	100	100
Mass Flow [kg·s^{-1}]	0.34	0.92	0.92	12.49	12.49	13.8	13.8	14.36	14.36

C.4. Closed liquefaction model with 95.5 vol% CO_2 input stream and N_2 and O_2 impurities

Tables C.7 through C.8 show the vapor fraction, temperature, pressure and mass flow of all streams, as shown and numbered in Figure C.1, for the main model of the closed liquefaction system with an input stream of 95.5 vol% CO_2 with N_2 and O_2 impurities.

Table C.7: Properties of stream 1 through 9, as referenced in Figure C.1, of the closed liquefaction system, modeled with an input stream of 95.5 vol% CO_2 with N_2 and O_2 impurities.

Stream Number	1	2	3	4	5	6	7	8	9
Vapor Fraction	1.00	1.00	1.00	1.00	1.00	1.00	1.00	0.14	1.00
Temperature [K]	30	128.6	35	134.9	35	135.6	35	-28	-28
Pressure [kpa]	100	279	279	779	779	2174	2174	2174	2174
Mass Flow [kg·s^{-1}]	3.65	3.65	3.65	3.65	3.65	3.65	3.65	3.65	0.48

Table C.8: Properties of stream 10 through 46, as referenced in Figure C.1, of the closed liquefaction system, modeled with an input stream of 95.5 vol% CO_2 with N_2 and O_2 impurities.

Stream Number	10	11	26	41	42	43	44	45	46
Vapor Fraction	0.00	1.00	0.06	0.00	0.00	0.00	0.00	0.00	0.00
Temperature [K]	-28	-33	-33	30	35	30	35	30	35
Pressure [kpa]	2174	103	103	100	100	100	100	100	100
Mass Flow [kg·s^{-1}]	3.17	0.9	0.9	15	15	16.34	16.34	17.36	17.36

C.5. Closed liquefaction model with 97.5 vol% CO_2 input stream and N_2 and O_2 impurities

Tables C.9 through C.10 show the vapor fraction, temperature, pressure and mass flow of all streams, as shown and numbered in Figure C.1, for the main model of the closed liquefaction system with an input stream of 97.5 vol% CO_2 with N_2 and O_2 impurities.

Table C.9: Properties of stream 1 through 9, as referenced in Figure C.1, of the closed liquefaction system, modeled with an input stream of 97.5 vol% CO_2 with N_2 and O_2 impurities.

Stream Number	1	2	3	4	5	6	7	8	9
Vapor Fraction	1.00	1.00	1.00	1.00	1.00	1.00	1.00	0.12	0.00
Temperature [K]	30	123.2	35	129.6	35	130.1	35	-28	-28
Pressure [kpa]	100	266	266	709	709	1888	1888	1888	1888
Mass Flow [kg·s^{-1}]	3.59	3.59	3.59	3.59	3.59	3.59	3.59	3.59	3.17

Table C.10: Properties of stream 10 through 46, as referenced in Figure C.1, of the closed liquefaction system, modeled with an input stream of 97.5 vol% CO_2 with N_2 and O_2 impurities.

Stream Number	10	11	26	41	42	43	44	45	46
Vapor Fraction	1.00	1.00	0.06	0.00	0.00	0.00	0.00	0.00	0.00
Temperature [K]	-28	-33	-33	30	35	30	35	30	35
Pressure [kpa]	1888	103	103	100	100	100	100	100	100
Mass Flow [kg·s^{-1}]	0.42	0.91	0.91	13.83	13.83	15.11	15.11	15.92	15.92

C.6. Closed liquefaction model with 99.5 vol% CO_2 input stream and N_2 and O_2 impurities

Tables C.11 through C.12 show the vapor fraction, temperature, pressure and mass flow of all streams, as shown and numbered in Figure C.1, for the main model of the closed liquefaction system with an input stream of 99.5 vol% CO_2 with N_2 and O_2 impurities.

Table C.11: Properties of stream 1 through 9, as referenced in Figure C.1, of the closed liquefaction system, modeled with an input stream of 99.5 vol% CO_2 with N_2 and O_2 impurities.

Stream Number	1	2	3	4	5	6	7	8	9
Vapor Fraction	1.00	1.00	0.06	0.00	0.00	0.00	0.00	0.00	0.00
Temperature [K]	-28	-33	-33	30	35	30	35	30	35
Pressure [kpa]	1599	103	103	100	100	100	100	100	100
Mass Flow [kg·s^{-1}]	0.36	0.91	0.91	12.59	12.59	13.88	13.88	14.44	14.44

Table C.12: Properties of stream 10 through 46, as referenced in Figure C.1, of the closed liquefaction system, modeled with an input stream of 99.5 vol% CO_2 with N_2 and O_2 impurities.

Stream Number	10	11	26	41	42	43	44	45	46
Vapor Fraction	1.00	1.00	1.00	1.00	1.00	1.00	1.00	0.10	0.00
Temperature [K]	30	116.9	35	123.8	35	123.8	35	-28	-28
Pressure [kpa]	100	251	251	635	635	1599	1599	1599	1599
Mass Flow [kg·s^{-1}]	3.53	3.53	3.53	3.53	3.53	3.53	3.53	3.53	3.17

C.7. External Refrigeration Cycle Sub Model

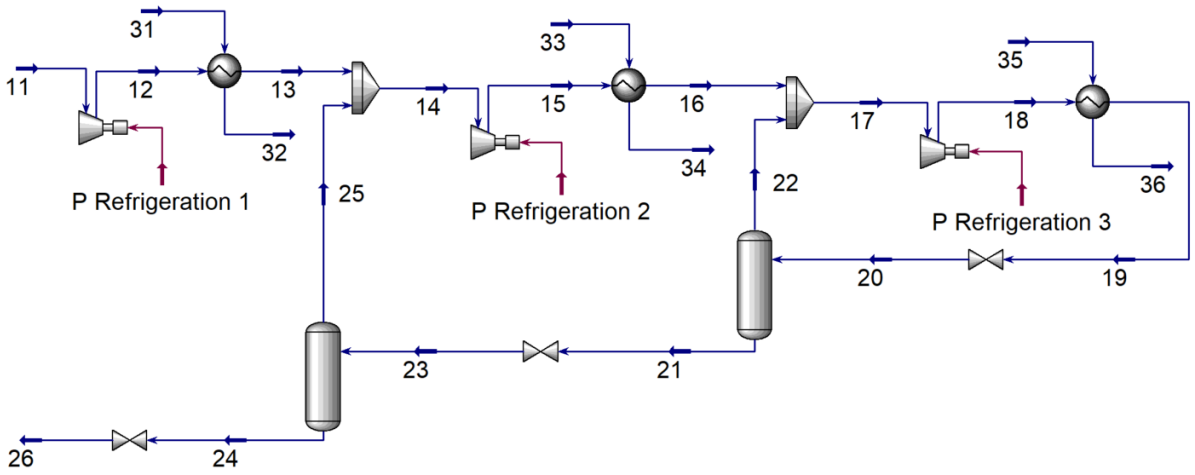

Figure C.2: Refrigeration cycle of the closed system liquefaction model consisting of three-stage compression with intercooling and three Joule-Thomson valves with separators in between which recycle the gaseous stream. As first shown in Figure 3.3.

Tables C.13through C.15 show show the vapor fraction, temperature and pressure of all streams, as shown and numbered in Figure C.2, for the external refrigeration cycle sub model. The mass flows are dependent on the input stream of the liquefaction system and are detailed for stream 11 and 26 in Section C.1 through C.6.

Table C.13: Properties of stream 11 through 19, as referenced in Figure C.2, of the external refrigeration cycle for the closed liquefaction system

Stream Number	11	12	13	14	15	16	17	18	19
Vapor Fraction	1.00	1.00	1.00	1.00	1.00	1.00	1.00	1.00	0.00
Temperature [K]	-33	35.6	35	30.9	118.1	35	32.1	117.4	35
Pressure [kpa]	103	241	241	241	581	581	581	1400	1400

Table C.14: Properties of stream 20 through 32, as referenced in Figure C.2, of the external refrigeration cycle for the closed liquefaction system

Stream Number	20	21	22	23	24	25	26	31	32
Vapor Fraction	0.10	0.00	1.00	0.08	0.00	1.00	0.06	0.00	0.00
Temperature [K]	8.4	8.4	8.4	-14.5	-14.5	-14.5	-33	30	35
Pressure [kpa]	581	581	581	241	241	241	103	100	100

Table C.15: Properties of stream 33 through 36, as referenced in Figure C.2, of the external refrigeration cycle for the closed liquefaction system

Stream Number	33	34	35	36
Vapor Fraction	0.00	0.00	0.00	0.00
Temperature [K]	30	35	30	35
Pressure [kpa]	100	100	100	100

D

Supplementary Techno-Economic Analysis

D.1. Detailed Closed Liquefaction System Equipment Cost

Table D.1 gives an overview of the various size parameters obtained through the APEA to calculate equipment cost for the closed liquefaction system. The cost correlations for compressors are dependent on power in kW, pressure vessel cost is dependent on mass which is calculated based on its size and internal pressure and the heat exchanger costs are dependent on heat exchanging area in m^2.

Table D.1: Overview of equipment parameters used with the equations shown in Section 5.1.1 to calculated equipment costs for the closed liquefaction system

CO_2 input purity [vol%]	**95.5**			**99.5**		
Process scale [kt · year^{-1}]	100	200	400	100	200	400
Compressors						
Compressor 1 Power [kW]	319	638	1276	271	543	1085
Compressor 2 Power [kW]	326	652	1304	277	555	1110
Compressor 3 Power [kW]	323	646	1291	272	544	1089
Refrigeration Compressor 1 Power [kW]	130	261	522	132	264	529
Refrigeration Compressor 2 Power [kW]	186	373	745	189	378	755
Refrigeration Compressor 3 Power [kW]	201	401	803	203	407	813
Pressure vessels						
Pressure vessel 1 diameter [m]	1.2	1.4	1.5	1.2	1.4	1.5
Pressure vessel 1 height [m]	3.7	4.0	4.6	3.7	4.0	4.6
Pressure vessel 1 pressure [kPa]	2417	2417	2417	1670	1670	1670
Refrigeration pressure vessel 1 diameter [m]	1.1	1.2	1.4	1.1	1.2	1.4
Refrigeration pressure vessel 1 height [m]	3.7	3.7	4.0	3.7	3.7	4
Refrigeration pressure vessel 1 pressure [kPa]	243	243	243	243	243	243
Refrigeration pressure vessel 2 diameter [m]	1.1	1.2	1.4	1.1	1.2	1.4
Refrigeration pressure vessel 2 height [m]	3.7	3.7	4.0	3.7	3.7	4
Refrigeration pressure vessel 2 pressure [kPa]	652	652	652	652	652	652
Heat Exchangers						
Heat exchanger 1 size [m^2]	75	150	262	76	152	304
Heat exchanger 2 size [m^2]	41	82	143	59	118	237
Heat exchanger 3 size [m^2]	37	75	130	40	79	158
Heat exchanger 4 size [m^2]	117	233	407	108	216	432
Refrigeration heat exchanger 1 size [m^2]	7	14	25	7	15	29
Refrigeration heat exchanger 2 size [m^2]	42	84	147	43	86	171
Refrigeration heat exchanger 3 size [m^2]	51	102	178	52	103	207

Tables D.2 and D.3 give the equipment cost of the closed liquefaction system as calculated with the correlation and variables from Equation 3.3 and Table 3.5 of Section 3.7.2. These costs therefore reflect the cost for a site located on the United Stated Gulf Coast in 2010 and have not yet been converted with a more recent CEPCI value and location factor for the Netherlands.

Table D.2: Overview of calculated costs for individual equipment units of the closed liquefaction system operating with a input purity of 95.5 vol% CO_2.

CO_2 input purity [vol%]	**95.5**		
Process scale [kt · year^{-1}]	100	200	400
Compressors			
Compressor 1 Price [€]	1 215 870	1 543 799	20 40 846
Compressor 2 Price [€]	1 224 080	1 556 242	2 059 707
Compressor 3 Price [€]	1 220 353	1 550 593	2 051 144
Refrigeration Compressor 1 Price [€]	951 726	1 143 431	1 434 002
Refrigeration Compressor 2 Price [€]	1 040 469	1 277 940	1 637 880
Refrigeration Compressor 3 Price [€]	1 061 451	1 309 744	1 686 085
Pressure vessels			
Pressure vessel 1 Price [€]	22 670	24 759	27 777
Pressure vessel 2 Price [€]	21 332	22 670	24 759
Pressure vessel 3 Price [€]	21 332	22 670	24 759
Heat Exchangers			
Heat exchanger 1 Price [€]	37 603	50 062	70 998
Heat exchanger 2 Price [€]	32 658	38 701	48 856
Heat exchanger 3 Price [€]	32 160	37 558	46 627
Heat exchanger 4 Price [€]	44 317	65 486	101 058
Refrigeration heat exchanger 1 Price [€]	28 575	29 321	30 575
Refrigeration heat exchanger 2 Price [€]	32 822	39 078	49 590
Refrigeration heat exchanger 3 Price [€]	34 043	41 883	55 058

Table D.3: Overview of calculated costs for individual equipment units of the closed liquefaction system operating with a input purity of 99.5 vol% CO_2

CO_2 input purity [vol%]	**99.5**		
Process scale [kt · year^{-1}]	100	200	400
Compressors			
Compressor 1 Price [€]	1 156 848	1 454 337	1 905 248
Compressor 2 Price [€]	1 164 702	1 466 242	1 923 292
Compressor 3 Price [€]	1 158 072	1 456 193	1 908 060
Refrigeration Compressor 1 Price [€]	954 648	1 147 860	1 440 715
Refrigeration Compressor 2 Price [€]	1 044 089	1 283 426	1 646 195
Refrigeration Compressor 3 Price [€]	1 065 236	1 315 480	1 694 779
Pressure vessels			
Pressure vessel 1 Price [€]	22 670	24 759	27 777
Pressure vessel 2 Price [€]	21 332	22 670	24 759
Pressure vessel 3 Price [€]	21 332	22 670	24 759
Heat Exchangers			
Heat exchanger 1 Price [€]	37 755	50 411	79 486
Heat exchanger 2 Price [€]	35 231	44 613	66 166
Heat exchanger 3 Price [€]	32 454	38 232	51 508
Heat exchanger 4 Price [€]	42 861	62 141	106 436
Refrigeration heat exchanger 1 Price [€]	28 584	29 342	31 083
Refrigeration heat exchanger 2 Price [€]	32 898	39 253	53 852
Refrigeration heat exchanger 3 Price [€]	34 139	42 103	60 399

D.2. Detailed Open Liquefaction System Equipment Cost

Table D.4 gives an overview of the various size parameters obtained through the APEA to calculate the equipment cost for the open liquefaction system. The cost correlations for compressors are dependent on power in kW, pressure vessel cost is dependent on mass which is calculated based on its size and internal pressure and the heat exchanger costs are dependent on heat exchanging area in m^2.

Table D.4: Overview of equipment parameters used with the equations shown in Section 5.1.1 to calculated equipment costs for the open liquefaction system

CO_2 input purity [vol%]	**95.5**			**99.5**		
Process scale [kt · year^{-1}]	100	200	400	100	200	400
Compressors						
Compressor 1 Power [kW]	399	798	1595	320	640	1279
Compressor 2 Power [kW]	414	828	1657	328	657	1313
Compressor 3 Power [kW]	216	431	862	230	460	920
Refrigeration Compressor 1 Power [kW]	180	359	719	192	384	767
Refrigeration Compressor 2 Power [kW]	412	824	1648	325	650	1301
Pressure vessels						
Pressure vessel 1 diameter [m]	1.2	1.4	1.5	1.2	1.4	1.5
Pressure vessel 1 height [m]	3.7	4	4.6	3.7	4	4.6
Pressure vessel 1 pressure [m]	2410	2410	2410	1667	1667	1667
Heat Exchangers						
Heat exchanger 1 size [m^2]	32	64	127	34	68	136
Heat exchanger 2 size [m^2]	42	84	168	45	90	179
Heat exchanger 3 size [m^2]	45	89	178	40	81	161
Heat exchanger 4 size [m^2]	44	88	177	37	74	149
Refrigeration heat exchanger 1 size [m^2]	66	133	265	114	229	457
Refrigeration heat exchanger 2 size [m^2]	71	142	285	76	152	304

Tables D.5 and D.6 give the equipment cost of the open liquefaction system as calculated with the correlation and variables from Equation 3.3 and Table 3.5 of Section 3.7.2. These costs therefore reflect the cost for a site located on the United Stated Gulf Coast in 2010 and have not yet been converted with a more recent CEPCI value and location factor for the Netherlands.

Table D.5: Overview of calculated costs for individual equipment units of the open liquefaction system operating with a input purity of 95.5 vol% CO_2.

CO_2 input purity [vol%]	**95.5**		
Process scale [kt · year^{-1}]	100	200	400
Compressors			
Compressor 1 Price [€]	1 306 976	1 681 889	2 250 151
Compressor 2 Price [€]	1 323 679	1 707 206	2 288 524
Compressor 3 Price [€]	1 082 459	1 341 586	1 734 348
Refrigeration Compressor 1 Price [€]	1 030 510	1 262 846	1 615 000
Refrigeration Compressor 2 Price [€]	1 321 313	1 703 620	2 283 090
Pressure vessels			
Pressure vessel 1 Price [€]	22 670	24 759	27 777
Heat Exchangers			
Heat exchanger 1 Price [€]	31 426	35 872	46 085
Heat exchanger 2 Price [€]	32 783	38 987	53 242
Heat exchanger 3 Price [€]	33 143	39 816	55 146
Heat exchanger 4 Price [€]	33 086	39 686	54 846
Refrigeration heat exchanger 1 Price [€]	36 279	47 020	71 696
Refrigeration heat exchanger 2 Price [€]	37 014	48 708	75 576

Table D.6: Overview of calculated costs for individual equipment units of the open liquefaction system operating with a input purity of 99.5 vol% CO_2

CO_2 input purity [vol%]	**99.5**		
Process scale [kt · year^{-1}]	100	200	400
Compressors			
Compressor 1 Price [€]	1 216 811	1 545 225	2 043 008
Compressor 2 Price [€]	1 226 868	1 560 469	2 066 113
Compressor 3 Price [€]	1 102 559	1 372 051	1 780 526
Refrigeration Compressor 1 Price [€]	1 048 532	1 290 162	1 656 404
Refrigeration Compressor 2 Price [€]	1 223 173	1 554 868	2 057 624
Pressure vessels			
Pressure vessel 1 Price [€]	22 670	24 759	27 777
Heat Exchangers			
Heat exchanger 1 Price [€]	31 706	36 514	47 561
Heat exchanger 2 Price [€]	33 173	39 884	55 302
Heat exchanger 3 Price [€]	32 561	38 479	52 075
Heat exchanger 4 Price [€]	32 144	37 520	49 872
Refrigeration heat exchanger 1 Price [€]	43 930	64 597	112 077
Refrigeration heat exchanger 2 Price [€]	37 749	50 398	79 458

D.3. Detailed Transportation Cost

Tables D.7 and D.8 show a detailed view of the OPEX and CAPEX costs which are summed in Figures 5.5 and 5.6 of Section 5.2. The OPEX in Figure 5.5 consists of summing the fuel, ship (adjusted to usage), buffer storage and loading facility OPEX from Tables D.7 and D.8. The CAPEX in Figure 5.6 consists of summing the buffer storage and loading facility CAPEX from Tables D.7 and D.8. The values in these tables are calculated with the equations and fixed variables shown in Sections 3.7.3 and 3.7.4 respectively.

Table D.7: Breakdown of annual operational expenditure and capital expenditure as summed in Figures 5.5 and 5.6 of Section 5.2 respectively for a CO_2 input purity of 95.5 vol%.

CO_2 input purity [vol%]	95.5		
Process scale [kt · year^{-1}]	100	200	400
Fuel OPEX [€ · year^{-1}]	400 140	800 280	1 600 560
Ship CAPEX [€ · year^{-1}]	92 092 750	92 092 750	92 092 750
Ship OPEX (total) [€ · year^{-1}]	4 604 638	4 604 638	4 604 638
Ship OPEX (adjusted to usage) [€ · year^{-1}	1 037 563	2 075 127	4 150 253
Buffer storage CAPEX [€ · year^{-1}]	13 859 719	13 859 719	13 859 719
Buffer storage OPEX [€ · year^{-1}]	831 583	831 583	831 583
Loading facilities CAPEX [€ · year^{-1}]	263 333	526 667	1 053 333
Loading facilities OPEX [€ · year^{-1}]	5 267	10 533	21 067

Table D.8: Breakdown of annual operational expenditure and capital expenditure as summed in Figures 5.5 and 5.6 of Section 5.2 respectively for a CO_2 input purity of 99.5 vol%.

CO_2 input purity [vol%]	99.5		
Process scale [kt · year^{-1}]	100	200	400
Fuel OPEX [€ · year^{-1}]	400 140	800 280	1 600 560
Ship CAPEX [€ · year^{-1}]	68 158 375	68 158 375	68 158 375
Ship OPEX (total) [€ · year^{-1}]	3 407 919	3 407 919	3 407 919
Ship OPEX (adjusted to usage) [€ · year^{-1}	767 907	1 535 813	3 071 626
Buffer storage CAPEX [€ · year^{-1}]	10 867 922	10 867 922	10 867 922
Buffer storage OPEX [€ · year^{-1}]	652 075	652 075	652 075
Loading facilities CAPEX [€ · year^{-1}]	263 333	526 667	1 053 333
Loading facilities OPEX [€ · year^{-1}]	5 267	10 533	21 067

Bibliography

[1] Tata Steel Nederland BV. *Beeldbank*. Online. Available: www.tatasteelnederland.com/nieuws/beeldbank. Accessed: 24 Oct. 2025.

[2] Intergovernmental Panel on Climate Change (IPCC). *History of the IPCC*. www.ipcc.ch/about/history/. Accessed: 24 Jul. 2025. 2025.

[3] United Nations. *UN Climate Change Conferences*. www.un.org/en/climatechange/un-climate-conferences. Accessed: 24 Jul. 2025. 2025.

[4] Council of the European Union (Consilium). *Paris Agreement on climate change*. www.consilium.europa.eu/en/policies/paris-agreement-climate/. Accessed: 24 Jul. 2025. 2025.

[5] L. van der Net *et al. Greenhouse Gas Emissions in the Netherlands 1990–2023: National Inventory Document 2025*. www.rivm.nl/publicaties/greenhouse-gas-emissions-in-netherlands-1990-2023-national-inventory-document-2025. RIVM Report 2025-0005, accessed: 24 Jul. 2025. 2025.

[6] PBL Netherlands Environmental Assessment Agency et al. *Climate and Energy Outlook of the Netherlands 2024*. www.pbl.nl/en/publications/climate-and-energy-outlook-of-the-netherlands-2024. PBL publication no. 5491, version 2, accessed: 24 Jul. 2025. 2024.

[7] Haskoning. *Vragen en antwoorden over het Groen Staal-Plan, Samenvatting van het Milieueffectrapport*. www.tatasteelnederland.com/duurzaamheid/groen-staal-plan/participatie/mer. Accessed: 24 Jul. 2025. 2025.

[8] Tata Steel Europe. *HIsarna: A Revolutionary Breakthrough Technology*. https://products.tatasteelnederland.com/sites/producttsn/files/tata-steel-europe-factsheet-hisarna.pdf. Accessed: 24 Jul. 2025. 2020.

[9] Nicole Bond, Robert Symonds, and Robin Hughes. “Pressurized chemical looping for direct reduced iron production: carbon neutral process configuration and performance”. In: *Energies* 15.14 (2022), p. 5219.

[10] Roberto Scaccabarozzi et al. “Techno-Economic and CO2 Emissions Analysis of the Molten Carbonate Fuel Cell Integration in a DRI Production Plant for the Decarbonization of the Steel Industry”. In: *Applied Energy* 376 (2024), p. 124264. DOI: 10.1016/j.apenergy.2024.124264.

[11] Darbaz Khasraw et al. “Devolatilisation characteristics of coal and biomass with respect to temperature and heating rate for HIsarna alternative ironmaking process”. In: *Fuel* 284 (2021), p. 119101.

[12] Abraham Aditya Takarianto. “Modeling of PSA System for Recovery of CO2 and CO from Industrial Proccess Gass Stream”. Accessed: 24 Jul. 2025. Master’s thesis. Delft, Netherlands: Delft University of Technology, 2024.

[13] Anne Carpenter. “CO2 abatement in the iron and steel industry”. In: *IEA Clean Coal Centre* 25 (2012), p. 193.

[14] M. Geerdes et al. *Modern Blast Furnace Ironmaking: An Introduction*. 3rd. Accessed: 2 Sep. 2025. Amsterdam: IOS Press, under the imprint of Delft University Press, 2015. URL: http://site.ebrary.com/id/11048358.

[15] Andreas Orth, Nikola Anastasijevic, and Heinz Eichberger. “Low CO2 emission technologies for iron and steelmaking as well as titania slag production”. In: *Minerals Engineering* 20.9 (2007), pp. 854–861.

[16] Koen Meijer et al. “Developments in alternative ironmaking”. In: *Transactions of the Indian Institute of Metals* 66.5 (2013), pp. 475–481.

[17] Ashkan Hosseini et al. “Off-Gas system scale-up of HIsarna iron-making process: A cfd-based approach”. In: *Metallurgical and Materials Transactions B* 53.6 (2022), pp. 3557–3574.

[18] José Maria M Pires, Stefania Moioli, and Laura A Pellegrini. “First techno-economic assessment of a monoethanolamine-based CO2 capture plant applied downstream the Electric Arc Furnace for steel production.” In: *Chemical Engineering Research and Design* (2025).

[19] IOGP Europe. *Interactive Map of CCUS Projects in Europe*. Accessed: 23 Sep. 2025. 2025. URL: https://iogpeurope.org/european-ccs-projects-map/.

[20] Ragnhild Korbøl and Aoued Kaddour. “Sleipner vest CO2 disposal-injection of removed CO2 into the Utsira formation”. In: *Energy Conversion and Management* 36.6-9 (1995), pp. 509–512.

[21] Netherlands Court of Audit. *Carbon storage under the North Sea: On profits under water*. Audit Report Report 2024/03/28. Netherlands Court of Audit, Mar. 2024. URL: https://english.rekenkamer.nl/publications/reports/2024/03/28/carbon-storage-under-the-north-sea.

[22] Sanne Akerboom et al. “Different this time? The prospects of CCS in the Netherlands in the 2020s”. In: *Frontiers in Energy Research* 9 (2021), p. 644796.

[23] PORTHOS CO2 Transport and Storage C.V. *Standard CO2 Transport and Storage Conditions in Respect of the Porthos System*. Technical Report. Version v1.1. Draft version 1.1, March 2022. PORTHOS CO2 Transport and Storage C.V., Mar. 2022. URL: www.porthosco2.nl/wp-content/uploads/2022/03/Porthos-standard-CO2-Transport-and-Storage-Conditions.pdf.

[24] BP Exploration Operating Company Limited and Xodus Group Ltd. *Offshore Environmental Statement for the Northern Endurance Partnership: Volume 1/2, Environmental Statement, Part A*. Environmental Statement D/4271/2021, Document: NS051-EV-REP-000-00021. BP, Sept. 2023. URL: www.bp.com/content/dam/bp/country-sites/en_gb/united-kingdom/home/images/nep/NEP-Environmental-Statement-Part-A.pdf.

[25] Northern Endurance Partnership / East Coast Cluster. *Northern Endurance Partnership greenlights UK’s first CO2 transportation and storage infrastructure project*. https://eastcoastcluster.co.uk/press-release/northern-endurance-partnership-greenlights-uks-first-co2-transportation-and-storage-infrastructure-project/. Accessed: 25 Sep. 2025. Dec. 2024.

[26] Cristel Lambton. *Northern Lights: A European CO2 Transport and Storage Network*. Presentation (PDF), Quebec CCUS Visioning Workshop, 15 March 2023. Accessed: 25 Sep. 2025. Mar. 2023. URL: https://inrs.ca/wp-content/uploads/Conf-5-Cristel-Lambton.pdf.

[27] Emil Yde Aasen. *Northern Lights: A European CO2 Transport and Storage Network*. Accessed: 23 Sep. 2025. Presented at the IEA Bioenergy ExCo84 workshop, Tallinn, Estonia, 22 October 2019. Tallinn, Estonia: IEA Bioenergy, Oct. 2019. URL: www.ieabioenergy.com/wp-content/uploads/2019/10/10_EmilYdeAasen-Northern-Lights_SharedVersion.pdf.

[28] CCS-ARAMIS Project. *Specification for CO2 supplied to Aramis via pipeline*. Accessed: 21 Oct. 2025. 2025. URL: www.aramis-ccs.com/files/13032025-ARM-CPT-BB8-PRO-MEM-0033-rev-6.2-public-version-NEW.pdf.

[29] Northern Endurance Partnership. *CO2 Pipelines Entry Specification, Version B02*. Technical Report. Published April 2025. Northern Endurance Partnership, Apr. 2025. URL: www.northernendurancepartnership.co.uk/wp-content/uploads/2025/04/PES-NEP00-EN-SPE-000-00001-Public-B02.pdf.

[30] Northern Lights JV DA and DNV. *Liquid CO2 Quality Specifications*. Technical Report. Version Rev 1. DOC NL-02-TE-SP01, updated liquid CO2 spec under reference conditions (13–15 bar (g), –30.5 to –26.5 °C vapour). Northern Lights JV DA, Feb. 2024. URL: https://safety4sea.com/wp-content/uploads/2024/03/Northern-Lights-GS-co2-2024_03.pdf.

[31] Engineering National Academies of Sciences, Medicine, et al. *Carbon Utilization Infrastructure, Markets, and Research and Development: A Final Report*. The National Academies Press, 2024.

[32] N Pedrosa et al. “Accurate Physical Property Modelling of CO2-Rich Mixtures with Impurities Within Typical CCS Feedstock”. In: *ISAVFT North American Conference on Multiphase Production Technology*. ISAVFT. 2024, ISAVFT–2024.

[33] Richard TJ Porter et al. “The range and level of impurities in CO2 streams from different carbon capture sources”. In: *International Journal of Greenhouse Gas Control* 36 (2015), pp. 161–174.

[34] Eleni G Nikolaidou et al. “The role of impurities in CCS from pilot capture plants to sequestration sites—A review”. In: *International Journal of Greenhouse Gas Control* 145 (2025), p. 104410.

[35] Arne Simons et al. “A review of corrosion in flowing conditions during dense phase CO2 transport for carbon capture, utilization, and storage (CCUS)”. In: *Engineering Failure Analysis* (2025), p. 109905.

[36] Erika De Visser et al. “Dynamis CO2 quality recommendations”. In: *International journal of greenhouse gas control* 2.4 (2008), pp. 478–484.

[37] Richard Barker, Yong Hua, and Anne Neville. “Internal corrosion of carbon steel pipelines for dense-phase CO2 transport in carbon capture and storage (CCS)–a review”. In: *International Materials Reviews* 62.1 (2017), pp. 1–31.

[38] Craig McKay et al. “Recommendations for the selection of equation of state during design and operation of impure CO2 transport and storage”. In: *Proceedings of the 16th Greenhouse Gas Control Technologies Conference (GHGT-16)*. 2022, pp. 23–24.

[39] D Turunawarasu and E Luna-Ortiz. “Thermodynamic Models in CCS Full-Chain Systems with CO2 Shipping”. In: *Offshore Technology Conference Asia*. OTC. 2024, D031S026R001.

[40] Tarek Ahmed. *Equations of state and PVT analysis*. Elsevier, 2013.

[41] Byeong Soo Shin et al. “Evaluation of Thermodynamic Models for Predicting Phase Equilibria of CO2 + Impurity Binary Mixture”. In: *International Journal of Thermophysics* 39.3, 44 (Mar. 2018), p. 44. DOI: 10.1007/s10765-018-2364-5.

[42] Øivind Wilhelmsen et al. “Thermodynamic modeling with equations of state: present challenges with established methods”. In: *Industrial & Engineering Chemistry Research* 56.13 (2017), pp. 3503–3515.

[43] Darshan Raju, Mahinder Ramdin, and Thijs JH Vlugt. “Thermophysical Properties and Phase Behavior of CO2 with Impurities: Insight from Molecular Simulations”. In: *Journal of Chemical & Engineering Data* 69.8 (2024), pp. 2735–2755.

[44] Sumit Sharma, Pramod Kumar, and Rakesh Chandra. “Introduction to molecular dynamics”. In: *Molecular dynamics simulation of nanocomposites using BIOVIA materials studio, Lammps and Gromacs*. Elsevier, 2019, pp. 1–38.

[45] Elke Goos et al. “Phase diagrams of CO2 and CO2–N2 gas mixtures and their application in compression processes”. In: *Energy Procedia* 4 (2011), pp. 3778–3785.

[46] E. W. Lemmon et al. *NIST Standard Reference Database 23: Reference Fluid Thermodynamic and Transport Properties–REFPROP, Version 10.0, National Institute of Standards and Technology*. 2018. DOI: 10.18434/T4JS3C. URL: www.nist.gov/srd/refprop.

[47] Haixia Wang, Jusheng Chen, and Qingling Li. “A review of pipeline transportation technology of carbon dioxide”. In: *IOP conference series: earth and environmental science*. Vol. 310. 3. IOP Publishing. 2019, p. 032033.

[48] Sunday Okoro et al. “Effects of non-condensable CCUS impurities (CH4, O2, Ar and N2) on the saturation properties (bubble points) of CO2-rich binary systems at low temperatures (228.15–273.15 K)”. In: *Greenhouse Gases: Science and Technology* 13.6 (2023). Open access under CC BY-NC-ND 4.0, pp. 1152–1169. DOI: 10.1002/ghg.2305. URL: www.researchgate.net/publication/377062915.

[49] Antonin Chapoy et al. “Hydrate and phase behavior modeling in CO2-rich pipelines”. In: *Journal of Chemical & Engineering Data* 60.2 (2015), pp. 447–453.

[50] Pauline Oeuvray et al. “Multi-criteria assessment of inland and offshore carbon dioxide transport options”. In: *Journal of Cleaner Production* 443 (2024), p. 140781.

[51] Y Sen et al. “Evaluation of CO2 liquefaction processes for ship-based carbon capture and storage (CCS) in terms of life cycle cost (LCC) considering availability”. In: *International Journal of Greenhouse Gas Control* 35 (2015), pp. 1–12.

[52] Simon Roussanaly et al. “At what pressure shall CO2 be transported by ship? An in-depth cost comparison of 7 and 15 barg shipping”. In: *Energies* 14.18 (2021), p. 5635.

[53] Desmond Winterbone and Ali Turan. *Advanced thermodynamics for engineers*. Butterworth-Heinemann, 2015.

[54] David Olsson Berstad et al. “Cryogenic CO2 condensation and membrane separation of syngas for large-scale LH2 production”. In: *Cryogenics 2017: Proceedings of the 14th IIR International Conference, Dresden, Germany, Mai 15-19, 2017.* International Institute of Refrigeration. 2017.

[55] Victor E Onyebuchi et al. “A systematic review of key challenges of CO2 transport via pipelines”. In: *Renewable and Sustainable Energy Reviews* 81 (2018), pp. 2563–2583.

[56] Munish Kumar Chandel, Lincoln F Pratson, and Eric Williams. “Potential economies of scale in CO2 transport through use of a trunk pipeline”. In: *Energy Conversion and Management* 51.12 (2010), pp. 2825–2834.

[57] Martha M Roggenkamp. “CCUS in the Netherlands”. In: *Carbon Capture Utilization and Storage: Law, Policy and Standardization Perspectives*. Springer, 2025, pp. 423–446.

[58] Tata Steel Netherlands, Research & Development - Blast Furnace Development and Alternative Ironmaking. *Internal Memo: [Off-gas cases for HIsarna]*. Internal company document. 2024.

[59] Peidong Hu et al. “Development of zeolite adsorbent with low water sensitivity for CO2 capture”. In: *Chemical Engineering Journal* 508 (2025), p. 161054.

[60] Khalid W Hameed. *Chemical Process Simulations using Aspen Hysys*. John Wiley & Sons, 2025.

[61] Marcia L Huber et al. “The NIST REFPROP database for highly accurate properties of industrially important fluids”. In: *Industrial & Engineering Chemistry Research* 61.42 (2022), pp. 15449–15472.

[62] JH Keenan and FG Keyes. “Thermodynamic and Transport Properties of Steam”. In: *Wiley and Sons* (1959).

[63] Han Deng, Simon Roussanaly, and Geir Skaugen. “Techno-economic analyses of CO2 liquefaction: Impact of product pressure and impurities”. In: *International Journal of Refrigeration* 103 (2019), pp. 301–315.

[64] European Commission. *F-gas legislation*. `climate.ec.europa.eu/eu-action/fluorinated-greenhouse-gases/f-gas-legislation_en`. Accessed: 11 Dec. 2025. European Commission — Climate Action, Feb. 2024.

[65] Gavin Towler and Ray Sinnott. *Chemical engineering design: principles, practice and economics of plant and process design*. Butterworth-Heinemann, 2021.

[66] University of Manchester. *Chemical Engineering Plant Cost Index*. `www.training.itservices.manchester.ac.uk/public/gced/CEPCI.html?reactors/CEPCI/index.html`. Accessed: 4 Jan. 2026. 2024.

[67] Northern Lights. *Northern Lights’ first CO_2 transport ship ready for delivery*. Accessed: 16 Dec. 2025. 2024. URL: `https://norlights.com/news/northern-lights-first-co2-transport-ship-ready-for-delivery/`.

[68] E□Bridge / Ministry of Economic Affairs and Climate Policy (EZK). *Electricity Cost Assessment for Large Industry in the Netherlands, Belgium, Germany and France: Final Report*. Technical Report. Accessed: 7 Jan. 2026. Rijksoverheid / Open Overheid, Mar. 2024. URL: `https://open.overheid.nl/documenten/17f8a8ea-2069-40ea-b4ce-c0138cd2fb71/file`.

[69] Breezada. *Bergen to Rotterdam – Sea Distance 509 Nautical Miles*. `www.breezada.com/en/routes/bergen/rotterdam`. Accessed: 8 Jan. 2026. 2026.

[70] CCS Midt-Norge Consortium. *CCS Midt-Norge: Final Report*. Project Report. Version 1.0, signed final report. Gassco AS, 2023.